Identification of Single Chain Variable Fragment (ScFv) Antibodies Specific to Immune Checkpoints by Phage Display

Mila Dimitrovska

June 2025

Supervisor: Prof. David Saliba B.Sc. (Hons) Ph.D. (Edin)

Master of Science in Applied Biomedical Science

Faculty of Health Sciences
University of Malta

L-Università ta' Malta

FACULTY/INSTITUTE/CENTRE/SCHOOL Faculty of Health Sciences

DECLARATIONS BY POSTGRADUATE STUDENTS

(a) Authenticity of Dissertation

I hereby declare that I am the legitimate author of this Dissertation and that it is my original work.

No portion of this work has been submitted in support of an application for another degree or qualification of this or any other university or institution of higher education.

I hold the University of Malta harmless against any third party claims with regard to copyright violation, breach of confidentiality, defamation and any other third party right infringement.

(b) Research Code of Practice and Ethics Review Procedures

I declare that I have abided by the University's Research Ethics Review Procedures. Research Ethics & Data Protection form code FHS - 2022 - 00465.

As a Master's student, as per Regulation 77 of the General Regulations for University Postgraduate Awards 2021, I accept that should my dissertation be awarded a Grade A, it will be made publicly available on the University of Malta Institutional Repository.

02.2023

Dedications

I would like to dedicate this work to my family and friends, who have been nothing but supportive throughout all of the months of work.

Acknowledgments

I would like to express my heartfelt thanks to my supervisor, Professor David Saliba, whose guidance was invaluable during every step of this process. Further thanks are also necessary towards many of his other students who made sharing lab space feel like a pleasure rather than an obstacle.

I would also like to extend my thanks more specifically to Ms Mariana Grima, and Ms Giuseppina Monda, for their impeccable laboratory management, and endless support.

Further thanks are necessary for all of the University of Malta staff, and especially to the Centre of Molecular Medicine and Biobanking for the use of their facilities as well as their constant aid.

Finally, I would like to acknowledge the contributions of the University of Edinburgh, as well as the International Centre for Cancer Vaccine Science in Gdansk, without which this project may have not even occurred.

Abstract

The inhibition of immune checkpoints is a significant emerging strategy in immunotherapy for the treatment of several malignancies, with much potential for further applications. However, currently there are many pitfalls and drawbacks to the widespread use of this therapy in a clinical setting. One such drawback is the lack of diverse options in the choice for immune checkpoints targeted. This study therefore aimed to identify, isolate, and validate high affinity single chain variable fragment (scFv) antibodies specific to three known immune checkpoints (CD47, TIGIT, and GITR), in an effort to further drive the research and development of new immunotherapeutic strategies for the treatment and management of various cancers. This was accomplished in collaboration with the International Centre for Cancer Vaccine Science in Gdansk, as well as the Roslin Institute, University of Edinburgh, using the phage display method. Numerous rounds of biopanning were performed, beginning from a naïve canine scFv bacteriophage library to create enriched libraries of phages carrying scFv with high affinity to the target proteins. The affinity of the generated scFv antibodies was verified using ELISA, after which, specific phage clones were selected from the biopanning round which showed highest affinity to the target, which were then further amplified and validated with ELISA. The protein sequences of these high affinity phage clones were determined using Sanger sequencing and manually compared. Of the three targets, high affinity scFv clones were only successfully produced against GITR His-tag, isolating 60 scFv phage clones, 43 of which showed high affinity and specificity against GITR protein. All but three clones were successfully sequenced, showing a relatively high amount of diversity of scFv sequences. Further research is required to fully explore the drawbacks of this methodology, as well as successfully identify high affinity scFvs against CD47 and TIGIT.

Table of Contents

List of Figures

List of Tables

List of Abbreviations

AML	Acute Myeloid Leukaemia
APC	Antigen Presenting cells
AUC	Area Under Curve
BSA	Bovine Serum Albumin
bsAb	Bispecific antibodies
CAF	Cancer associated fibroblast
CAR	Chimeric antigen receptor
CD	Cluster of Differentiation
cDNA	Complementary DNA
CDR	Complementarity-determining region
CI	Confidence Interval
COVID-19	Coronavirus Disease
CTLA-4	Cytotoxic T-lymphocyte antigen 4
CV	Coefficient of Variation
DNA	Deoxyribonucleic acid
DNAM-1	DNAX accessory molecule 1
E. coli	*Escherichia coli*
ECIS	European Cancer Information System
ECM	Extracellular matrix
ELISA	Enzyme-linked Immunosorbent Assay
ERK	Extracellular signal-regulated kinase 1/2
EU	European Union
Fab	Antigen-binding Fragment
FDA	Food and Drug Authority
Fv	Fragment variable
GITR	Glucocorticoid-Induced TNFR-Related protein
GITRL	Glucocorticoid-Induced TNFR-Related protein Ligand
HAMA	Human Anti-Mouse Antibody
IAP	Integrin-Associated protein
ICCVS	International Centre for Cancer Vaccine Science
ICI	Immune Checkpoint Inhibitor

IFNγ	Interferon gamma
Ig	Immunoglobulin
IL-2	Interleukin-2
ITIM	Immunoreceptor Tyrosine-based Inhibitory Motif
ITT	Immunoglobulin Tail Tyrosine
IRAE	Immune-Related Adverse Events
JNK	c-Jun N-terminal kinase
LAG-3	Lymphocyte-activation gene 3
LB	Luria-Bertani
mAbs	Monoclonal Antibodies
MAPK	Mitogen-activated protein kinase
MDSC	Myeloid derived suppressor cells
MNPs	Magnetic Nanoparticles
NEB	New England Biolabs
NF-κB	Nuclear Factor kappa-light-chain-enhancer of activated B cells
NK	Natural Killer
NPC	No Protein Control
ORR	Overall response rate
PADLOCK	Phage DispLay of Immune ChecKpoints
PBS	Phosphate Buffered Saline
PC	Phage Culture
PCR	Polymerase Chain Reaction
PCSK9	Proprotein Convertase Subtilisin/Kexin type 9
PD-1	Programmed Cell Death Protein 1
PD-L1	Programmed Cell Death Protein 1 Ligand
PEG	Polyethylene glycol
rpm	Revolutions per minute
SARS-CoV-2	Severe Acute Respiratory Syndrome Coronavirus 2
scFv	Single-chain Variable Fragment
SIRP	Signal Regulatory Protein
SIRPα	Signal Regulatory Protein alpha
TACTILE	T cell activation, increased late expression
TCR	T cell receptor

TEA	Triethylamine
TIGIT	T cell Immunoglobulin and ITIM domain
TILs	Tumour-infiltrating Lymphocytes
TIM-3	T cell immunoglobulin domain and mucin domain 3
TIM-4	T cell immunoglobulin domain and mucin domain 4
TNF	Tumour Necrosis Factor
TNFRSF	TNF receptor superfamily
Treg	Regulatory T cells
US	United States
VH	Variable Fragment Heavy chain
VISTA	V-domain Ig suppressor of T cell activation
VL	Variable Fragment Light chain

1. Introduction

In the current age of modern medicine, cancer remains one of the leading causes of mortality in nearly all developed countries. According to official European cancer statistics, in the year 2017, roughly 25% of all deaths in the European Union (EU) were cancer related, with some EU countries exceeding 30% from the total number of deaths by the year 2019 (Eurostat 2022, European Cancer Information System [ECIS] 2023). In a review written by Dyba, Randi et al. (2021) summarising the overall cancer burden of the EU in the year 2020, over 4 million new cancer cases were recorded, not counting non-melanoma skin cancers, with nearly half of those cases being estimated to have resulted in the death of the patient.

Similarly, The American Cancer Society reports up to 1.9 million new cancer cases in the United States of America in the year 2022. Furthermore, it reports that while cancer death rates have overall dropped in the past 30 years, cancer still remains the second most common cause of death for children below the age of 14 (American Cancer Society [ACS] 2022).

Therefore, from the above statistics, it is simple to conclude that the development and implementation of novel and patient-centred treatment and management strategies, aimed at eliminating malignant cells, while minimising harm to the patient still remains an incredibly important pursuit in medicine (McDowell 2018). One such strategy in particular is the use of immunotherapeutic techniques, and more specifically Immune checkpoint inhibitors (ICI), either as a monotherapy, or in conjunction with other therapies, for an improved patient outcome (Vanneman, Dranoff 2012).

The main focus of this study is, therefore, the production and validation of high affinity single chain variable fragment (scFv) antibodies targeting three novel checkpoints in the tumour microenvironment (TME). This will be done through the use of phage display biopanning, and

thus also highlighting the validity of this methodology in the synthesis on antibodies as a secondary aim of this project. This shall all be carried out with the ultimate goal of improving current immunotherapy strategies, as well as expanding the panel of available ICIs for the treatment of various cancers.

1.1 Tumour Microenvironment

As the knowledge available on the pathogenicity of various malignancies increases, it should be noted that an increasing amount of attention is being diverted away from the tumour cells themselves, and towards the TME. There are many complex processes that occur between the different components making up the TME and the infiltrating cells of both the innate and the acquired immune system, all of which may have different effects on the tumour (Anderson, Simon 2020).

The TME is composed of a constantly evolving collection of various cells, including T cells, B cells, dendritic cells, fibroblasts and others, as well as the extracellular matrix (ECM) and other non-cellular components making up the extracellular environment, in which they are all found. The interactions and rearrangement of these various components is considered to be one of the main driving factors in tumour growth, and depending on the processes which occur, may either lead to tumour elimination by the immune cells, or evasion of the immune response and even development of resistance by the tumour to various cancer treatment strategies (Baghban, Roshangar et al. 2020).

A summary of the TME and some of the various cells and processes that occur within it may be seen in **Figure 1.1**.

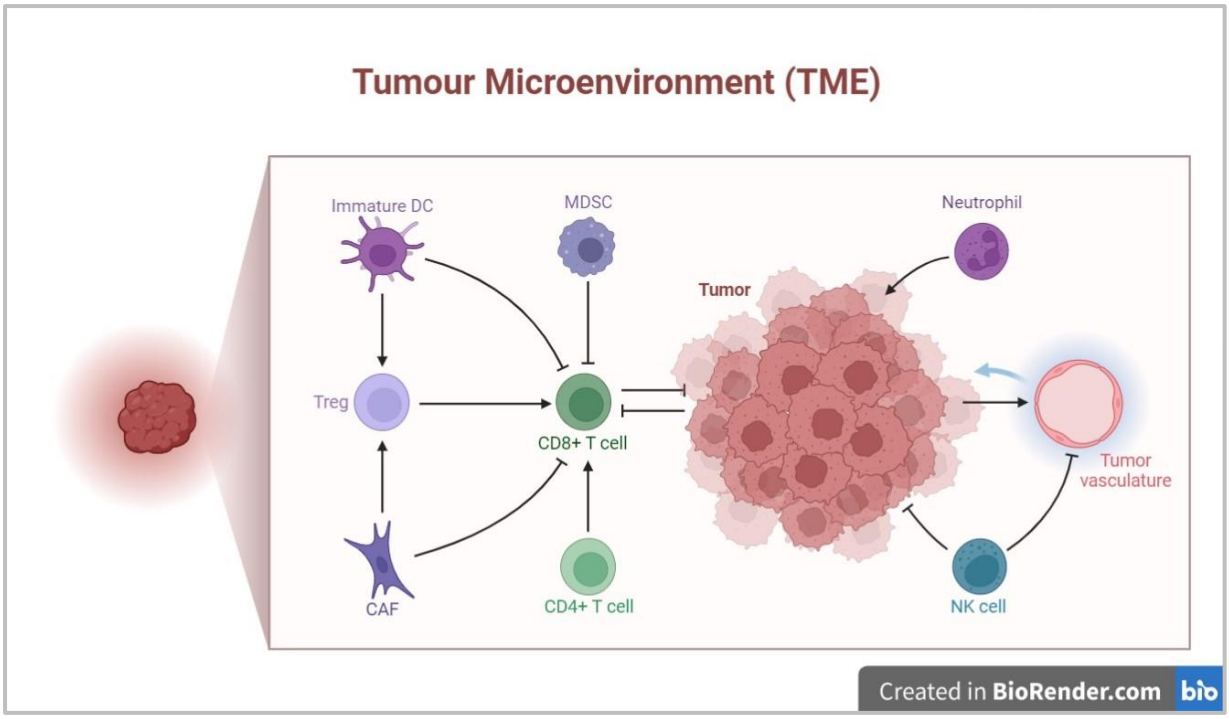

Figure 1.1: A simplified representation of some of the different cells making up the TME, their various interactions, and their effects on the tumour*. The main anti-tumour effects are driven by the actions of $CD8^+$ T cells, $CD4^+$ T cells and Natural Killer (NK) cells. Conversely the anti-tumour effect of these cells may be suppressed through several means, including the action of cells such as regulatory T cells (Tregs), myeloid-derived suppressor cells (MDSC), and cancer-associated fibroblasts (CAF) which may also be found in the TME. This image was produced using the online software BioRender.*

Of the different components of the TME, infiltrating lymphocytes are by far considered the main drivers of the anti-tumour immune response, and through understanding these processes as well as the mechanisms utilised by the tumour cells to avoid them, several new targets for therapy have been discovered. This of course includes the use of ICIs targeting specific checkpoints present on infiltrating T cells such as Programmed Cell Death Protein 1 (PD-1) and its ligand PD-L1, as well as Cytotoxic T-lymphocyte antigen 4 (CTLA-4), although these may not always be present in the TME of every tumour (Bożyk, Wojas-Krawczyk et al. 2022).

Depending on the level of immune infiltration, the TME of the various types of tumours may be divided into three distinct categories. These are Type I, characterised by a relatively large amount of infiltrating T cells, Type II, which are seen to have a minimal amount of infiltrating T cells, and Type III, which shows the immune cells sequestered to the peripheries of the TME only. These differences in composition of the TME have often been found to affect both the prognosis of the patient, as well as the reaction to various immunotherapy treatment strategies, including immune checkpoint blockade (Smyth, Ngiow et al. 2015).

Most often tumours exhibiting Type I TME, otherwise known as “hot” cancers, are found to show the best response to ICIs, both as a monotherapy, as well as in combination with other therapies such as surgery, chemotherapy, and targeted therapy. Some types of malignancy which may be commonly characterised by a Type I TME include melanoma and neuroendocrine tumours, meaning these types of cancers are often seen to respond favourably to immunotherapy (Takkenkamp, Jalving et al. 2020). On the other hand, cancers characterised by Type II and Type III TME, or “cold” cancers, such as pancreatic cancer, and prostate cancer, often show a poor response to immune checkpoint blockade due to the lack of infiltrating T cells, despite the fact that the target checkpoints may be expressed (Smyth, Ngiow et al. 2015).

However, in the case of pancreatic adenocarcinoma in particular, a study by Karamitopoulou (2019) making use of animal models has shown the possibility of modulating the TME through the activation of CD40 as a way of stimulating T cell activity and infiltration, and thus converting a “cold” tumour into a “hot” one. This would therefore pave the way for the action of ICIs and other modulators, which would have otherwise had minimal effect on these tumours, thus further opening the door for the application of this type of treatment.

On the other hand, while the study of the TME has proven intrinsic to the deepening understanding of tumour growth and treatment, one criticism that has emerged to this TME-centric view is that, similarly to the previously dominant tumour-centric views on cancer, it can be rather restrictive in the way cancer is treated and managed. Many reviews have highlighted the importance of considering the organism as a whole rather than simply the TME on its own, with Spitzer et.al (2017) suggesting the usefulness of maintaining lymphocyte activation in peripheral lymph nodes as well as systemic immune remodelling, both during and after immunotherapy, as a way of improving and prolonging anti-tumour response, as well as further preventing tumour growth and metastasis, especially in multifocal disease (Laplane, Duluc et al. 2019).

Nevertheless, the increased awareness of the TME has greatly helped to shape the next wave of cancer treatment strategies, as well as allowed for the emergence of checkpoint modulation and blockade for the treatment of various cancers.

1.2 Immunotherapy

Immunotherapy, as a treatment for cancer, is a type of biological therapy (biotherapy), developed in large part thanks to an increase in knowledge of cancer pathogenesis, the TME, as well as the modes of action of the human immune system in regard to cancer. It along with other therapies, such as targeted therapy, have started supplanting the use of broader, non-specific anti-cancer therapies such as the use of cytotoxic agents and radiation, which for the longest time were seen as the cornerstone for cancer treatment (Vanneman, Dranoff 2012).

Unlike the traditional cancer treatments, rather than attempting to destroy malignant cells directly, immunotherapy functions by acting on the immune system in order to stimulate an

immune response against the cancer cells, without causing untoward damage to healthy cells and tissues. This goal may be accomplished with a variety of different techniques, allowing immunotherapy to be split into five different branches, depending on the part of the immune system targeted and the route of action taken, although there also may be overlap between the different methodologies (National Cancer Institute [NCI] 2019). These five, by order of development, starting from the oldest to the most recent, include the use of Cytokines, Immune Checkpoint Inhibitors (ICIs), Monoclonal Antibodies (mAbs), Chimeric antigen receptor (CAR) T cell therapy, and Treatment Vaccines (Cancer Research UK 2021, Khan, Maker et al. 2021)

While each of the mentioned types of immunotherapy are fascinating topics for further research, the main focus of this study lies in the use of ICIs. As previously mentioned, the main mode of action of this treatment lies in the targeting of specific immune checkpoints in the TME, most often with the use of synthesized high affinity antibodies or antibody fragments, and thus allowing for an enhanced anti-tumour response, mostly carried out by activated T cells, making use of the complex regulatory mechanisms of the immune system (Cancer Research UK 2022, Khan, Maker et al. 2021). As of the writing of this review, there are a total of sixteen different immune checkpoint molecules recognised by the United States Food and Drug Authority (FDA) as feasible avenues in the treatment of several cancers (Luke 2023). However, only two of them, PD-1 and CTLA-4, currently have ICIs commercially available for use in a clinical setting, although much research is continuously being carried out on several of the other ICIs due to the promising nature of this anti-cancer therapy (De Sousa Linhares, Leitner et al. 2018) Thus, the main aim of this research project is the examination of three ICIs in particular, Cluster of Differentiation 47 (CD47), T cell Immunoglobulin and immunoreceptor tyrosine-based inhibitory motif (ITIM) domain (TIGIT), and Glucocorticoid-Induced TNFR-

Related protein (GITR), in an effort to determine their feasibility as highly specific, antibody based anti-cancer agents, and therefore add to the breadth of knowledge available on this subject with the aim of furthering practical developments in this field (Sherbet 2017).

1.3 Immune Checkpoints

The use of ICIs as anti-cancer agents, while not the most recently discovered strategy in the case of immunotherapy-based cancer treatments, was and still is considered one of the most ground-breaking breakthroughs in the development of specific, low-toxicity cancer treatments in recent times (Khan, Maker et al. 2021).

Immune checkpoint molecules are a group of membrane bound proteins, usually expressed as ligand-receptor pairs, found on various cells of both the innate and the adaptive immune system. Their leading role is in the regulation of immune responses through various inhibitory or stimulatory effects on different immune cells. However, when these processes become hijacked by malignant cells, these checkpoint molecules have not only been found to prevent tumour elimination, but also to enhance tumour development by improving properties such as self-renewal, metastasis, drug resistance, and more (Zhang, Zheng 2020).

Of the several different checkpoints available as possible targets of inhibition in cancer treatment, ICIs for only two of them are commercially available and used on a semi-widespread basis. These are CTLA-4, and PD-1/PD-L1, which are often used in combination with each other for improved effects due to their complementary modes of action. These are both normally expressed on activated T cells and are negative regulators of T cell function during an immune response. CTLA-4 is believed to regulate T cell proliferation in the early immune response, primarily in lymph nodes, whereas PD-1 suppresses T cells at a later stage

of the immune response, and primarily in peripheral tissues. Therefore, anti-CTLA-4 and anti-PD-1 inhibitors have been found, both as monotherapies and in conjunction with each other, to cause significantly increased anti-tumour activity against several distinct types of cancers, such as non-small lung carcinoma, renal carcinoma, and melanoma, among others (Buchbinder, Desai 2016, Rotte 2019).

However, there are several drawbacks that have been observed to continuously occur with the prolonged use of these ICIs. The first is the possible development of inflammatory adverse effects, known as immune-related adverse events (IRAEs), due to the improved action of activated T cells, and often present with similar symptoms to autoimmune disease. Some of the most common IRAEs found to occur in association with the use of these specific inhibitors include the development of hypophysitis, primary thyroid dysfunction, and type 1 diabetes mellitus, among others. In cancer patients which already present with these diseases, the use of these ICIs is usually not recommended (Byun, Wolchok et al. 2017, Haanen, Ernstoff et al. 2020).

A review by Albandar et al. (2021) investigating the incidence rates of IRAEs in patients treated with ICIs for CTLA-4 and PD-1/PD-L1 concluded that the different ICIs presented different rates of toxicity, with CTLA-4 showing much higher rates of both incidence and severity of developed IRAEs. Furthermore, it was found that severity was the worst in cases where both ICIs were utilised as a joint therapy. However, it should be noted that IRAE related deaths for both monotherapies as well as the combination therapy remained at less than 1% of all the patients tested. Furthermore, the overall response rate (ORR) of the patients treated with these therapies seemed to correlate with that of the incidence of IRAEs, with combination therapies showing the best response, followed by CTLA-4 monotherapy, with PD-1/PD-L1

showing comparatively worse ORR (El Osta, Hu et al. 2017). This is further corroborated by another study which posited the emergence of IRAEs to be a biomarker of ICI effectiveness upon onset of treatment, although in this study, PD-1/PD-L1 was credited with a stronger IRAE onset (Das, Johnson 2019). Furthermore, it has been definitively quoted that patients who had developed IRAEs had a much higher cancer survival rate to those who had not, further showing the level of interconnection which currently exists between the effectiveness of currently available ICIs and IRAE development (Albandar, Fuqua et al. 2021).

Another drawback often associated with these ICIs is the eventual development of tolerance by the tumour over time. While an increased anti-tumour response may be seen initially with the treatment, as previously stated, there are multiple different immune checkpoints which may be expressed or hijacked by the malignant cells. Therefore, a prolonged treatment with anti-PD-1 and anti-CTLA-4 has often been linked to a clonal evolution of the malignant cells, and subsequently a downregulation of PD-1 or CTLA-4 and an upregulation of other immune checkpoint molecules, thus decreasing the effectiveness of these drugs (Andrews, Wargo 2017, Riaz, Havel et al. 2017). The main way in which this is currently combatted is through the combination of ICI treatment with other anti-cancer therapies, such as chemotherapy, radiotherapy, surgery and other non-ICI immunotherapy treatments. While these strategies have been seen to improve the effectiveness of therapy with the currently available ICIs, both in cases of adaptive immunity, as well as in patients who showed an innate resistance to the ICIs, these issues were never completely eliminated. Furthermore, regardless of the strives taken, there still remains a pressing need for new ICI options and combinations in the case of certain cancers, such as pancreatic and prostate cancer, which are known for very low response rates with the currently available ICIs (Sharma, Goswami et al. 2023). Therefore, it is currently vitally important to synthesise novel ICIs targeting other immune checkpoints

expressed in the tumour microenvironment in order to improve the effectiveness of this immunotherapy strategy in anti-cancer treatment.

1.3.1 CD47

The first checkpoint which will receive focus in this review is CD47, originally named Integrin-Associated protein (IAP). CD47 is an integral membrane spanning glycoprotein receptor that is part of the immunoglobulin superfamily, and is widely expressed on all human tissue cells, including red blood cells (Fenalti, Villanueva et al. 2021). It is characterised with an extracellular N-terminal IgV domain, five transmembrane domains, and a short C-terminal cytoplasmic tail (Eladl, Tremblay-Lemay et al. 2020). Its main function is the inhibition of phagocytosis of self-cells through its preferential binding to its ligands, Signal Regulatory Proteins (SIRP) and most notably Signal Regulatory Protein alpha (SIRPα), exhibited on the surfaces of most phagocytes, such as macrophages and dendritic cells (Yang et al. 2023). Upon the binding of CD47 to SIRPα, a phosphorylation of the intracellular ITIMs of SIRPα is triggered, activating a pathway that eventually leads to the deactivation of Myosin IIA, an important component of the cytoskeleton responsible for cell motility, and thus inhibiting phagocytosis. In this way, CD47 acts as a “Don’t Eat Me” signal on healthy cells and is an important marker for self-tolerance (Jia et al. 2021).

Furthermore, this checkpoint has also been found to display an inhibitory effect on T cell action through the CD47-thrombospondin-signaling pathway, posited to come about due to the activation of Hydrogen sulphide (H_2S) signalling, although the exact mode of action remains unknown (Miller et al. 2013, Nath et al. 2022). Further functions of CD47 and its various ligands include the regulation and mediation of mitochondrial biogenesis, cell

adhesion, motility, and stem cell self-renewal, among others (Cham et al. 2020, Soto-Pantoja et al. 2015).

However, this immune checkpoint has often been observed to be overexpressed on the surfaces of malignant cells in the case of several haematological cancers, as well as some solid tumours, thus inhibiting both phagocytosis and T cell action, and promoting malignant cell replication, and tumour growth and metastasis, often leading to a poor prognosis for the patient (Eladl, Tremblay-Lemay et al. 2020). In many pre-clinical trials, antibodies against both CD47 and SIRPα have been seen to exhibit significant anti-tumour activity in several different tumour types (Veillette, Chen, 2018).

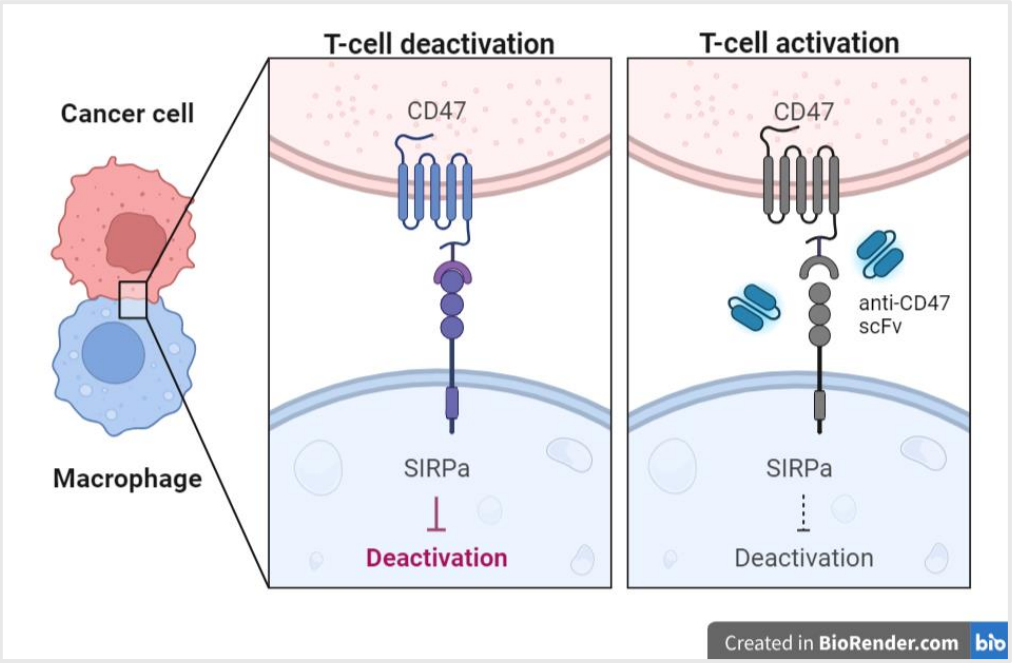

Figure 1.2: A figure summarising T cell deactivation via the interaction between CD47 and SIRPα, as well as the effects of CD47 blockade through the use of anti-CD47 scFv*. This image was produced using the online software BioRender.*

In a study by Eladl, Tremblay-Lemay, et al. (2020) investigating the effects of several different ICIs targeting CD47 overexpressed in many of the most common haematological malignancies, it was found that in many cases the use of anti-CD47 monoclonal antibodies

such as Hu5F9-G4, CC-90002, SRF231, and others led to a significant increase in anti-cancer activity by macrophages, and a general improvement in prognosis, though the efficacy and potency of the therapeutic effects were seen to vary between cases. Some issues which emerged during the course of the investigation however, include a general lack of specificity, leading to the development of IRAEs, the most common of which being anaemia, although in many cases, these treatment-related adverse events remained at grade 1 or 2. Furthermore, similarly to PD-1 and CTLA-4, the development of a resistance to the anti-CD47 agents was often observed over time in the patients, mostly due to tumour heterogeneity, often leading to a diminishing response after about three to four months.

In a similar study by Weiskopf, Jahchan et al. (2016), investigating the action of anti-CD47 antibody Hu5F9-G4, in conjunction with other inhibitory molecules in small cell carcinoma of the lungs, it was found that the disruption of the CD47-SIRPα pathway on the surface of tumour cells with the use of anti-CD47 antibodies almost invariably increased macrophage-mediated tumour phagocytosis in the small cell lung carcinoma cells in culture, as well as in animal models. This was largely credited to be due to the high levels of expression of CD47 found on the surface of most small cell carcinoma cells. Furthermore, this effect was found to be increased further when used in conjunction with inhibitors to other regulatory molecules overexpressed on the surface of these malignant cells, such as anti-CD56, CD24, and CD99. The actions of both the variable fragment heavy chain (VH) and light chain (VL) domains of the antibody in question were investigated, and both were found to have inhibitory effects on the CD47 molecule, especially when complexed, forming a structure bearing a large similarity to SIRPα in complex with CD47, thus explaining the antagonistic abilities of Hu5F9-G4 antibody.

These, along with other similar studies, investigating the effects of different CD47 antagonist antibodies in the case of in malignancies where CD47 was found to be overexpressed, nearly all showed a positive effect in the increase of tumour phagocytosis and the decrease of tumour growth and metastasis. This therefore makes it an incredibly attractive prospect in the development of new immunotherapy strategies and thus the creation of more personalised treatment plans for several different cancers. Clinical trials for several different CD47 antagonists have already been approved in several countries as of 2019, with the best results as of now being observed with the use of anti-CD47 monoclonal antibodies such as CC-90002 and Hu5F9-G4, while the safest inhibitors were largely found to be CD47-targeted bispecific antibodies (bsAb), and the SIRPα/Fc fusion protein antibodies, which were able to bind to the tumour antigens more preferentially and thus decrease the presentation of IRAEs (Jiang, Sun et al. 2021, Yang, Xun et al. 2023).

Further studies into the use of bispecific therapies, targeting CD47 together with a second marker expressed on the surface of some cancer cells have also been carried out and found to have largely positive effects, displaying similar anti-cancer effects as monoclonal anti-CD47 antibodies, with an increased specificity towards the malignant cells. One specific example is a bispecific antibody targeting both CD47 as well as the marker CD20, which is normally expressed on B-lymphocytes, and can act as a tumour marker for several lymphomas (Yang, Yang et al. 2021). Bispecific antibodies such as the one described, are often produced in the form of scFv-based bsAbs, in large part due to their smaller size when compared to monoclonal antibodies, allowing for optimum recognition and thus improved effects (Ahamadi-Fesharaki, Fateh et al. 2019).

Research has also been carried out on the development of scFv antibodies solely against CD47, and in 2017, Rezaei, Habibi-Anbouhi et al. discovered their positive effects in the treatment of human bladder cancer when conjugated with magnetic nanoparticles (MNPs), allowing for precise targeting of the specific malignant cells when used in conjunction with thermotherapy. This study, and others like it therefore highlight the great deal of versatility in this area of research, as well as the potential for the development of completely novel techniques in cancer detection and treatment that this may lead to in the near future.

1.3.2 TIGIT

The immune checkpoint known as TIGIT, is an immunosuppressive receptor expressed on the surfaces of various activated T cells, including $CD8^+$ T cells, $CD4^+$ T cells, Regulatory T cells (Treg), and Natural Killer (NK) cells. It is composed mainly of a single extracellular Immunoglobulin (Ig) variable domain, as well as an intracellular domain containing an Ig tyrosine tail (ITT) domain as well as an ITIM domain (Jeong, Nam et al. 2022).

The main ligands to which TIGIT binds are primarily Poliovirus receptor (PVR), also known as CD155, and Nectin-2, also known as CD112, among other members of the Nectin superfamily. These receptors may both be found on the surfaces of Antigen Presenting cells (APC), and once complexed with TIGIT, play a significant role in cell adhesion and the deactivation of a T cell response, mainly of the NK cells, and thus preventing apoptosis (Stengel, Harden-Bowles et al. 2012). These ligands have also been found to be shared with other immune receptor molecules, such as CD226, also known as DNAX accessory molecule 1 (DNAM-1) and CD96, or T cell activation increased late expression (TACTILE), both of which have very similar effects on NK cells to TIGIT, and thus may act as co-inhibitors (Chauvin, Zarour 2020, Ge, Peppelenbosch et al. 2021).

However, in the cases of certain solid tumours, both PVR and Nectin-2, among other members of the nectin superfamily, have been found to be overexpressed on the surface of malignant cells, and upon binding to TIGIT carrying T cells infiltrating the TME, an inhibition of T cell activation and NK cell action is observed. This, therefore, leads to the protection of the tumour cells from apoptosis. In many cancer types, the presence of TIGIT has often been found to be upregulated as well, with elevated levels of TIGIT expression often being indicative of a poor prognosis, as well as in some cases being positively correlated with late stage cancer and T cell exhaustion (Wen, Mao et al. 2021). Therefore, this makes TIGIT a very promising potential target for inhibition in the treatment of cancers, either as a monotherapy, or in conjunction with other ICIs (Annese, Tamma et al. 2022, Dougall, Kurtulus et al. 2017).

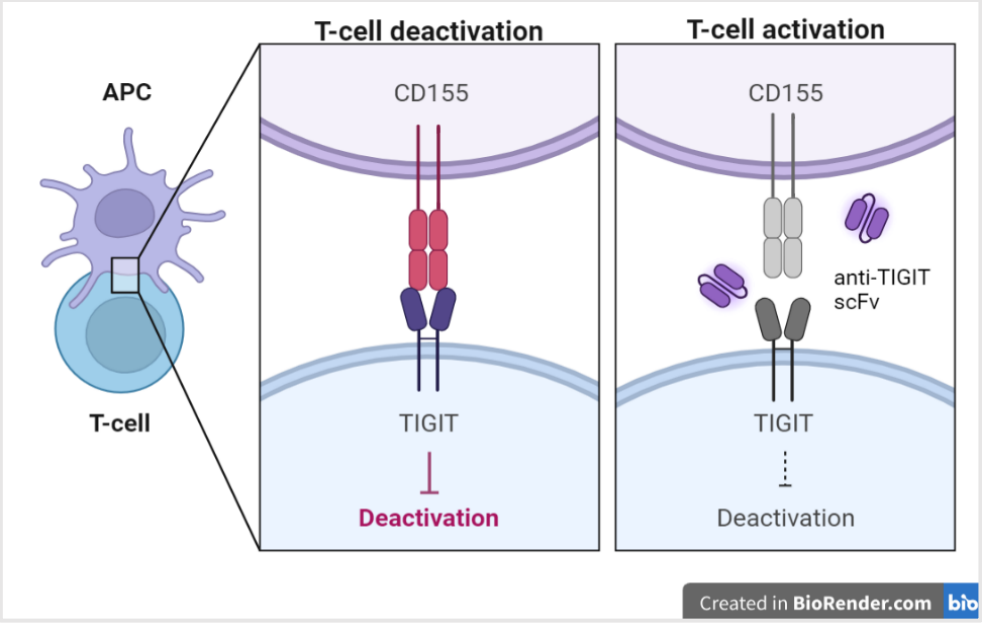

***Figure 1.3**: **A figure summarising T cell deactivation via the interaction between TIGIT and one of its ligands, CD155, as well as the effects of TIGIT blockade through the use of anti-TIGIT scFv.** This image was produced using the online software BioRender.*

The use of TIGIT as an immunotherapy target in the treatment of solid tumours has shown positive results in both pre-clinical and clinical trials as of the writing of this review, both as a

monotherapy and in combination therapies (Blake, Dougall et al. 2016, Chauvin, Zarour 2020). Moreover, quite a few groups have already discovered the successes of using a combined TIGIT and PD-1/PD-L1 strategy in improving the efficacy of the ICI therapy. Ge, Peppelenbosch et al. (2021), investigated this particular relationship in detail, and discovered that in patients who presented with cancers resistant to anti-PD-1, the inhibition of TIGIT lead to a greatly enhanced anti-cancer effect in most trials. This was discovered to be due in large part to the coordinate expression of both TIGIT and PD-1 on $CD8^+$ T cells, as both tend to be simultaneously upregulated in exhausted $CD8^+$ cells. This also potentially makes them useful markers in gauging T cell exhaustion and dysfunction in late stage cancer. In mouse studies, it was also noticed that while anti-PD-1 treatment alone only resulted in partial tumour regression, often followed by tumour escape, a combination of anti-PD-1 and anti-TIGIT treatment regularly led to full regression in most subjects (Ge, Peppelenbosch et al. 2021).

Other studies found similar success in the use of anti-TIGIT treatment against haematological malignancies, decreasing cancer replication rate, and aiding in the prevention of T cell exhaustion, as well reduction in the number of Tregs produced. Similarly, the synergistic use of anti-TIGIT and anti-PD-1 mAbs in Acute Myeloid Leukaemia (AML) patients provided an enhanced efficacy in treatment and remission (Wang, Bu et al. 2018)

Synergistic effects were also noted with other potential ICIs, such as Lymphocyte-activation gene 3 (LAG-3), which is also an immune receptor found on activated $CD4^+$ and $CD8^+$ T cells and NK cells and often found to be upregulated in the TME. Similarly to TIGIT and PD-1, it also acts as a negative regulator of T cell action and expansion and is partly responsible for the promotion of Treg expansion. It is therefore, also considered a marker for T cell exhaustion,

and thus shows similar potential to its synergistic inhibition with both TIGIT and PD-1 (Anderson, Joller et al. 2016, Joller, Kuchroo 2017).

While there have been some initial concerns regarding TIGIT toxicity with prolonged use, it is widely agreed upon that the most commonly observed IRAEs that tend to present rarely exceed grade 1 or 2 of severity, with some of the most frequent including development of diarrhoea, a pruritic rash, or mild anaemia (Frentzas, Meniawy et al. 2021). Rarely are the adverse effects deemed harmful enough to stop treatment, and as of the writing of this review, there has not been a single IRAE related death as a result of anti-TIGIT treatment in any of the clinical trials that have been carried out up to this point (Niu, Maurice-Dror et al. 2022). In a randomized placebo study to further validate the safety of anti-TIGIT antibodies, it was concluded that the occurrence of IRAEs between both the drug and the placebo were comparable, although it should be noted that the sponsor of this particular study was listed as a known manufacturer of tiragolumab, an anti-TIGIT antibody based drug (Rodriguez-Abreu, Johnson et al. 2020). Nevertheless, anti-TIGIT antibodies are currently widely regarded as relatively well-tolerated by the majority of patients, although it is advisable to perform further studies on this topic.

Hence, due to the potential of anti-TIGIT technology, there are several companies currently in the process of pre-clinically and clinically testing several different anti-TIGIT agents. The vast majority are IgG based mAbs, and most of them are humanised. Due to the synergistic effects of combined anti-TIGIT/PD-1 therapies, bispecific antibodies targeting both receptors simultaneously are also of interest by several parties. (Rotte, Sahasranaman et al. 2021) The use of scFv anti-TIGIT antibodies has also been under investigation, and the efficacy of using scFv-TIGIT loaded oncolytic viruses on solid tumours has been studied and deemed to have

shown successful anti-tumour effects, with best effects noted when used synergistically with other scFv ICI, such as anti-PD-1, or anti-LAG-3 (Lin, Ren et al. 2020, Zuo, Wei et al. 2021).

Overall, TIGIT is a highly promising immune checkpoint target, with multiple positive trials, and several types of antibodies and antibody-based drugs under investigation. Therefore, the more knowledge available on novel anti-TIGIT agents would invariably be useful in the driving of this therapy.

1.3.3 GITR

The final immune checkpoint of interest for this review is GITR, a Type I transmembrane protein belonging to the Tumour Necrosis Factor (TNF) receptor superfamily of proteins. Similarly to TIGIT, it is largely expressed on the surface of various T cells and NK cells and is involved in the stimulation of both the innate and acquired immune systems (Nocentini & Riccardi 2009). This checkpoint mainly interacts with its one natural ligand, (GITRL), a Type II transmembrane receptor also part of the TNF receptor superfamily (TNFRSF), which is expressed on various APCs, such as macrophages, B cells and dendritic cells (Zhou, Tone et al. 2008).

Upon activation of $CD4^+$ and $CD8^+$ T cells through the stimulation of T cell receptor (TCR), GITR expression is upregulated, and then activated through binding to GITRL. Upon activation, GITR commences a co-stimulatory effect on the immune system, promoting T cell proliferation and activation, as well as inhibition of the action of Tregs (Chattopadhyay, Ramagopal et al. 2007). This is widely posited to be accomplished through the upregulation of CD25, as well as the induction of Interleukin-2 (IL-2) and Interferon gamma (IFNγ) expression. GITR signalling is in large part mediated through the activation of Nuclear Factor kappa-light-chain-enhancer of activated B cells (NFκB), as well as members of the Mitogen-activated protein kinase (MAPK)

pathway, such as Extracellular signal-regulated kinase 1/2 (ERK), p38, and c-Jun N-terminal kinase (JNK) (Knee, Hewes et al. 2016).

This mode of action is diametrically opposed to the actions of the previously described immune checkpoints, as the main function of this protein is the stimulation and enhancement of an immune response by activated T cells, rather than an inhibition of their functions. Therefore, when investigating the potential of this protein as a therapeutic target in the treatment of cancers, it is with the express goal of stimulating its effective actions and thus facilitating a greater anti-tumour effect (Wang, Chau et al. 2021).

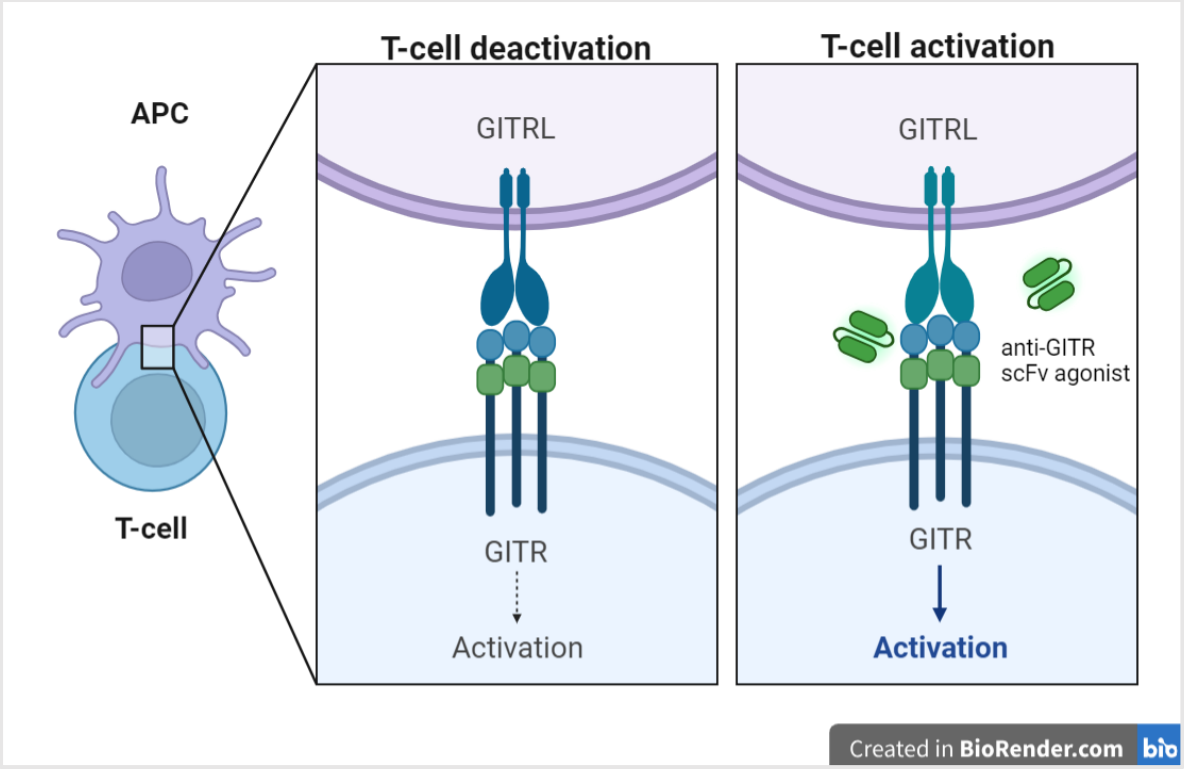

***Figure 1.4**: **A figure summarising T cell activation via the interaction between GITR and its ligand GITRL, as well as the effects of anti-GITR agonist scFv in the stimulation of T cell action.** This image was produced using the online software BioRender.*

GITR modulation using anti-GITR mAbs has been postulated as a potential immunotherapeutic avenue in the treatment of cancers for several years now (Coe, Begom

et al. 2010). There has been much research into the development and use of antibody based agonists for several members of the TNFRSF, with GITR being one of the most attractive targets, although other receptors have also been put into consideration, such as 4-1BB, OX40, and CD27 (Buzzatti, Dellepiane et al. 2019).

Anti-tumour effects from GITR modulation arise through the reduction and inhibition of Tregs, and the stimulation of $CD8^+$, $CD4^+$, and NK cells, as well as an increase in the level of resistance of effector T cells to Treg action, thus prolonging the immune response. While not normally expressed on the tumour cells themselves, GITR has often been found expressed on the surface of tumour-infiltrating lymphocytes (TILs) in the TME of several types of solid cancers, such as melanomas, renal cell carcinomas, and lung carcinomas, among others (Nocentini, Ronchetti et al. 2012, Wang, Chau et al. 2021).

Several *in vitro* and *in vivo* studies on the use of GITR agonist Abs have been performed and found to show a significant anti-tumour effect. The most commonly used anti-GITR agonist Ab is undoubtedly DTA-1, a rat monoclonal IgG based antibody generated through the immunisation of rats with a $CD4^+/CD25^+$ mouse T cell line, although other Abs are also available. Another anti-GITR agonist of interest would be anti-GITR mAb G3c, another murine antibody which showed even better stimulatory effects than DTA-1 *in vitro*, although *in vivo* studies showed a higher level of stimulation of Tregs over $CD4^+$ cells, thus displaying reduced effects, revealing that different agonist antibodies may have differing effects (Nocentini, Ronchetti et al. 2012). Another emerging anti-GITR agonist antibody is TRX518, described by Zappasodi, Sirard et al. (2019) to exhibit quite positive anti-tumour activity in phase 1 human clinical trials, showing its potential as a monotherapy, while also suggesting its use in combination therapies with existing ICIs for compounded results.

Strives have been made into the development of combination therapies between GITR agonist Abs, and Abs against other targets. A study by Avogadri, Yuan et al. (2010), posited the use of a combined anti-GITR DTA-1 antibody and anti-CTLA-4 therapy, finding that a combined therapy of CTLA-4 blockage and GITR stimulation led to enhanced anti-tumour effects in mouse models over monotherapies of the two types of antibodies, owing to their largely complementary effects, leading to a longer anti-tumour immune response. Research has also been carried out into combined GITR/PD-1 targeting, found to have positive effects in the reinvigoration of exhausted $CD8^+$ cells in murine models, as well as a greater rate of remission of established tumours over the monotherapies of each, which rarely lead to full remission (Wang, Zhang et al. 2018).

The use of anti-GITR agonist scFv as an alternative to DTA-1 and other mAbs has also been investigated. In mouse studies carried out by Fellermeier, Beha et al. (2016), the use of generated scFv against several members of the TNFRSF were investigated, including GITR, as well as 4-1BB and OX40. The actions of the scFv were investigated both on their own, and when combined with a suitable ligand for the receptor of choice, creating tumour-directed Ab fusion proteins, providing an increased serum stability and bioavailability. This synthesis of bifunctional fusion scFv proteins for the induction of an immune response against tumour cells is an interesting approach for anti-GITR scFv, as well as that of other markers (El-Mesery, Trebing et al. 2013).

1.4 Phage Display

The main method through which specific scFv antibodies will be produced during the course of this study is known as phage display biopanning. Phage display is a complex biological

technique making use of modified bacteriophage viruses for the production of several types of proteins or peptides of any origin, both for research purposes as well as for pharmaceutical development (Fermin, Rampersad et al. 2018, Pansri, Jaruseranee et al. 2009). With the manner in which phage libraries are constructed, made up of fusion phages displaying both the peptide of interest and the DNA sequence coding for it, this links both the phenotype and genotype of these peptides, making this technique extremely useful for research purposes, although it has several other applications (Wu, Liu et al. 2016).

As a methodology, it was first developed by biologist George P. Smith, in 1985, wherein the peptides of interest were displayed on the surface of filamentous M13 class phages through the insertion of foreign DNA fragments coding for the peptide into the gene coding for surface protein pIII of the filamentous phage, thus creating a fusion protein expressed on the surface of these phages. Since its inception, this method has gone on to be utilised for numerous purposes without much variation, thus showing its versatility in various areas of research.

The first step to any research utilising the phage display method is the construction of a suitable library of phages. In order to construct a phage library with a vast repertoire, such as antibody phage libraries displaying rearranged V-gene repertoires, or scFv with different specificities, a method utilising Ribonucleic acid (RNA) extracted from B cells is used. In this method, naïve or immunised B cells are obtained either from a human source, or an animal source, as is the case for this study which makes use of a canine phage library. The extracted RNA is first converted into complementary DNA (cDNA) through reverse transcription, after which, both the VL and VH sequences of any antibodies coded for by those cells may be amplified and ligated into the phagemid, thus creating a library of great diversity (Bashir & Paeshuyse 2020).

Depending on the original B cells used, a phage library may either be naïve or immunised. Naïve libraries made use of B cells originating from healthy individuals and thus tend to generate highly diverse libraries. On the other hand, immunised libraries are those constructed from B cells originating from individuals carrying a particular disease, often leading to phage libraries with higher affinities towards the antigens of interest, but with reduced diversity (Alfaleh, Alsaab et al. 2020). Further binding affinity and diversity may also be obtained through the lengthening of complementarity-determining region (CDR) loops, especially CDR3 of the VH residues, improving the functionality and binding affinity of the synthesised scFv (Ledsgaard, Ljungars et al. 2022).

Today, there are several phage libraries commercially available, such as the one obtained from the University of Edinburgh for the purposes of this study, thus greatly saving on time and labour. Once an appropriate phage library has been identified and obtained, the phages carrying the scFv of interest may then be purified, and amplified at will, using the normal mechanisms of the phages. This method has since grown to be one of the most important methods for protein and antibody synthesis, especially in the case of pharmaceutical development (Jaroszewicz, Morcinek-Orłowska et al. 2022).

Once the library has been obtained, the main steps involved in phage display are fairly simple and may be broken down into four main phases: binding to immobilised target, several washing steps, elution, and finally amplification and purification of the selected phages (CUSABIO 2023, Wu, Liu et al. 2016). This procedure may be seen summarised in **Figure 1.5**.

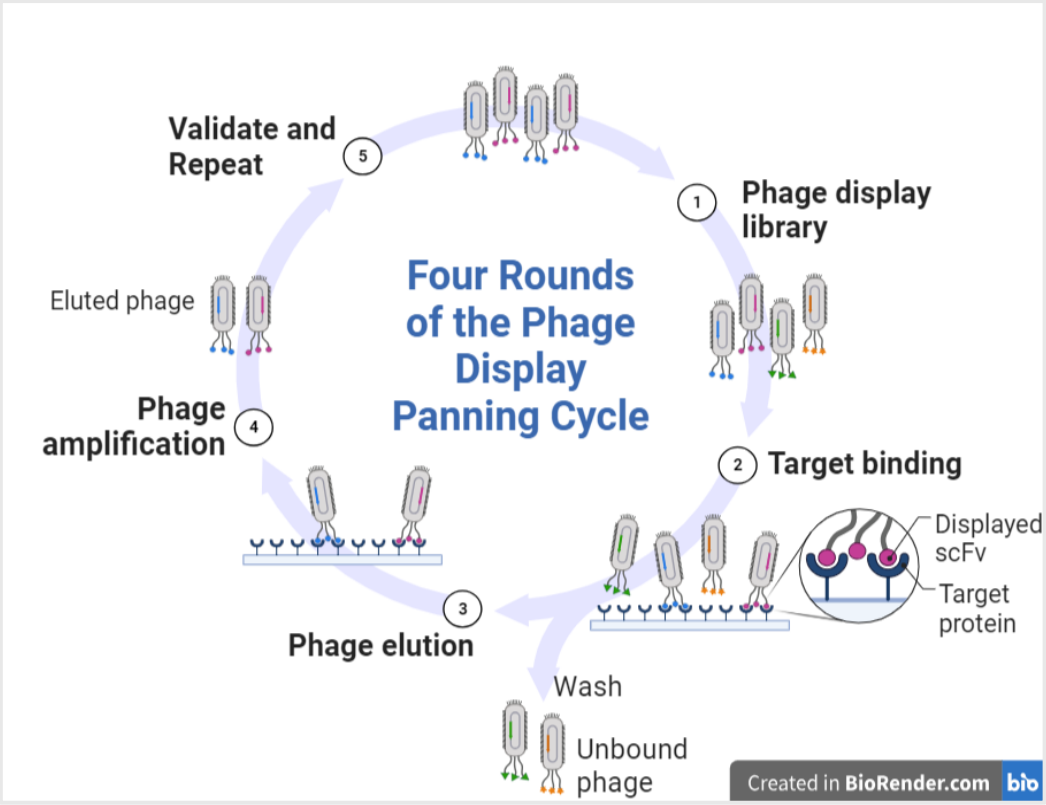

Figure 1.5: A figure summarising the main steps of the phage display cycle, beginning from the original phage library. *The first step, which is the binding of the selected target phages displaying the scFv of interest, is done usually with an antigen specific to the displayed target antibody, immobilised on either plates or beads. Any unbound phages which do not display the target antibody will in turn be washed away in the next step, after which the remaining target phages are recovered through elution. The final step is the amplification of the eluted phages, through the infection of host cells, such as Escherichia coli (E. coli) bacteria, which may be facilitated through the use of a helper phage such as M13KO7. These are then cultured, thus facilitating the replication of the target phage. The phages may then be extracted from the host bacterial cells, and the above steps may be repeated in order to purify and enrich the selected phage target. After a maximum of four rounds of this biopanning procedure, the end result is an enriched phage library, carrying only the peptide of interest. This image was produced using the online software BioRender.*

Throughout this biopanning and amplification process, mutations may occur in the peptide carrying phages, leading to the production of higher affinity clone mutants, with a better binding capacity to the proteins of interest. These rare clones may be isolated from the enriched library and further propagated through more biopanning rounds against captured target protein, although competition from clones with weaker affinities is often a confounding factor in this process (Kiguchi, Oyama et al. 2020). However, these higher affinity phage clones

may still be captured and identified, and the DNA sequences may be studied in order to identify the variations which have led to the improved effectiveness of the scFv of these phages.

Phage display as a methodology for the production of immunotherapeutic drugs is a commonly emerging use for this technique. Since its inception, it has been used as the underlying method to create eight of the twenty most popular pharmaceutical products on the market. While it may be utilised in the production of whole mAbs, more recently, attention has been drawn to the production of antibody fragments as an alternative, including antigen-binding fragments (Fab), fragment variable (Fv) which consist of either a VL or VH region only, scFv, and others. Of those listed scFvs are currently one of the more popular antibody fragments used, either unchanged, or modified as bivalent or bispecific antibodies. The main reason for the switch from whole antibodies to antibody fragments in this area largely lies with the fact that it has been found to be far easier for the viruses to hold and express these smaller peptide fragments over the entire mAb molecule (Alfaleh, Alsaab et al. 2020, Bazan, Całkosiński et al. 2012).

In fact, the use of the phage display technology in the production of Ab based fragments is deemed by many to be the reason for the recent breakthroughs in immunotherapy. Many of the failures of earlier immunotherapy techniques, making use of mouse derived mAbs, were largely due to the stimulation of a human anti-mouse antibody (HAMA) response against the mouse mAbs. This response may be mitigated or even outright prevented using phage display created antibodies and antibody fragments, either through the use of human derived scFvs directly, or through its use as a guided selection method to humanise animal mAbs using hybridoma technology (Nagano, Tsutsumi 2021).

The antibodies and antibody fragments produced may then in turn be utilised in various pharmaceutical applications, such as in the treatment of cancers, or even in infectious diseases. After the Coronavirus (COVID-19) pandemic, new importance was shed over the need for more effective treatments of infectious disease, and much research has recently been initiated into the use of phage display for the production of antibody-based treatments for severe acute respiratory syndrome coronavirus 2 (SARS-CoV-2) and its various mutants. Research into the applications of phage display derived antibodies for the treatment of long-running bacterial infections has also been investigated and found favourable results (Roth, Wenzel et al. 2021).

Further applications of this technology have been described by Dong, Meng et al. (2020), who produced a phage library of recombinant scFv, starting from a primary library created from human peripheral whole blood, and human umbilical cord blood in order to successfully identify and produce antibodies against proprotein convertase subtilisin/kexin type 9 (PCSK9), as a potential hypolipidemic therapy. These are only a few examples of the myriads of potential uses for antibody-based pharmaceuticals derived from phage display, other than for cancer treatment.

The use of phage display in the creation of antibodies to be used in anti-cancer therapy has also been investigated. Wang, Gao et al. (2019) described phage display as a relatively efficient and inexpensive method for the creation of anti-cancer antibodies. Anti-tumour scFvs from a phage display library have been described in multiple sources of literature, and for various types of cancers. Hall, Boroughs et al. (1998) described the creation of novel scFv cancer treatments for colon cancer derived from two human antibody phage display libraries

and Rezaei, Habibi-Anbouhi et al. (2017) described the successful utilisation of phage display in the creation of CD47 scFv conjugated MNPs in the treatment of bladder cancer.

Monoclonal antibodies against TIGIT have also been reportedly synthesised from phage display libraries, and shown to have been able to initiate a not-insignificantly increased NK response against solid tumour cells in several *in vivo* and *ex vivo* studies (Han, Xu et al. 2021). A report has also been made over the identification and synthesis of Affimer proteins specific to members of the TNFRSF such as GITR through phage display, as an alternative to Ig derived TNF agonists in the treatment of cancers (Basran 2019).

All of the mentioned examples simply go to show the sheer amount of versatility of the phage display method, in the development of antibody and peptide based pharmaceuticals for the treatment of several different diseases, including cancers. The advancements in medicine gained through the advent of phage display, either through the discovery of multiple novel potential immunotherapy targets, or through advancements in cancer screening technology, have caused this methodology to be deemed of great enough importance to be made the recipient of a Nobel Prize in Chemistry, in the year 2018 (Saw, Song 2019).

This all goes to show why this method was chosen for this study, as the main method to identify and synthesise scFv for the three immune checkpoint molecules of interest in this project.

1.5 The PADLOCK Project

From the literature examined up to this point, the advantages of immunotherapy as a cancer treatment have become clear, as has the importance of further improving upon it through

the discovery of new immunotherapeutic strategies. It has also been established that for the branch of immunotherapy making use of ICIs to stimulate immune responses against malignant cells and tumours, one of the most pressing limiting factors is the lack of checkpoint regulators targeting novel immune checkpoints that have been approved for widespread clinical use, either as monotherapies or as combination therapies.

The production methods for these new potential antibody-based checkpoint regulators have also been explored, with the phage display method showing to be a very valid, efficient, and relatively cost-effective emerging strategy for the production of human or humanised antibodies, or antibody fragments targeting specific immune regulating protein receptors in the tumour microenvironment.

There is therefore no surprise over the amount of research being carried out on these particular topics. This study, along with several others concurrently occurring, are all part of an ongoing initiative known as the Phage Display of Immune Checkpoints (PADLOCK) project, with the main aim of using phage display technology in order to identify, isolate and synthesise high affinity scFv against several immune checkpoint proteins that have been deemed as potential targets for regulation in order to stimulate enhanced anti-cancer effects.

Other than the three checkpoints which have already been explored in this review, CD47, TIGIT, and GITR, as part of project PADLOCK, research is also being carried out on several other checkpoint proteins, including PD-1, T cell immunoglobulin domain and mucin domain 3 (TIM-3), T cell immunoglobulin domain and mucin domain 4 (TIM-4), and V-domain Ig suppressor of T cell activation (VISTA), with yet more being considered for future projects as well (D Saliba 2023, pers. comm. 3 May).

With the amount of attention this topic has been drawing in recent years, and the great strides made in this field, it is more important than ever to offer contributions to this area of study, both by providing information on new targets, as well as assessing economical production methods. Therefore, it is with these reasons, among others, that projects such as this one are not only considered necessary, but should also be highly encouraged, both for their potential for kick-starting further research, as well as for the possible contributions to the pharmaceutical industry, and even the medical field as a whole, in the never-ending drive for improved cancer treatments.

1.6 Aims and Objectives

In summary, the main aim of this research study is the generation of scFv antibodies against the three mentioned immune markers CD47, TIGIT, and GITR. This was achieved through the following methods:

- Multiple rounds of phage display and biopanning, in order to isolate the scFv antibodies with the highest affinities to the three target proteins from a phage library;
- ELISA of the enriched libraries from the different biopanning rounds as well as of specific phage clones against both target and non-target proteins in order to test the specificity of the isolated scFv antibodies;
- Plasmid DNA extraction and sanger sequencing of individual phage clones, as well as comparison and alignment of the sequences of different clones in order to determine similarity in the structure of the scFv antibodies identified, and thus, to determine the level of diversity of the generated enriched library.

2. Materials and Methods

The following sections go into detail about the exact methodology that was used in this research project. A basic outline of the overall workflow carried can be seen in **Figure 2.1**.

Figure 2.1: A workflow diagram summarising the steps taken throughout the course of this research study with the aim of producing unique scFv specific to the targets of interest using phage display. *During phage display, four rounds of phage display biopanning were carried out for all three targets, calculating phage titres of the enriched libraries between rounds. Following that, affinity and specificity of the scFv isolated in each round was confirmed with ELISA. The enriched libraries were incubated against both target and non-target control protein. After the initial ELISA, the phage display protocol was adjusted and repeated for the targets with unsatisfactory levels of amplification. Individual phage clones were selected from the round showing highest level of amplification. The affinity of each individual clone was determined using another ELISA. Finally, plasmid extraction was performed on all clones for Sanger sequencing. The amino acid sequences of the clones were analysed and compared to determine the level of diversity of scFv within the enriched library. Each of the mentioned stages and all of the individual steps necessary to successfully carry them out are explained in detail within this chapter.*

2.1 Growth and Maintenance of *Escherichia coli* ER2738

One of the most important elements to this protocol was the growth and maintenance of the strain *Escherichia coli* ER2738, a male strain (F-pilus), which was provided for our use by the International Centre for Cancer Vaccine Science (ICCVS). This bacterial strain provided the main method through which the M13 bacteriophages of the phage library could be amplified during the biopanning process and was done in accordance with the recommendation of the New England BioLabs Phage Display Peptide Library instruction manual (*Ph.D. phage display peptide library instruction manual* 2020).

The M13 phages, being classified as male specific (F+) coliphages, could infect *E. coli* through the male strain of the F (fertility) pilus, present on the surface of most members of the Enterobacteriaceae family. This pilus is coded for by the F-factor of the coliform, also known as the F-plasmid, a type of conjugative circular DNA plasmid found in most members of Enterobacteriaceae, with the purpose of facilitating gene transfer and recombination between individual bacteria (Koraimann 2018). The F-factor of the ER2738 strain of *E. coli* in particular is capable of granting the bacterium resistance to the antibiotic tetracycline, allowing for it to be grown selectively on tetracycline containing media (*Method 1643: Male-specific (F+) and Somatic Coliphage in Secondary (No Disinfection) Wastewater by the Single Agar Layer (SAL) Procedure* 2018). Therefore, all of the cultures used in the amplification of M13 phages were grown on media containing tetracycline.

2.1.1 Preparation of Solid and Liquid Media

The media used to grow *E. coli* ER2738 mainly consisted of a Luria-Bertani (LB) agar [HiMedia Laboratories GmbH, Einhausen, Germany] dissolved in deionised water at a concentration of 35 g/L. The LB agar would then be autoclaved to ensure sterility at a temperature of 121^{o}C for 15 minutes immediately after preparation. After the autoclave step, often antibiotics would have been added to the prepared media once it had cooled to a minimum of 50^{o}C, in order to create selective media. The LB agar could then be poured evenly into petri dishes and allowed to cool completely and solidify, after which the completed LB agar plates were stored at 2-8^{o}C until needed.

During some steps of the biopanning procedure, a liquid LB broth [HiMedia Laboratories GmbH, Einhausen, Germany] would have also been used, such as during the preparation of overnight mid-log phase cultures. This was prepared at a concentration of 25 g/L in deionised

water. Similarly, the sterile LB broth was also autoclaved at 121^{o}C for 15 minutes, cooled, and then stored in a fridge at 2-8^{o}C. All of the described media preparation processes were carried out within Class II Laminar Flow Cabinets [Faster S.R.L., Ferrara, Italy] in order to maintain sterility of the media.

Several different antibiotics were used at different points in this study. For the preparation of the primary streak plate of ER2738, tetracycline was used at a working concentration of 10 µg/mL. Tetracycline stock was prepared in advance, at a concentration of 10 mg/mL through the addition of tetracycline hydrochloride [Gibco, New York, United States, Catalogue No. A39246] to a 70% ethanol solution. On the other hand, for the preparation of media used in titrations of the phage library rounds, ampicillin LB agar plates were produced instead, although this would later be replaced by carbenicillin. Both ampicillin and carbenicillin are semi-synthetic antibiotics belonging to the β-lactam class, with structures similar enough to each other that resistance to one often led to resistance to the other antibiotic (*A Guide for Choosing Between Commonly Used Antibiotics* 2025). However, carbenicillin was found to have better stability at high temperatures and acidic environments as opposed to ampicillin and has been suggested to contribute to a reduction in growth of satellite colonies during longer incubations, due to its ability to better withstand breakdown by β-lactamases (*Can carbenicillin be substituted for ampicillin when selecting for the pGEM Vectors* 2025).

Ampicillin and carbenicillin were both prepared at a stock concentration of 100 mg/mL through the dilution of ampicillin sodium salt [Gibco, New York, United States, Catalogue No. 11593027] or carbenicillin disodium salt [Gibco, New York, United States, Catalogue No. 10177012] respectively in deionised water. Both were used at a working concentration of 100 µg/mL.

All prepared stock of antibiotics were filter sterilised to ensure sterility and then aliquoted into sterile microcentrifuge tubes while inside a Class II Laminar Flow cabinet. These were then stored at a temperature of -20°C in order to improve long term stability, as well as to avoid multiple freeze-thaw cycles.

2.1.2 Primary Streak Plate

Glycerol stocks of the *E. coli* ER2738 were first prepared by inoculating tetracycline LB broth with the bacteria in a conical bottom falcon tube, while inside the Class II Laminar flow cabinet. This was then incubated at 37^{o}C with agitation at 250 revolutions per minute (rpm) in an Eppendorf New Brunswick™ Innova 42 Incubator Shaker [Eppendorf, Massachusetts, United States] for a minimum of 16 hours. A 50% glycerol solution was also prepared through the mixture of equal parts 100% glycerol with deionised water which was then filter-sterilised. After the overnight incubation step, a volume of 500 µL of the overnight culture was mixed with 500 µL of the sterile 50% glycerol solution until completely homogenous. This final mixture was referred to as the glycerol stock culture and could then be stored frozen at a temperature of -80°C for months at a time until needed.

When preparing the primary streak plate, 10 µL of the ER2738 glycerol stock culture were used to form a pool on one side of a tetracycline LB agar plate. This pool was then spread using a 1µL sterile loop using the motions demonstrated in the diagram of **Figure 2.2**. During each step, it was ensured that a sterile side of the loop was used, either by turning it over or replacing it with a fresh loop.

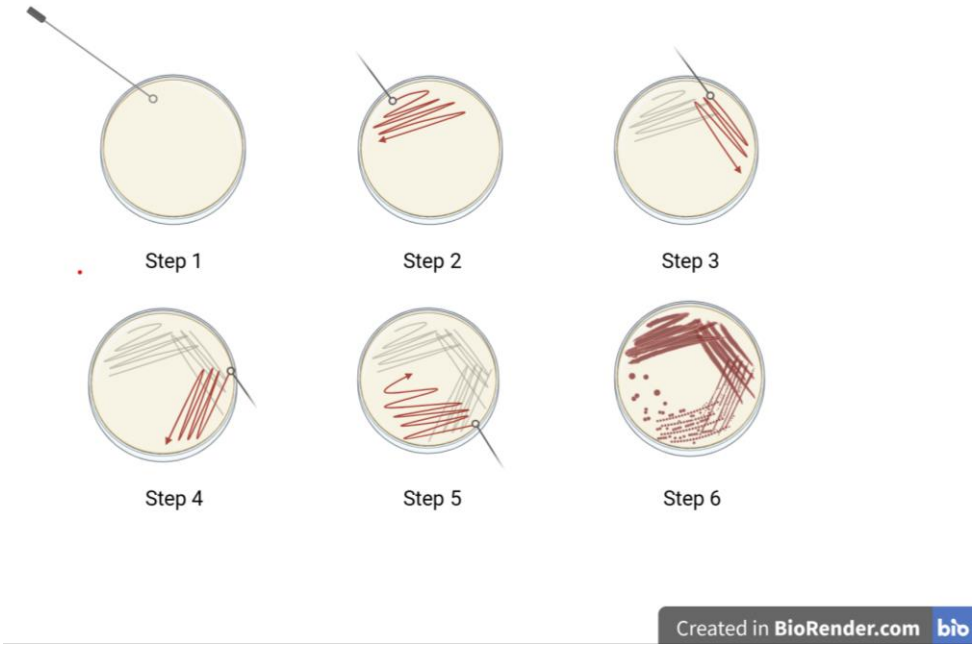

Figure 2.2: A figure summarising the streaking technique used to produce a primary streak plate with discrete colonies of tetracycline resistant E. coli ER2738. *The image was produced with the online software BioRender.*

After the inoculation, the plates were air-dried while in the Class II Laminar Flow cabinet, covered and then incubated upside down at 37^{o}C in a Binder BD53 Natural Convection incubator [BINDER GmbH, Tuttlingen, Germany] for 16 hours, after which the plates, now containing distinct colonies of tetracycline resistant ER2738 bacteria, were stored at 4^{o}C in the fridge for up to 2 weeks, after which a new primary streak plate would have to be made. A sterility plate was simultaneously incubated in order to ensure no contamination had occurred.

2.1.3 Preparation of Mid-Log phase *E. coli*

In order to facilitate the infection of the *E. coli* ER2738 by the M13 phages during biopanning, a liquid LB broth culture was prepared. As has been previously stated, this infection occurs through the binding of the phage to the F pili expressed on the surface of the bacterial cells. If this F pilus is lost or becomes blocked, infection of the bacteria by the phages can no longer

successfully occur (Malmborg, Söderlind et al. 1997). However, many studies into the structure and actions of *E. coli* during growth of the culture have suggested that the F-pilus is naturally lost from the cell over time after infection with M13 phages, either through resorption by the cell, or the breaking of the pilus into the medium (O'Callaghan, Bradley and Paranchych 1973, Jacobson 1972, Novotny and Fives-Taylor 1974). Therefore, in order to optimise infection rates with the M13 phages during biopanning and phage titering, it was made sure to use bacterial cultures in the mid-log phase of their growth.

This was done through the preparation of an LB broth containing 10 µg/mL of tetracycline in a sterile falcon tube, which was inoculated with a single colony of ER 2738 from the primary streak plate, while inside a Class II Laminar flow cabinet. This preparation was then incubated in an Eppendorf New Brunswick™ Innova 42 incubator shaker at 37°C and 220 rpm for 16 hours. If work could not be immediately done with this culture, it was stored in the fridge at 4°C for a few hours, until needed.

After this incubation, a new 10 µg/mL tetracycline LB broth was prepared at a volume of 25 mL, into which 250 µL of the overnight culture were then pipetted. This new culture was then also incubated in an Eppendorf New Brunswick™ Innova 42 incubator shaker at 37°C and 250 rpm for at least 1.5 hours. After this time, a small sub-sample of this culture was placed into a cuvette and measured using the Eppendorf BioPhotometer spectrophotometer [Eppendorf Corporate, Hamburg, Germany], after blanking with a cuvette containing sterile tetracycline LB broth. This was done in order to measure the level of growth of the ER2738 and the moment at which it had entered mid-log phase, which was determined to be when the OD600 was measured at 0.4 to 0.6. If on the first reading, the culture was seen to not have reached the required OD600 reading, it was returned back to the incubator for some minutes, and the

spectrophotometer reading was repeated again until mid-log phase was reached. This process was usually observed to take between 1.5 to 3 hours. Once the desired OD600 reading was observed, the mid-log phase culture was stored in the fridge at 4^{o}C until needed or for at most 3-4 days. Once the OD600 reading exceeded 0.6, this process would have to be repeated, and a new mid-log phase culture was prepared.

2.2 Phage Display and Biopanning

2.2.1 Reagent Preparation

Before any work was begun, it was made sure to have all necessary reagents prepared and ready to use in advance, in order to improve workflow. Many of the reagents necessary utilised Phosphate buffered saline (PBS) solution, in their preparations, which was a solution consisting of several salts, phosphates and deionised water, most commonly containing a mixture of sodium chloride, disodium hydrogen phosphate, and in some formulations, potassium chloride, among others. After preparation, this solution was autoclaved at 121^{o}C for 15 minutes. This solution was used in several steps of the protocol, but also in the preparation of several buffers utilised during biopanning as well as candidate phage clone preparation.

Firstly, was Binding buffer, composed of a mixture of PBS and 0.01% Tween-20, a non-ionic detergent often used in biochemical research for the creation of various stabilising, washing and blocking buffers. Similarly, a wash buffer was also prepared, using PBS and 0.05% Tween-20 for biopanning and 0.1% Tween-20 for ELISA and phage clone preparation. Finally, a Blocking buffer was prepared using PBS, 0.1% Tween-20 and 3% Bovine Serum Albumin (BSA), a monomeric protein produced from bovine blood plasma, which has many possible

applications in biochemical research, but in this case, was used to block non-specific binding between proteins (*Bovine Serum Albumin (BSA Protein),* 2025). Each of these buffers were filter sterilised after they had been produced and then stored in the fridge at 4^{o}C.

A 100mM Triethylamine (TEA) solution was also prepared in advance by adding 700 µL of the TEA to 50 mL of deionised water, ensuring that the pH of the final solution was around 11.3 using a pH meter. This was then stored covered in the fridge at 4^{o}C.

Finally, a mixture of 20% Polyethylene glycol (PEG 8000) and 2.5M sodium chloride (NaCl) was prepared by dissolving both completely in deionised water. This was done by heating the mixture to 50^{o}C on a hot plate, with constant stirring by a magnetic stirrer until fully dissolved. Once the PEG/NaCl mixture was homogenous, it was also autoclaved at 121^{o}C for 15 minutes without removing the magnet, as this solution had to be stirred once again after autoclaving in order to prevent the separation of the phases during cooling. This high concentration solution was used in the precipitation of phages during the final stages of biopanning through a volume exclusion reaction and attractive depletion model, by binding to the water molecules surrounding the phages, thus causing them to clump together (Carme Pons Royo and Jungbauer 2025). All plasticware used in this procedure was autoclaved beforehand and kept sterile until use.

2.2.2 Phage Display and Biopanning Rounds

As previously mentioned in **Section 1.4**, phage display is a molecular technique through which M13 phage genomes can be modified in order to hold the sequences of various proteins and peptides in a way which allows said proteins to be expressed upon the protein coat (capsid) of the phage (Fermin, Rampersad and Tennant 2018). For this specific application, a canine scFv phage library was obtained through collaborations with the University of Edinburgh, as

well as the ICCVS, University of Gdansk, with each individual phage displaying one specific type of scFv antibody. Research has shown a surprising amount of similarity in the tumour immune markers that are seen in humans and canines, thus leading to the production of scFv that should be able to target human proteins as well. The scFvs expressed were composed of both the VH and VL domains joined together by a short linker peptide sequence (Lisowska, Worrall et al. 2025).

As already stated, the targets for biopanning in this experiment were scFvs specific for the following proteins: Recombinant Human CD47 Protein (ECD, His Tag) [Sino Biological Inc., Beijing, China, Catalogue No. 12283-H08H], Recombinant Human TIGIT Protein (Dimer, ECD, His Tag) [Sino Biological Inc., Beijing, China, Catalogue No. 10917-H08H3], and Recombinant Human GITR/TNFRSF18/AITR Protein (ECD, His Tag) [Sino Biological Inc., Beijing, China, Catalogue No. 13643-H08H]. These proteins were reconstituted using sterile PBS to a working concentration of 100 µg/mL and then aliquoted and stored at -20^{o}C to avoid multiple freeze thaw cycles.

Four sterile low-retention microcentrifuge tubes were labelled with R (round) followed by a roman numeral denoting the round number (either i, ii, iii, or iv), as well as a number corresponding to a specific target protein as shown below:

- Tube Ri 1 – No protein control (NPC)
- Tube Ri 2 – CD47
- Tube Ri 3 – TIGIT
- Tube Ri 4 – GITR

In each tube, 10 µL of the respective reconstituted protein (100 µg/mL) were added along with 90 µL of binding buffer (PBS + 0.01% Tween-20) to create a total volume of 100 µL, with

the NPC tube only receiving 100 µL of binding buffer. This tube was used as the negative control for this procedure and would only isolate phages with non-specific binding.

The first true steps of this process involved the binding of the reconstituted target proteins to Dynabeads™ His-Tag Isolation and Pulldown [Invitrogen, Massachusetts, USA, Catalogue No. 10103D] magnetic beads. These beads were obtained at a concentration of 40 mg beads/ml in 20% ethanol and had a binding capacity of 40 µg of 28 kDa histidine tagged (His-Tag) protein per 25 µL beads (*Dynabeads™ His Tag Isolation & Pulldown package insert* 2025). Therefore, the exact volume of beads necessary per tube, while taking into account losses during washing steps was calculated using the following calculations:

- Dynabeads concentration= 40 mg/mL
- Binding capacity= 40 µg of protein/25 µL of beads
- 2.5 µg of protein requires 1.5625 µL of beads
- Prepared as: 2 µL of beads/tube
- Total volume for 4 tubes: 8 µL, rounded up to 10 µL to compensate for losses.

Before use, the 10 µL of beads were washed once using a Dynamag™-2 magnet [Invitrogen, Massachusetts, USA, Catalogue No. 12321D] in 500 µL binding buffer. This was then reconstituted in 110 µL of binding buffer to create a final volume of 120 µL. This was added at a volume of 20 µL to each of the pre-labelled tubes containing their respective proteins and then incubated on a rotator for a minimum of 30 minutes at room temperature to allow for the proteins to bind to the beads. These were then washed twice with 500 µL of washing buffer (PBS + 0.05% Tween-20) and then blocked with 150 µl of blocking buffer (3% BSA in PBS+0.1% Tween-20) for 1 hour at room temperature on a rotator. These steps were

performed in order to wash away excess protein, as well as prevent non-specific binding in the following steps. After this step, the blocking buffer was removed.

After the beads had been prepared and coated with protein, the next steps involved the addition of the scFv phage library. During Round 1 (Ri) the original scFv dog library (titre $5x10^{12}$ PFU/mL) was diluted in blocking buffer. In the first round, 2 µL of the library were added to 148 µL of blocking buffer, for a final volume of 150 µL of library for each tube. In all subsequent rounds, 5 µL of the enriched library produced from the previous round, were added to 145 µL of blocking buffer per tube. This volume was doubled if the enriched library of previous rounds had been stored in 50% glycerol, thus 10 µL of library would be used with 140 µL blocking buffer per tube. Therefore, to each tube of protein coated magnetic beads, 150 µL of diluted phage library were added, after which the tubes were once again incubated on a rotator at room temperature for a minimum of 1 hour, in order to allow phages expressing scFvs with a high affinity to the bound target proteins to also bind to the beads. After this step, the beads were thoroughly washed 10 times using 500 µL wash buffer to remove any unbound non-specific phages. The isolated phages were then eluted off of the beads using 150 µL of 100 mM TEA solution (pH 11.3) for 10 minutes at room temperature on a rotator. The eluates were then transferred to newly labelled sterile low-retention tubes containing 35 µL of 1 M TRIS solution (pH 6.8) in order to neutralise the high pH from the previous step. The magnetic beads, remaining in the original tubes could now be discarded and the phage eluates were then stored at 4^{o}C until the following day. Each of the steps involving the pipetting of phages made use of filtered tips in order to avoid contamination of the pipettes.

Day 2 of this procedure involved the amplification and purification of the eluates obtained from the first day of biopanning. This made use of the mid-log phase *E. coli* ER2738 in LB/Tetracycline broth as described in **Section 2.1.3**. In freshly labelled tubes, 1 mL of the mid-log phase ER2738 culture were added along with 90 µL of the neutralised phage from the previous step. This was incubated at 37^{o}C for 15 minutes on a thermoblock. This was then diluted into 20 mL of LB broth containing 20 µL of ampicillin (working concentration 100 µg/mL) and allowed to incubate at 37^{o}C and at 250 rpm for 1.5 hours. This allowed for initial infection of the bacteria by the phages, as well as created ampicillin resistance within the phages. After this incubation, 20 µL of a M13KO7 helper phage (stock titre was 6.9x10^{11} PFU/ml) were added to each tube, incubated static for 10 minutes, and then at 37^{o}C and 250 rpm for another 1.5 hours. The addition of the helper phage was a crucial step to the procedure as it carried all necessary genes for infection, replication and assembly of the phages. This allowed any phagemids carrying the genes specific to certain scFvs to be able to properly bind with the proteins necessary for amplification, leading to an increase in viral production as well as facilitating production of plasmid-containing particles for DNA sequencing. They are also able to confer kanamycin resistance (*Working with Helper Phages* 2024).

After the incubation with the helper phage, a volume of 10 µL of kanamycin was added to each of the four tubes. Kanamycin stock was prepared at a concentration of 50 mg/mL, through the dissolution of kanamycin sulphate [Gibco, New York, United States, Catalogue No. 35 11593-027] in deionised water. After this, the tubes were incubated overnight at 30^{o}C and 250 rpm for a maximum of 16 hours.

During the third and final day of biopanning, the first step involves the centrifugation of the overnight samples at 4000 rpm for 10 minutes, in order to separate the bacteria from the phages in the supernatant. Without disturbing the pellet at the bottom of the tubes, as much of the supernatants as possible was transferred to fresh pre-labelled falcon tubes containing 3.5 mL of PEG/NaCl and incubated on ice for a minimum of 2 hours and often up to 4 hours. This is the main step in which the amplified phages from the previous step were precipitated out of the solution. This precipitation step was then followed by two consecutive centrifugation steps at 4000 rpm and 4^{o}C for 20 minutes each, discarding the supernatant each time, while preserving the phage pellet. Each of the phage pellets were then resuspended in 200 µL of sterile PBS and centrifuged one final time at 10000 rpm and 4^{o}C for 10 minutes. The resultant supernatant, now called the enriched phage library, was transferred to fresh low retention tubes and then stored at 4^{o}C for at most a month. For long term storage, in order to preserve the integrity of the phage library, sterile glycerol was added to each tube, making a final concentration of 50% glycerol, allowing for the enriched libraries to be stored at -80^{o}C for years at a time. Each subsequent round of biopanning should have ideally resulted in an enriched library more specific to the target protein than the previous round.

2.2.3 Method Modifications and Flow Cytometry

The results obtained from the first attempt at biopanning outlined in the previous section are fully explained in **Chapter 3**, however, while the procedure seemed to have succeeded in producing high affinity phages against GITR target protein, it failed to produce phages carrying scFv specific to CD47 and TIGIT. Therefore, due to the unsatisfactory levels of amplification and sensitivity noticed with two of the three target proteins, biopanning was repeated for these two targets with some modifications to the biopanning method.

A common failure of His-tagged proteins is the inaccessibility of the histidine tag within the tertiary structure of the protein in question, thus not allowing for strong binding to the beads. A hypothesis was made that this was the main cause for the low levels of affinity and specificity noticed in two of the three targets (*Affinity His-Tag Purification Troubleshooting Guide* 2019).

Therefore, the first major modification made in the method was in the type of magnetic beads used, in this case being the Dynabeads™ Protein G [Invitrogen, Massachusetts, USA, Catalogue No. 10009D], which bind specifically to an Fc tag on proteins, rather than binding to a histidine tag. Therefore, new proteins were also obtained, those being Recombinant Human CD47 Protein (ECD, hFc Tag) [Sino Biological Inc., Beijing, China, Catalogue No. 12283-H02H], and Recombinant Human TIGIT Protein (ECD, hFc Tag) [Sino Biological Inc., Beijing, China, Catalogue No. 10917-H02H]. However, to ensure proper binding of these targets to the Protein G beads before biopanning was repeated, binding affinity was tested using Flow Cytometry. For this method, the antibodies Anti-CD47 Antibody (PE), Mouse Monoclonal [Sino Biological Inc., Beijing, China, Catalogue No. 12283-MM07-P] and Anti-TIGIT Antibody, Mouse Monoclonal [Sino Biological Inc., Beijing, China, Catalogue No. 10917-MM52] were obtained.

Firstly, five different sets of dilutions were prepared for both of the bait proteins under investigation, as shown in **Table 2.1**, with a total of 20 tubes being prepared. Later, the PE-labelled antibodies would be added to half of these tubes, while the tubes without antibodies would be the negative controls.

Table 2.1: A table showing the levels of serial dilution of CD47 Fc protein and TIGIT Fc protein that were used to perform Flow cytometry. *The table shows the prepared concentration of each of these bait protein dilutions, as well as the volume of reconstituted protein (stock concertation of 100 µg/mL) and volume of binding buffer (PBS + 0.01% Tween-20) used to prepare each. These bait proteins from each serial dilution were immobilised on Protein G magnetic beads, and their presence was detected using specific PE-labelled antibodies, in order to ensure compatibility between proteins and beads.*

Conc. (µg/mL)	Vol. Of CD47 / TIGIT (µL)	Vol. of Binding Buffer (µL)
5	10	190
0.5	20 of 5 µg/mL	180
0.05	20 of 0.5 µg/mL	180
0.005	20 of 0.05 µg/mL	180
0.0005	20 of 0.005 µg/mL	180
0	0	200

The next steps involved the reconstitution of the Protein G beads, similarly to the calculations done in **Section 2.2.2** with the aim of preparing 2 µL of beads per tube. Therefore, 50 µL of Protein G beads were washed in 500 µL of binding buffer (PBS + 0.01% Tween-20), discarding the wash, and then reconstituting in 450 µL of binding buffer. Then to each prepared tube, 20 µL of the beads were pipetted and incubated on a rotator at room temperature for 30 minutes. Each tube was then washed twice with 500 µL wash buffer (PBS + 0.05% Tween-20) and then blocked with 150 µL of blocking buffer (3% BSA in PBS + 0.1% Tween-20) per tube. At this point, the contents of the tubes were split in half, with one half being incubated for 1 hour with rotation, while the other was incubated overnight. This extra step was added in order to determine if a longer blocking step would affect binding of the antibodies, and therefore, if an extra overnight step could be added to Day 1 of biopanning, allowing for better time management and a less laborious procedure.

After the respective blocking steps, blocking buffer was removed, and antibodies were added to the required tubes. The anti-CD47 and anti-TIGIT antibodies were diluted in blocking buffer with a final volume of 140 µL and a working concentration of 1 µg/mL of each antibody. A volume of 20 µL of the prepared antibody was then added to each tube with their respective target, including the ones labelled 0, acting as negative controls. These were then incubated in the dark for 1 hour with rotation, and then washed once with 500 µL wash buffer.

In the case of TIGIT, since a PE labelled antibody could not be found, an extra step was added in which a Goat anti-Mouse IgG Fc Cross-Adsorbed Secondary Antibody, PE [Invitrogen, Massachusetts, USA, Catalogue No. 31861] was added, similarly prepared in blocking buffer with a working concentration of 1 µg/mL and a volume of 20 µL per tube of TIGIT/Anti-TIGIT antibody. This was followed by an extra hour-long incubation on a rotator, in the dark, followed by another washing step.

After the final wash, all tubes of beads were reconstituted in 500 µL blocking buffer and transferred to flow cytometry tubes. The level of fluorescence was measured in each of the 20 prepared tubes, including for those in which antibody was not added using the Attune™ NxT Flow Cytometer [Invitrogen, Massachusetts, USA, Catalogue No. A24858]. The results were analysed using FlowJo™ Software v10.10 [BD Life Sciences, New Jersey, USA].

Once this optimisation was completed, showing satisfactory levels of binding for both CD47-Fc and TIGIT-Fc to the Protein G beads, with and without the extra overnight blocking step, biopanning was repeated for these two protein targets on Protein G beads. A fresh scFv original phage library was obtained as well, and was prepared in the same way as previously, by diluting in blocking buffer. During round one, this was added as a volume of 20 µL per tube (CD47 Fc, TIGIT Fc and NPC), as opposed to the 2 µL originally used, in order to increase the

chances of encountering phages carrying scFvs with high affinities to the targets. For similar reasons, in subsequent rounds, 10 µL of enriched library were used per tube, increased to 20 µL if they had been stored in 50 % glycerol. The final modification was that carbenicillin was used as opposed to ampicillin during the amplification of phages on the second day of the phage display biopanning procedure. All other biopanning steps remained identical to the original method.

2.2.4 Phage Library Titrations

Titrations of the enriched phage libraries were performed at the end of each round of biopanning in order to confirm that there were phages present, as well as to calculate the titre (PFU/mL) of each enriched library. A set of serial dilutions of the enriched library for each target protein from the particular round in question was prepared in sterile LB broth as shown in **Table 2.2**.

Table 2.2: A table showing the different levels of dilution of the enriched phage library rounds created in order to carry out a phage titration. *The phage rounds were diluted with NEAT sterile LB broth. The tubes were mixed by gently pipetting up and down a minimum of 10 times with a sterile filtered tip before transferring the required volume (20 µL) into the next tube and discarding the tip, changing the pipette tip between each dilution.*

Tube	Dilution	LB broth	Phage library
1	10^{-2}	198 µL	2 µl from the stock
2	10^{-3}	180 µL	20µl from tube 1
3	10^{-4}	180 µL	20µl from tube 2
4	10^{-5}	180 µL	20µl from tube 3
5	10^{-6}	180 µL	20µl from tube 4
6	10^{-7}	180 µL	20µl from tube 5
7	10^{-8}	180 µL	20µl from tube 6
8	10^{-9}	180 µL	20µl from tube 7
9	10^{-10}	180 µL	20µl from tube 8

A volume of 100 µl of the same mid-log phase liquid culture used during biopanning was pipetted into fresh pre-labelled tubes, to which 100 µl of the 10^{-8}, 10^{-9}, and 10^{-10} phage library dilutions were added and allowed to incubate for no longer than 5 minutes to allow for infection. After infection of the bacteria with phage library, 200 µl of the mixture were pipetted onto ampicillin/carbenicillin LB agar plates and spread evenly. The plates were allowed to dry completely and then incubated upside down at 37ºC in a Binder BD53 Natural Convection incubator [BINDER GmbH, Tuttlingen, Germany] for 16 hours, together with a sterility plate. The following day, the number of colonies were counted on the plate observed to have between 30 and 300 distinct colonies. Each distinct colony represented a unique clone of the scFv phagemid due to the low multiplicity of infection. Furthermore, due to the ampicillin resistance inserted into the phagemid during library preparation, only bacteria infected with phagemid would have been able to grow on the ampicillin/carbenicillin containing selective media plates (Qi, Lu et al. 2012). Thus, the titre of phages (PFU/mL) present correlated exactly with the titre of infected bacterial cells (CFU/mL) which was calculated with the following equation:

CFU/ml=PFU/ml = (Number of colonies on the plate x dilution factor)/(0.5 x 0.1 mL)

2.2.5 ELISA Screening of Phage Rounds

In order to determine the affinity of the enriched libraries obtained from each round of biopanning an ELISA was performed, during which various dilutions of the phage libraries were tested against the immobilised target protein as well as an unrelated control protein. In **Figure 2.3**, the main concept behind this process can be summarised.

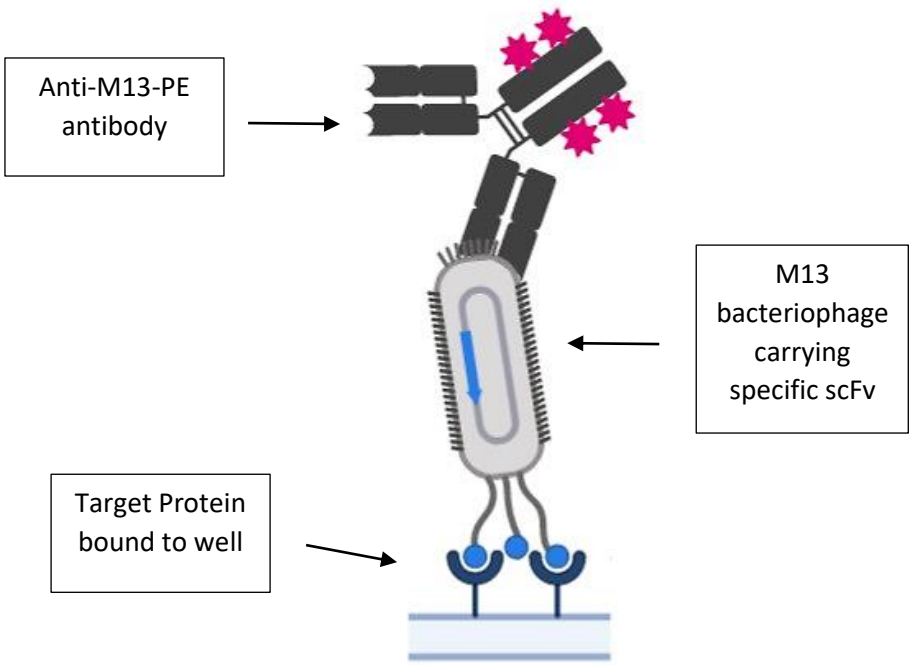

Figure 2.3: A figure showing the mechanism through which an ELISA of the enriched rounds was carried out. *The high affinity M13 phages of the enriched library in each well were bound to immobilised bait proteins and were measured using PE-labelled monoclonal mouse anti-M13 antibodies.*

The first step was the coating of a COSTAR® 96-Well Black Polystyrene Plate [Corning Inc., New York, United States, Catalogue No. 3915] with 50 ng of protein diluted in PBS per well and incubated for 2 hours at room temperature. The ELISA performed on the enriched phage libraries produced from the original biopanning method made use of the following proteins: Recombinant Human CD47 Protein (ECD, His Tag), Recombinant Human TIGIT Protein (Dimer, ECD, His Tag), Recombinant Human GITR/TNFRSF18/AITR Protein (ECD, His Tag), and SARS CoV-2 (2019-nCoV) Spike S1-His Recombinant Protein (HPLC-verified) [Sino Biological Inc., Beijing, China, Catalogue No. 40591-V08H] as the non-target protein (NPC). Two 96-well plates were used to accommodate the number of rounds and dilutions of enriched library, with the layouts outlined in **Figures 2.4 and 2.5**.

On each plate, a negative control of only immobilised protein with no library was included as a background fluorescence measurement, as well as a positive control of a phage round that is known to be a good binder as a positive control of the ELISA itself. In this case, the positive control chosen was the enriched library of Round iv GITR, at a dilution of 1/10, which was determined to showcase a high level of specificity and affinity to the target GITR (His-Tag) protein from a previous simplified ELISA of the rounds made with fewer phage dilutions, which is further explained in **Appendix D**.

After incubating with protein, each well was washed 3 times with 100 µL wash buffer (PBS + 0.1% Tween-20) per well and then blocked overnight with 200 µL blocking buffer (3% BSA in PBS + 0.1% Tween-20) per well at 4^{o}C. The following day, dilutions of each round of phage library were prepared for all three target proteins as well as the no protein control libraries, using PBS in the following dilutions: 1/10, 1/100, 1/200, 1/500, and 1/1000. After removing the blocking buffer, 100 µL of the phage library were added to each appropriate well, as shown once again in **Figures 2.4 and 2.5**. The wells labelled as no library were instead only filled with 100 µL of PBS. Both plates were incubated for one hour at room temperature.

Plate 1	1	2	3	4	5	6	7	8	9	10	11
A	Ri CD47 1/10 on CD47	RiCD47 1/100 on CD47	Ri CD47 1/200 on CD47	Ri CD47 1/500 on CD47	Ri CD47 1/1000 on CD47	Ri TIGIT 1/10 on TIGIT	Ri TIGIT 1/100 on TIGIT	Ri TIGIT 1/200 on TIGIT	Ri TIGIT 1/500 on TIGIT	Ri TIGIT 1/1000 on TIGIT	CD47 no library
B	Rii CD47 1/10 on CD47	Rii CD47 1/100 on CD47	Rii CD47 1/200 on CD47	Rii CD47 1/500 on CD47	Rii CD47 1/1000 on CD47	Rii TIGIT 1/10 on TIGIT	Rii TIGIT 1/100 on TIGIT	Rii TIGIT 1/200 on TIGIT	Rii TIGIT 1/500 on TIGIT	Rii TIGIT 1/1000 on TIGIT	TIGIT no library
C	Riii CD47 1/10 on CD47	Riii CD47 1/100 on CD47	Riii CD47 1/200 on CD47	Riii CD47 1/500 on CD47	Riii CD47 1/1000 on CD47	Riii TIGIT 1/10 on TIGIT	Riii TIGIT 1/100 on TIGIT	Riii TIGIT 1/200 on TIGIT	Riii TIGIT 1/500 on TIGIT	Riii TIGIT 1/1000 on TIGIT	Riv GITR 1/10
D	Riv CD47 1/10 on CD47	Riv CD47 1/100 on CD47	Riv CD47 1/200 on CD47	Riv CD47 1/500 on CD47	Riv CD47 1/1000 on CD47	Riv TIGIT 1/10 on TIGIT	Riv TIGIT 1/100 on TIGIT	Riv TIGIT 1/200 on TIGIT	Riv TIGIT 1/500 on TIGIT	Riv TIGIT 1/1000 on TIGIT	
E	Ri CD47 1/10 on CP	Ri CD47 1/100 on CP	Ri CD47 1/200 on CP	Ri CD47 1/500 on CP	Ri CD47 1/1000 on CP	Ri TIGIT 1/10 on CP	Ri TIGIT 1/100 on CP	Ri TIGIT 1/200 on CP	Ri TIGIT 1/500 on CP	Ri TIGIT 1/1000 on CP	
F	Rii CD47 1/10 on CP	Rii CD47 1/100 on CP	Rii CD47 1/200 on CP	Rii CD47 1/500 on CP	Rii CD47 1/1000 on CP	Rii TIGIT 1/10 on CP	Rii TIGIT 1/100 on CP	Rii TIGIT 1/200 on CP	Rii TIGIT 1/500 on CP	Rii TIGIT 1/1000 on CP	
G	Riii CD47 1/10 on CP	Riii CD47 1/100 on CP	Riii CD47 1/200 on CP	Riii CD47 1/500 on CP	Riii CD47 1/1000 on CP	Riii TIGIT 1/10 on CP	Riii TIGIT 1/100 on CP	Riii TIGIT 1/200 on CP	Riii TIGIT 1/500 on CP	Riii TIGIT 1/1000 on CP	
H	Riv CD47 1/10 on CP	Riv CD47 1/100 on CP	Riv CD47 1/200 on CP	Riv CD47 1/500 on CP	Riv CD47 1/1000 on CP	Riv TIGIT 1/10 on CP	Riv TIGIT 1/100 on CP	Riv TIGIT 1/200 on CP	Riv TIGIT 1/500 on CP	Riv TIGIT 1/1000 on CP	

Figure 2.4: A figure showing the full plate layout of plate 1 in the ELISA of the initial biopanning using His-Tag proteins. *Plate 1 included 5 dilutions of each round of CD47 phages and TIGIT phages against both target and non-target SARS-COV Spike S1 control (CP) proteins, with Round IV GITR library acting as a positive control.*

Plate 2	1	2	3	4	5	6	7	8	9	10	11
A	Ri NPC 1/10 on GITR	Ri NPC 1/100 on GITR	Ri NPC 1/200 on GITR	Ri NPC 1/500 on GITR	Ri NPC 1/1000 on GITR	Ri GITR 1/10 on GITR	Ri GITR 1/100 on GITR	Ri GITR 1/200 on GITR	Ri GITR 1/500 on GITR	Ri GITR 1/1000 on GITR	GITR no library
B	Rii NPC 1/10 on GITR	Rii NPC 1/100 on GITR	Rii NPC 1/200 on GITR	Rii NPC 1/500 on GITR	Rii NPC 1/1000 on GITR	Rii GITR 1/10 on GITR	Rii GITR 1/100 on GITR	Rii GITR 1/200 on GITR	Rii GITR 1/500 on GITR	Rii GITR 1/1000 on GITR	
C	Riii NPC 1/10 on GITR	Riii NPC 1/100 on GITR	Riii NPC 1/200 on GITR	Riii NPC 1/500 on GITR	Riii NPC 1/1000 on GITR	Riii GITR 1/10 on GITR	Riii GITR 1/100 on GITR	Riii GITR 1/200 on GITR	Riii GITR 1/500 on GITR	Riii GITR 1/1000 on GITR	
D	Riv NPC 1/10 on GITR	Riv NPC 1/100 on GITR	Riv NPC 1/200 on GITR	Riv NPC 1/500 on GITR	Riv NPC 1/1000 on GITR	Riv GITR 1/10 on GITR	Riv GITR 1/100 on GITR	Riv GITR 1/200 on GITR	Riv GITR 1/500 on GITR	Riv GITR 1/1000 on GITR	
E	Ri NPC 1/10 on CP	Ri NPC 1/100 on CP	Ri NPC 1/200 on CP	Ri NPC 1/500 on CP	Ri NPC 1/1000 on CP	Ri GITR 1/10 on CP	Ri GITR 1/100 on CP	Ri GITR 1/200 on CP	Ri GITR 1/500 on CP	Ri GITR 1/1000 on CP	
F	Rii NPC 1/10 on CP	Rii NPC 1/100 on CP	Rii NPC 1/200 on CP	Rii NPC 1/500 on CP	Rii NPC 1/1000 on CP	Rii GITR 1/10 on CP	Rii GITR 1/100 on CP	Rii GITR 1/200 on CP	Rii GITR 1/500 on CP	Rii GITR 1/1000 on CP	
G	Riii NPC 1/10 on CP	Riii NPC 1/100 on CP	Riii NPC 1/200 on CP	Riii NPC 1/500 on CP	Riii NPC 1/1000 on CP	Riii GITR 1/10 on CP	Riii GITR 1/100 on CP	Riii GITR 1/200 on CP	Riii GITR 1/500 on CP	Riii GITR 1/1000 on CP	
H	Riv NPC 1/10 on CP	Riv NPC 1/100 on CP	Riv NPC 1/200 on CP	Riv NPC 1/500 on CP	Riv NPC 1/1000 on CP	Riv GITR 1/10 on CP	Riv GITR 1/100 on CP	Riv GITR 1/200 on CP	Riv GITR 1/500 on CP	Riv GITR 1/1000 on CP	

Figure 2.5: A figure showing the full plate layout of plate 2 in the ELISA of the initial biopanning using His-Tag proteins. *Plate 2 Shows the 5 dilutions of the rounds of No protein control (NPC) phages and GITR phages against GITR protein as the target and the SARS-COV Spike S1 non-target control protein (CP).*

Once the incubation step had finished, each well was washed 5 times with 100 µL wash buffer per well, in order to remove any unbound phages. Each well was then incubated for one hour in the dark with 70 µL of Anti-M13 Antibody (PE), Mouse Monoclonal [Sino Biological Inc., Beijing, China, Catalogue No. 11973-MM05T-P], diluted in blocking buffer at a working concentration of 1 µg/mL. Each well was then once again washed 5 times with 100 µL wash buffer, and once more with 100 µL of PBS. After the final wash, 100 µL of fresh PBS were added to each well, and the fluorescence of the plates was read using the TECAN Spark® Multimode Microplate Reader using the following settings:

Mode: Fluorescence
Top Reading Excitation: Monochromator
Excitation wavelength: 561 nm
Excitation Bandwidth: 20 nm
Emission: Monochromator
Emission wavelength: 606 nm
Emission Bandwidth: 20 nm
Gain: Optimal
Mirror: AUTOMATIC
Number of flashes: 10
Integration Time: 40 µs
Lag time: 0 µs
Settle time: 0 ms
Z-Position: 20000 µm
Z-Position mode: Manual
Multiple Reads per Well (Circle (filled)): 4 x 4
Multiple Reads per Well (Border): 450 µm

An ELISA was also performed of the second attempt at biopanning using the modified method. The steps taken were identical to the previous ELISA, other than the proteins used, this time being the Recombinant Human CD47 Protein (ECD, hFc Tag), and Recombinant

Human TIGIT Protein (ECD, hFc Tag). For the sake of consistency, the non-target protein used was once again the SARS-CoV-2 Spike S1. The layout used for these plates can be seen in **Figures 2.6 and 2.7**.

Plate 1	1	2	3	4	5	6	7	8	9	10	11
A	Ri CD47 1/10 on CD47	Ri CD47 1/100 on CD47	Ri CD47 1/200 on CD47	Ri CD47 1/500 on CD47	Ri CD47 1/1000 on CD47	Ri TIGIT 1/10 on TIGIT	Ri TIGIT 1/100 on TIGIT	Ri TIGIT 1/200 on TIGIT	Ri TIGIT 1/500 on TIGIT	Ri TIGIT 1/1000 on TIGIT	CD47 no library
B	Rii CD47 1/10 on CD47	Rii CD47 1/100 on CD47	Rii CD47 1/200 on CD47	Rii CD47 1/500 on CD47	Rii CD47 1/1000 on CD47	Rii TIGIT 1/10 on TIGIT	Rii TIGIT 1/100 on TIGIT	Rii TIGIT 1/200 on TIGIT	Rii TIGIT 1/500 on TIGIT	Rii TIGIT 1/1000 on TIGIT	TIGIT no library
C	Riii CD47 1/10 on CD47	Riii CD47 1/100 on CD47	Riii CD47 1/200 on CD47	Riii CD47 1/500 on CD47	Riii CD47 1/1000 on CD47	Riii TIGIT 1/10 on TIGIT	Riii TIGIT 1/100 on TIGIT	Riii TIGIT 1/200 on TIGIT	Riii TIGIT 1/500 on TIGIT	Riii TIGIT 1/1000 on TIGIT	Riv GITR pos cntrl
D	Riv CD47 1/10 on CD47	Riv CD47 1/100 on CD47	Riv CD47 1/200 on CD47	Riv CD47 1/500 on CD47	Riv CD47 1/1000 on CD47	Riv TIGIT 1/10 on TIGIT	Riv TIGIT 1/100 on TIGIT	Riv TIGIT 1/200 on TIGIT	Riv TIGIT 1/500 on TIGIT	Riv TIGIT 1/1000 on TIGIT	
E	Ri CD47 1/10 on CP	Ri CD47 1/100 on CP	Ri CD47 1/200 on CP	Ri CD47 1/500 on CP	Ri CD47 1/1000 on CP	Ri TIGIT 1/10 on CP	Ri TIGIT 1/100 on CP	Ri TIGIT 1/200 on CP	Ri TIGIT 1/500 on CP	Ri TIGIT 1/1000 on CP	
F	Rii CD47 1/10 on CP	Rii CD47 1/100 on CP	Rii CD47 1/200 on CP	Rii CD47 1/500 on CP	Rii CD47 1/1000 on CP	Rii TIGIT 1/10 on CP	Rii TIGIT 1/100 on CP	Rii TIGIT 1/200 on CP	Rii TIGIT 1/500 on CP	Rii TIGIT 1/1000 on CP	
G	Riii CD47 1/10 on CP	Riii CD47 1/100 on CP	Riii CD47 1/200 on CP	Riii CD47 1/500 on CP	Riii CD47 1/1000 on CP	Riii TIGIT 1/10 on CP	Riii TIGIT 1/100 on CP	Riii TIGIT 1/200 on CP	Riii TIGIT 1/500 on CP	Riii TIGIT 1/1000 on CP	
H	Riv CD47 1/10 on CP	Riv CD47 1/100 on CP	Riv CD47 1/200 on CP	Riv CD47 1/500 on CP	Riv CD47 1/1000 on CP	Riv TIGIT 1/10 on CP	Riv TIGIT 1/100 on CP	Riv TIGIT 1/200 on CP	Riv TIGIT 1/500 on CP	Riv TIGIT 1/1000 on CP	

Figure 2.6: A figure showing the full plate layout of plate 1 used in the ELISA of the modified biopanning procedure using Fc proteins on Protein G beads. *Plate 1 included 5 dilutions of each round of CD47 phages and TIGIT phages against both target and non-target SARS-COV Spike S1 control (CP) proteins, with Round IV GITR library acting as a positive control.*

Plate 2	1	2	3	4	5	6
A	Ri NPC 1/10 on CD47	Ri NPC 1/100 on	Ri NPC 1/200 on CD47	Ri NPC 1/500 on CD47	Ri NPC 1/1000 on CD47	CD47 no library
B	Rii NPC 1/10 on	Rii NPC 1/100 on	Rii NPC 1/200 on CD47	Rii NPC 1/500 on CD47	Rii NPC 1/1000 on CD47	Riv GITR 1/10 pos
C	Riii NPC 1/10 on CD47	Riii NPC 1/100 on CD47	Riii NPC 1/200 on CD47	Riii NPC 1/500 on CD47	Riii NPC 1/1000 on CD47	
D	Riv NPC 1/10 on CD47	Riv NPC 1/100 on CD47	Riv NPC 1/200 on CD47	Riv NPC 1/500 on CD47	Riv NPC 1/1000 on CD47	
E	Ri NPC 1/10 on CP	Ri NPC 1/100 on CP	Ri NPC 1/200 on CP	Ri NPC 1/500 on CP	Ri NPC 1/1000 on CP	
F	Rii NPC 1/10 on CP	Rii NPC 1/100 on CP	Rii NPC 1/200 on CP	Rii NPC 1/500 on CP	Rii NPC 1/1000 on CP	
G	Riii NPC 1/10 on CP	Riii NPC 1/100 on CP	Riii NPC 1/200 on CP	Riii NPC 1/500 on CP	Riii NPC 1/1000 on CP	
H	Riv NPC 1/10 on CP	Riv NPC 1/100 on CP	Riv NPC 1/200 on CP	Riv NPC 1/500 on CP	Riv NPC 1/1000 on CP	

Figure 2.7: A figure showing the full plate layout of plate 2 used in the ELISA of the modified biopanning procedure using Fc proteins on Protein G beads. *Plate 2 included 5 dilutions of the rounds of No protein control (NPC) phages against CD47 Fc protein and the SARS-COV Spike S1 non-target control protein (CP).*

2.3 Candidate Phage Clone Preparation

Once biopanning was successfully completed, individual clones were randomly chosen from the enriched library of the round showing highest amount of binding to the target protein, which was established by the ELISA. These were then amplified, through a method similar to biopanning, and then screened with an ELISA to identify the individual clones with the highest affinity to the target protein. Clones were chosen by picking individual distinct colonies from the selective LB agar plates used to perform the phage titration of the rounds, ensuring that the plates used were no older than 4 days. Only GITR clones were isolated during the course of this project.

The first step involved the labelling of sterile 1.5 mL microcentrifuge tubes with the round number of the enriched library (e.g. Riii), Phage Culture (PC) 1, and a number chosen to designate the individual clone. In this case, up to 60 clones were picked in total, although for the sake of convenience, work was carried out with only 30 clones at a time, to avoid errors. To each of these prepared tubes, 400 µL of an LB/Carbenicillin broth with a working concentration of 100 µg/mL was pipetted, into which a single colony from the titration plate of the chosen round of enriched library was inoculated using a sterile 10 µL pipette tip. Additionally, as negative controls, one microcentrifuge tube was left with only sterile LB/Carbenicillin broth and no bacteria nor phages, while another was inoculated with a single colony of ER2738 from the primary streak plate and thus containing no phages. All tubes were then incubated for 16 hours at 37^{o}C with shaking at 250 rpm. These PC1 tubes were considered the master stocks of individual phagemid clones in ER2738.

On the following day, fresh 1.5 mL microcentrifuge tubes were prepared similarly to the first batch by labelling with the round number, PC2, and the individual clone number. To each of

the PC2 tubes 400 µl of LB/Carbenicillin broth containing $5x10^8$ PFU (about 1 µL per tube) of Hyperphage M13 KO7ΔpIII [PROGEN Biotechnik GmbH, Heidelberg, Germany, Catalogue No. PRHYPE-XS]. The Hyperphage is used in this procedure as a substitute to the M13KO7 helper phage as it has been found to increase the generation of phage particles by over two or three orders of magnitude. This is due to the fact that, while carrying the wild type pIII phenotype on their surface, allowing for the infection of F+ *E. coli*, Hyperphage, unlike the M13KO7 helper phage lacks the full gene coding for pIII. This means that upon infection, the only pIII source in the phage assembly would be the pIII-antibody fusion encoded in the clone phagemids themselves, thus greatly increasing the number of phage particles produced which express the scFv antibody fragment on their surfaces, leading to a larger yield of high affinity phages. This was considered especially important during the picking and amplification of individual clones, as any loss of high binding phages at this stage could have led to the complete loss of a high affinity clone (Rondot, Koch et al. 2001, Breitling, Broders et al. 2010). Similarly to the M13KO7 Helper phages, Hyperphages also grant kanamycin resistance.

To each of the prepared PC2 tubes, now containing the Hyperphage, 50 µL of the respective overnight PC1 culture were transferred to their corresponding tubes. These were then incubated at 37°C and at 250 rpm for 60-90 minutes. To the remaining PC1 culture, sterile glycerol was added to make up a final concentration of 15% glycerol, and these PC1 master stocks were then stored at -80°C for future experiments.

A kanamycin dilution of a working concentration of 5 mg/mL was prepared from the kanamycin stock (stock concentration 50 mg/mL) with 450 µL of deionised water. A volume of 5.6 µL of this solution was then pipetted into each of the PC2 tubes once their 60-90 minute

incubation had been completed. These were then incubated again at 37^{o}C and 250 rpm for 16 hours.

The following day, another two fresh sets of tubes were prepared with the round number, clone number and PC3, one set of which were low retention tubes to be used to purify the amplified phagemid clones. The PC2 tubes were centrifuged at 4000 rpm for 10 minutes at room temperature. The supernatant was transferred to one set of the prepared PC3 tubes, without disturbing the pellet, and the centrifugation was repeated. A volume of 400 µL of the supernatant from the second centrifugation step was transferred to the corresponding low-retention PC3 tube, to each of which 400 µL of blocking buffer (3% BSA in PBS + 0.1% Tween-20) was added. This was incubated on ice for 10 minutes, after which a volume of 160 µL of sterile 20 % PEG/2.5M NaCl was added to each tube, which were once again incubated on ice (at 4^{o}C) for 1-2 hours. This was followed by a final centrifugation at 10000 rpm at 4^{o}C for 20 minutes. The supernatant was discarded, and the resulting phage pellet was carefully resuspended in 100 µL of sterile PBS. These samples were then immediately used to perform a monoclonal ELISA.

2.3.1 Monoclonal ELISA of the Prepared Clones

The monoclonal ELISA of the individual phagemid clones was usually performed as soon as purification was completed. Similarly to the ELISA of the biopanning rounds, the 96-well flat-bottom black ELISA plate was coated with 50 ng of protein per well, using both a target and a non-target control protein for a minimum of 2 hours, followed by 3 washing steps, and an overnight blocking step. The following day, 50 µL of sterile PBS were added to each of the PC3 preparations, for a final volume of 150 µL. A 1/10, and 1/100 dilution of the enriched library from which the clones were isolated was also prepared as a positive control. After removing

the blocking buffer from the wells, 50 µL of the PC3 were added to the respective wells, along with the polyclonal phage library positive control, as shown in the plan in **Figure 2.8**. These were then incubated for 2 hours at room temperature.

Clones 1-30	1	2	3	4	5	6	7	8	9
A	1 on GITR	9 on GITR	17 on GITR	25 on GITR	1 on CP	9 on CP	17 on CP	25 on CP	Riii GITR 1/10 on GITR
B	2 on GITR	10 on GITR	18 on GITR	27 on GITR	2 on CP	10 on CP	18 on CP	27 on CP	Riii GITR 1/100 on GITR
C	3 on GITR	11 on GITR	19 on GITR	28 on GITR	3 on CP	11 on CP	19 on CP	28 on CP	Riii GITR 1/10 on CP
D	4 on GITR	12 on GITR	20 on GITR	29 on GITR	4 on CP	12 on CP	20 on CP	29 on CP	Riii GITR 1/100 on CP
E	5 on GITR	13 on GITR	21 on GITR	30 on GITR	5 on CP	13 on CP	21 on CP	30 on CP	
F	6 on GITR	14 on GITR	22 on GITR	no phage on GITR	6 on CP	14 on CP	22 on CP	no phage on CP	
G	7 on GITR	15 on GITR	23 on GITR	ER2738 on GITR	7 on CP	15 on CP	23 on CP	ER2738 on CP	
H	8 on GITR	16 on GITR	24 on GITR		8 on CP	16 on CP	24 on CP		

Clones 31-60 (with 26)	1	2	3	4	5	6	7	8	9
A	26 on GITR	38 on GITR	46 on GITR	54 on GITR	26 on CP	38 on CP	46 on CP	54 on CP	no phage on GITR
B	31 on GITR	39 on GITR	47 on GITR	55 on GITR	31 on CP	39 on CP	47 on CP	55 on CP	no phage on CP
C	32 on GITR	40 on GITR	48 on GITR	56 on GITR	32 on CP	40 on CP	48 on CP	56 on CP	Riii GITR 1/10 on GITR
D	33 on GITR	41 on GITR	49 on GITR	57 on GITR	33 on CP	41 on CP	49 on CP	57 on CP	Riii GITR 1/100 on GITR
E	34 on GITR	42 on GITR	50 on GITR	58 on GITR	34 on CP	42 on CP	50 on CP	58 on CP	Riii GITR 1/10 on CP
F	35 on GITR	43 on GITR	51 on GITR	59 on GITR	35 on CP	43 on CP	51 on CP	59 on CP	Riii GITR 1/100 on CP
G	36 on GITR	44 on GITR	52 on GITR	60 on GITR	36 on CP	44 on CP	52 on CP	60 on CP	
H	37 on GITR	45 on GITR	53 on GITR	ER2738 on GITR	37 on CP	45 on CP	53 on CP	ER2738 on CP	

Figure 2.8: A figure showing the ELISA plate layout of clones 1 to 60 against GITR His-Tag protein (target) and SARS-Cov2 Spike S1 (non-target). *Due to an error made during the preparation of clones 1-30, the clone designated as number 26 was lost. Therefore, a new clone was picked and labelled as 26 when picking clones 31-60 and was therefore included in the second plate. The negative controls used in this ELISA were the wells labelled as no phage, which provide a background reading, as well as the wells labelled ER2738, which were used as a negative control during monoclonal preparation and also contain no phages.*

Each well was then washed 5 times with 100 µL wash buffer, after which they were incubated with 70 µL per well of anti-M13-PE antibody (working concentration of 1 µg/mL) and incubated for 1 hour in the dark at room temperature. This was followed by washing 5 times with 100 µL wash buffer, followed by once more with 100 µL PBS. After discarding the final wash, a new volume of 100 µL PBS was added to each well, and the plates were read on the TECAN Spark, using the same settings as the previous ELISA described in **Section 2.2.5**.

2.4 Plasmid Extraction of Individual Clones

During the procedure carried out in Section 2.3, before the addition of the glycerol to the PC1 master stock, a 50 µL subsample of the PC1 master stock cultures of each clone was collected and transferred to sterile 14 mL round bottom tubes containing 3 mL of LB/Carbenicillin broth (100 µg/mL) and labelled with the round number and the individual clone number. These were used for *E. coli* propagation in preparation for plasmid DNA extraction using the Monarch® Plasmid Miniprep Kit [New England BioLabs Inc., Massachusetts, United States, Catalogue No. T1010L]. These were then incubated at 37^{o}C and 250 rpm for 16 hours, after which they were centrifuged at 4000 rpm for 10 minutes. The supernatant was carefully removed, ensuring not to disturb the pellet. In the event that DNA extraction could not be carried out the same day, these pellets were stored at -80^{o}C until ready to process. Two control tubes were also prepared, one with no bacteria and no phage, while to the other only ER2768 bacteria was added with no phage. These were the negative controls, in which no growth should have occurred.

Once ready to carry out the procedure, the pellets were thawed, and the extraction was carried out based on the manufacturer instructions of the Monarch miniprep kit, which made

use of a variety of alkaline and high salt reagents as well as several buffers to lyse the bacterial cells, releasing the plasmids and binding them to a silica matrix while all cell debris was removed. Due to the precise timings of the incubation steps involved in this method, DNA extraction was carried out several times in groups of no more than 6 clones at a time.

The first step involved the resuspension of the bacterial pellet in 200 µL of the resuspension buffer (Pink) provided by the kit, and then transferring each suspension to a labelled microcentrifuge tube. The suspension was gently vortexed for at most 10 seconds to ensure homogeneity, after which 200 µL of a lysis buffer (Blue) were added immediately to each tube. The tubes were mixed by gentle inversion until the contents turned viscous, and a dark pink/purple colour was observed. This was then incubated for no longer than 1 minute at room temperature. The following step consisted of the addition of 400 µL of a neutralization buffer (Yellow), which was the only reagent of the kit normally stored in the fridge at 4^{o}C when not in use. The tubes were once again mixed by gentle inversion until a precipitate was observed to have formed and the contents became a uniform yellow colour, with no more pink being observed. This was incubated for no longer than 2 minutes at room temperature. The tubes were then centrifuged at 10000 rpm for 5 minutes. New England Biolabs (NEB) columns, which were also provided in the Monarch miniprep kit were prepared and labelled, and the supernatant from the previous centrifugation step was carefully transferred in the respective NEB columns, to bind the DNA. These were then centrifuged at 10000 rpm for 1 minute after which the flowthrough was discarded. The columns were replaced in their respective tubes, and 200 µL of a Plasmid Wash Buffer 1 were added into it. The 1 minute centrifugation step was repeated, and the flowthrough once again discarded. A volume of 400 µL of Plasmid Wash Buffer 2 was then also added to each column, followed by another 1 minute centrifugation, discarding the flowthrough. This wash with 400 µL of Plasmid Wash

Buffer 2 was repeated once again, discarding the flowthrough after centrifugation. The columns were then transferred to fresh labelled tubes, and a 1 minute dry spin was performed to remove any remaining wash buffer. Finally, the columns were transferred to a final labelled tube, and 35 µL of the elution buffer were pipetted into each of them, ensuring to cover the centre of the matrix without puncturing it. This was incubated at room temperature for 1 minute, followed by a final centrifugation step, which released the bound DNA from the NEB columns. The columns were then discarded, and the eluates collected and stored at 4^{o}C while wrapped in paraffin films to avoid evaporation losses (*Monarch® Plasmid Miniprep Kit Instruction Manual* 2021).

2.4.1 NanoDrop and Sanger Sequencing

In order to confirm the presence of DNA in the collected eluates of the 60 phage clones, the NanoDrop™ 2000 Spectrophotometer [ThermoScientific, Massachusetts, United States, Catalogue No. ND-2000] was used to measure the concentration of DNA extracted from each phage clone. A single drop of 2 µL of each sample was pipetted onto the pedestal of the NanoDrop, after which the arm was dropped, and the sample was measured using the appropriate NanoDrop software (Nucleic acid) settings. It was made sure to clean the pedestal between each sample using lint-free tissue paper, and a blank of just the elution buffer was read before any samples.

Once each sample was confirmed to have a satisfactory concentration of phage clone plasmid DNA, the samples were packaged properly and sent abroad to LGC genomics, Berlin for sanger sequencing. The primer chosen for sequencing was the M13-29R primer.

2.5 Data Analysis

2.5.1 GraphPad Prism

The software primarily used in the analysis of both the individual rounds, as well as the monoclones was GraphPad Prism 10 software [GraphPad Software, San Diego, California, US], using the fluorescence data obtained from the various ELISAs. Twelve replicate readings were obtained for each well using the TECAN Spark, all of which were inputted into the software, and the mean ± SEM were calculated. In the case of the rounds, the Area Under the Curve (AUC) was obtained for each round, which were then compared to each other as well as to the negative control using the Browne-Forsythe and Welch ANOVA in order to determine whether the variances in each round were statistically significant and thus concluding the success of the biopanning. This method was chosen as it did not assume equal variance between rounds and allowed for more accuracy in multiple comparisons (*The Ultimate Guide to ANOVA* 2025). This was done for the measurements of the rounds against both the target protein as well as the non-target protein. Estimation plots were also prepared for the AUCs of round 4 specifically, for a more direct comparison. Only p values of less than 0.05 were considered statistically significant.

For monoclonal analysis, fluorescence data from the ELISA was used once again, and a Shapiro-Wilk test was performed in order test for normality for each clone. This was followed by a multiple unpaired t-test of the data that was normally distributed or a Mann Whitney test if the data was not, in order to compare the fluorescence of individual phage clones on target and non-target and determine if the difference was statistically significant ($p \leq 0.05$). The data was once again given as the mean ± SEM. A legend of the symbols used to denote statistical significance may be found in **Table 2.3** below.

***Table 2.3: Legend of symbols denoting statistical significance and their respective p-value**, as specified by the GraphPad Software (What is the meaning of * or ** or *** in reports of statistical significance from prism or instat 2025).*

Symbol	Meaning
Not Significant (ns)	$p > 0.05$
*	$p \leq 0.05$
**	$p \leq 0.01$
***	$p \leq 0.001$
****	$p \leq 0.0001$

2.5.2 Sequence Comparisons of Individual Clones

Once the genetic sequences of the scFvs encoded by the phage monoclones were obtained, they were processed using the SnapGene [GSL Biotech LLC, California, United States] software, from which amino acid sequences were generated, and labelled. Once all of the Complementarity Determining Regions (CDRs) of each scFv were identified, they could then be manually sorted, aligned, and compared in order to identify differences in sequence between the high binding clones.

A Sequence Analysis software was also designed by Ms. Francesca Chircop, a bioinformatics student at the University of Malta, which made use of the amino acid sequences of the CDR3 of both the heavy chain (VH) and the light chain (VL), collected in a csv file, in order to generate a dendrogram summarising the structural similarity between all clones successfully sequenced. The CDR3 regions were focused on specifically due to the observed high level of variability in those regions (*Antibody CDR annotation, NovoPro labs* 2025). This diagram could then be used to better visualise the level of diversity in the scFv of the enriched library, as well as act as a guide during manual comparisons of individual sequences.

The online software SWISS-MODEL was used to obtain crystalline structures of some of the clones, as well as generate Ramachandran plots summarising the phi and psi angles of each amino acid, separated out into alpha-helical and beta strand conformations (Waterhouse, Bertoni et al. 2018, Guex, Peitsch et al. 2009).

Protein docking experiments were carried out between one of these generated structures and the structure of the target immune checkpoint protein, which was obtained from the online AlphaFold Protein Structure Database (Tumour necrosis factor receptor superfamily member 18) and UniProtKB (Q9Y5U5 - TNR18_HUMAN) (Ahmad, Da Costa Gonzales et al. 2025, Guex, Peitsch et al. 2009, Waterhouse, Bertoni et al. 2018). This was carried out through the use of HADDOCK 2.4 (High Ambiguity Driven protein-protein DOCKing) online software, to generate accurate protein docking models between the scFv obtained from the isolated phage clone and the target immune checkpoint (Honorato, Trellet et al. 2024, Honorato, Koukos et al. 2021). It was made sure to follow HADDOCK basic protein-protein docking tutorials in order to ensure all parameters are chosen correctly for the specific docking study in question (van Zundert, Rodrigues et al. 2015, de Vries, van Dijk et al. 2010, Bonvin 2025a). The exact parameters used for this docking study may be found in **Appendix J**.

3. Results

3.1 Biopanning rounds

Biopanning of the original phage library against all three target proteins, as well as the NPC, was carried out simultaneously. Of the three initial targets, biopanning was only successful against GITR His-tagged protein, with both CD47 and TIGIT showing no enrichment of specific scFv.

3.1.1 GITR

By the end of this project, four biopanning rounds were successfully carried out against the target GITR, leading to the identification and amplification of enriched polyclonal phage libraries expressing scFvs with high affinity and specificity to GITR (His-Tag) protein. At the end of each round, a phage library titration was carried out in order to confirm the presence of phages, as well as to calculate the CFU, and therefore the PFU present in each round of enriched library, which showed satisfactory numbers of phage present, as well as similar levels of amplification for each round. These results may be seen summarised in **Table 3.1**.

Table 3.1: A table showing the Colony forming unit (CFU/mL) and therefore the phage concentration (PFU/mL) of each round of GITR His-tag phages. *This was calculated with the formula described in Section 2.2.4 using the dilution factor of the enriched library and the number of colonies counted.*

GITR (His-Tag)			
Protein	**Number of Colonies**	**Dilution Factor**	**Colony Forming Unit (CFU/ml)**
I	155	10^9	3.1×10^{12}
II	37	10^9	7.4×10^{11}
III	152	10^9	3.04×10^{12}
IV	36	10^9	7.2×10^{11}

Five dilutions of each round of enriched library were prepared (1/10, 1/100, 1/200, 1/500, 1/1000) and an ELISA was used to determine the affinity of the generated scFvs towards the

immobilised target protein (GITR His-tag). Each round of the enriched library was also tested against a bound non-target protein (SARS-Cov2 Spike S1 His-tag) to show the specificity of the generated scFvs. Five dilutions of the four rounds of the No protein Control (NPC) were also prepared and measured with ELISA against one of the bound targets and the non-target protein, as a negative control for the biopanning rounds. As stated in **Section 2.2.2**, no protein was added to the tubes used to perform biopanning of the NPC, with beads being incubated with only 100 µL of sterile binding buffer (PBS + 0.01% Tween-20).

With each ELISA plate, a no library control well was included, in which no phage library was added to a well coated in target protein. This acted as a blank for the ELISA, as well as provided a negative control. Anti-M13-PE antibody was pipetted into each well and was used as the detection antibody in this assay. The larger the quantity of bound phages, the higher the amount of fluorescence (Arbitrary Units [A.U.]) produced, thus allowing an accurate measurement of scFv affinity. The raw data obtained was inputted into the software GraphPad Prism, and graphically represented, as seen in **Figure 3.1**.

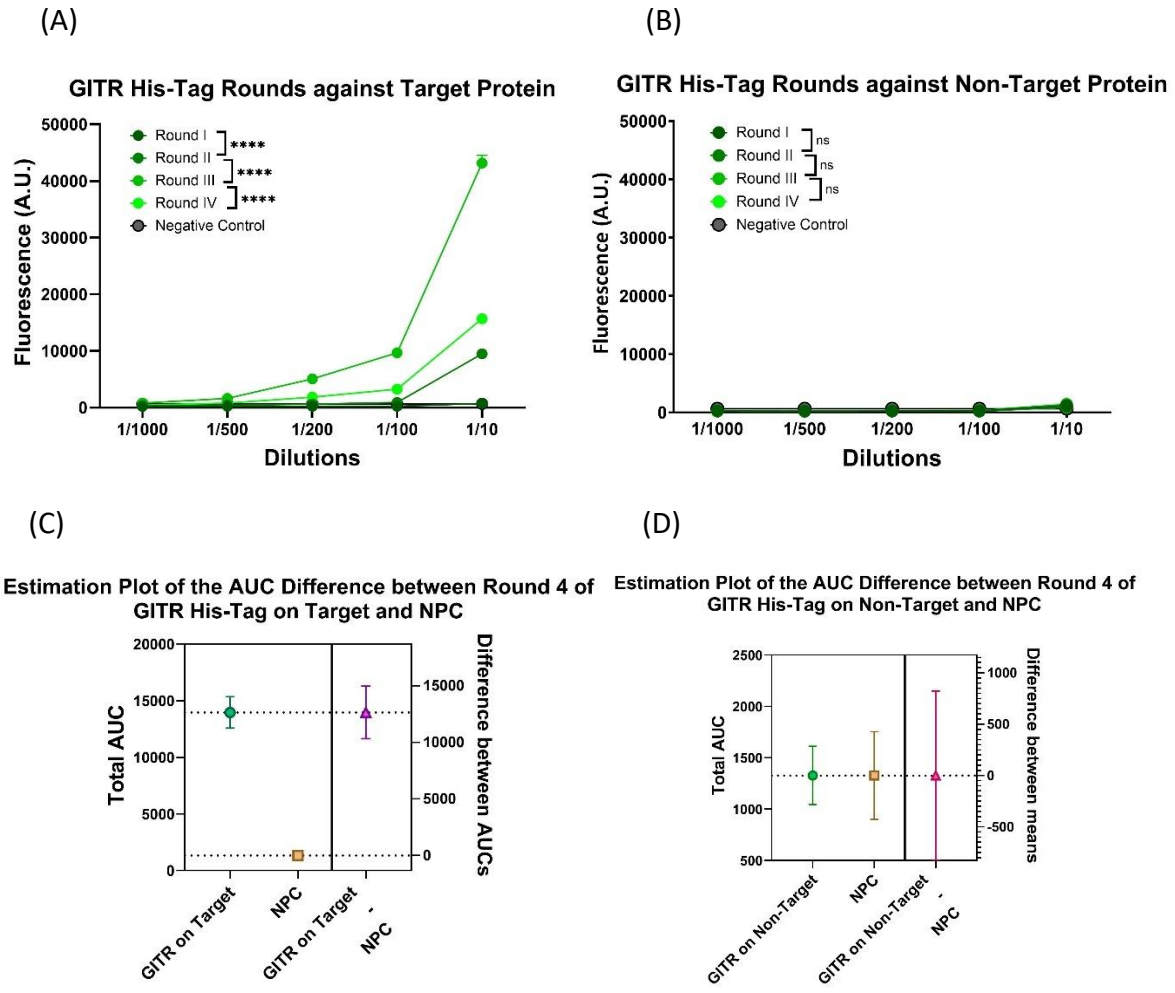

Figure 3.1: A figure showing the graphs of the 5 phage dilutions of rounds 1-4 GITR against the measured fluorescence in Arbitrary Units (A.U.) of the anti-M13-PE. *Graph (A) shows the four rounds of enriched phage library bound to GITR protein, while (B) shows the four rounds on non-target protein. Graphs (C) and (D) show estimation plots comparing the total AUC of round 4 GITR enriched library and round 4 of the NPC. All fluorescence measurements were performed in 12 replicates for each well. The error bars of each graph show 95% Confidence Interval (CI).*

From the above figures, it could be seen that biopanning against GITR protein was successful, with the differences between the AUC of rounds being statistically significant ($p \leq 0.0001$). Furthermore, from the graph showing the ELISA of the rounds against non-target protein, it can be seen that fluorescence levels measured are comparable to the negative (no library) control, thus showing that there is almost no non-specific binding of the scFvs expressed by the phages of the enriched library. Estimation plots comparing the fourth round of anti-GITR scFv phages against the fourth NPC phage round were also plotted to further Illustrate this conclusion.

As was expected, the lowest level of fluorescence of the rounds was observed in round one, While the highest level was measured by round 3, with some loss of affinity being observed in round 4. An additional Estimation plot of round 3 GITR phages against round 3 NPC was further generated to confirm this conclusion and may be seen in **Figure 3.2**.

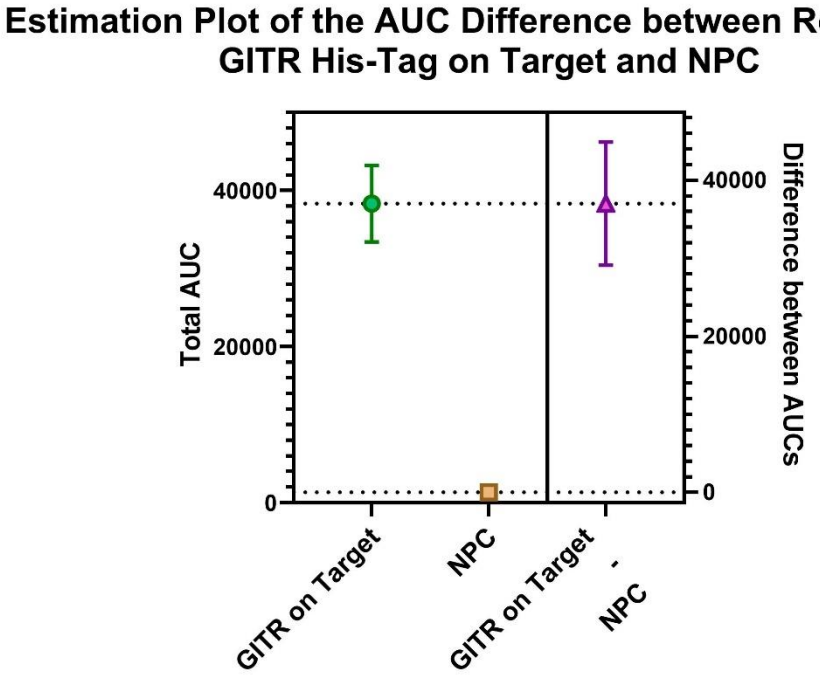

Figure 3.2: A figure showing the estimation plot of total AUC of round 3 GITR and Round 3 NPC. *This was created in order to confirm that the strongest fluorescence reading was observed in round 3. The error bars show the 95% CI.*

3.1.2 CD47

By the end of this study, four rounds of biopanning against CD47 His-tag protein were carried out. Phage library titrations were performed between each round, the results of which may be seen in **Table 3.2**. From the results, it can be seen that the phage titre of each round never fell below 6.8×10^{11} PFU/mL, which was considered an acceptable phage titre, showing similar levels of amplification between each round as was seen in GITR.

Table 3.2: A table showing the Colony forming unit (CFU/mL) and therefore the phage concentration (PFU/mL) of each round of CD47 His-tag phages. *This was calculated with the formula described in Section 2.2.4 using the dilution factor of the enriched library and the number of colonies counted.*

CD47 (His-Tag)			
Rounds	**Number of Colonies**	**Dilution Factor**	**Colony Forming Unit (CFU/ml)**
I	34	10^9	6.8×10^{11}
II	129	10^9	2.58×10^{12}
III	241	10^9	4.82×10^{12}
IV	116	10^9	2.32×10^{12}

Five dilutions of each round of enriched phage library were prepared and similarly to GITR, their affinity was tested against both target protein (CD47 His-tag) and non-target protein (SARS-Cov2 Spike S1 His-tag). A no library negative control well was also included as a negative control, and a single well of round 4 GITR (1/10) on target protein was used as a positive control for the assay. Anti-M13-PE antibody was added to each well, and the fluorescence (A.U.) of each round of enriched phage library was measured against target and non-target. The NPC used was the same as that for the GITR rounds.

Upon completion of the ELISA of each CD47 round against bound target and non-target protein, it was found that the generated scFvs had a very large amount of non-specific binding to the control protein, with few high affinity phages to the CD47 target protein isolated.

Graphs showing all rounds of CD47, as well as estimation plots comparing the total AUC of round 4 CD47 phages and round 4 of the NPC were generated to further illustrate this conclusion. All of the mentioned graphs may be seen in **Figure 3.3**.

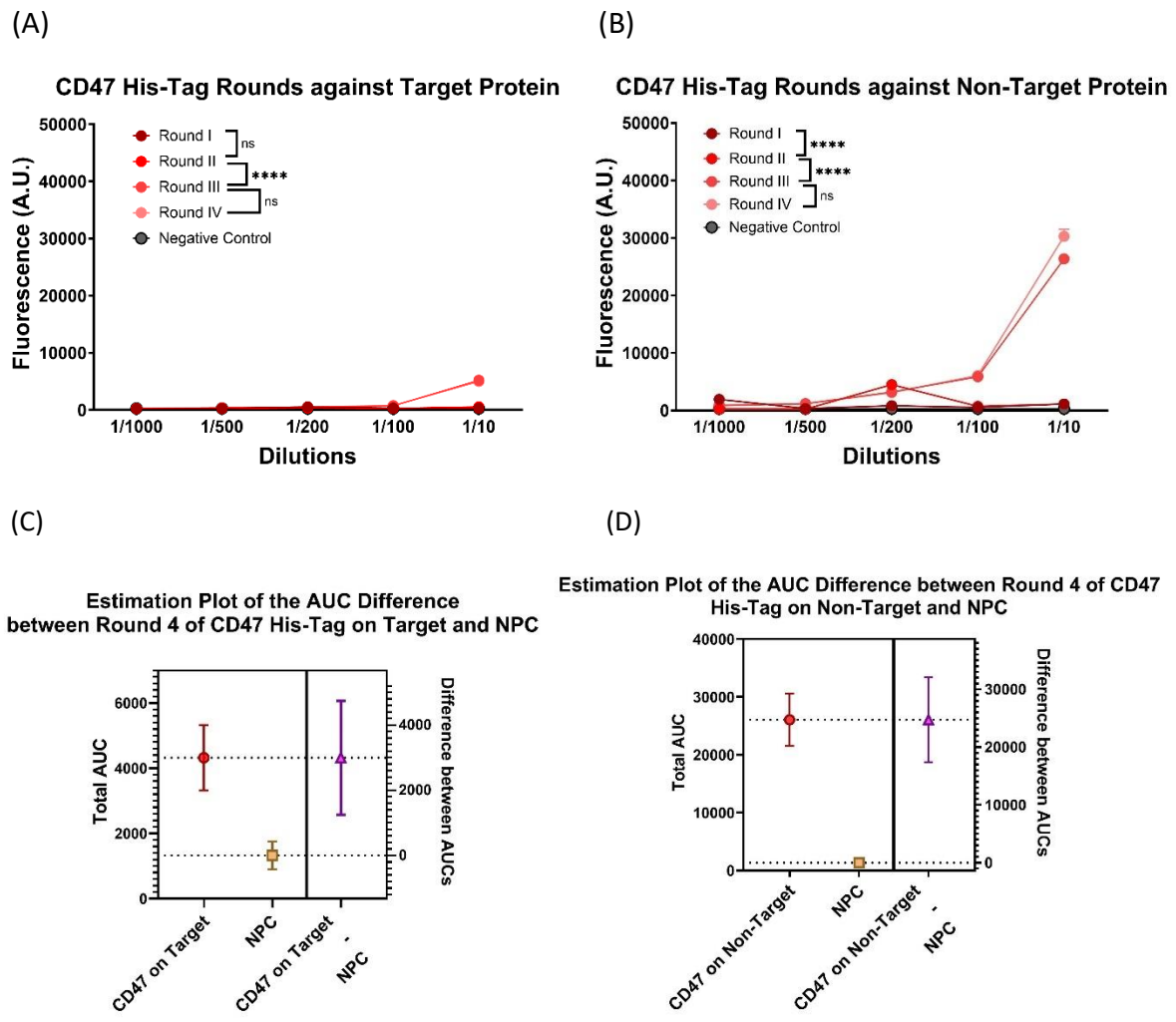

Figure 3.3: A figure showing the graphs of the 5 phage dilutions of rounds 1-4 CD47 His-tag against the measured fluorescence in Arbitrary Units (A.U.) of the anti-M13-PE. *Graph (A) shows the four rounds of enriched library bound to CD47 His-tag protein, while (B) shows the four rounds on non-target protein. Graphs (C) and (D) show estimation plots comparing the total AUC of round 4 CD47 enriched library and round 4 of the NPC. All fluorescence measurements were performed in 12 replicates for each well. The error bars of each graph show 95% CI.*

From the results, it can be seen that the highest level of affinity against both target and non-target was reached by the third round of biopanning, with the difference in the level of amplification between rounds 3 and 4 not being considered statistically significant. Furthermore, the estimation plots show that while there was a noted difference in fluorescence between round 4 of CD47 and round 4 of the NPC, it was far more statistically significant when on the non-target protein rather than the target, showing that the phages amplified do not have particularly strong affinity or specificity to CD47. This shows that while

there likely were some phages with affinity to CD47 present in the original phage library, they were largely outcompeted by less specific phages during biopanning and amplification (Derda, Tang et al. 2011, Hoen, Jirka et al. 2011). Due to this perceived loss of high affinity phages from the enriched libraries, as well as the lack of a notable increase in amplification between rounds 3 and 4, it was decided that additional biopanning rounds of the enriched libraries would most probably only lead to further loss of phages and therefore not improve these results. Instead, biopanning was repeated, starting from a new fresh original phage library, and making use of CD47 Fc proteins on Protein G beads, in an effort to ensure correct orientation of target proteins when immobilised on the magnetic beads and thus, hopefully improve specific binding of high affinity phages (Liu, Yu 2016). This was further validated using flow cytometry of the protein-coated beads and PE labelled antibody, the results of which may be seen in **Appendix C**.

In an effort to expedite the process, rather than performing a titration of each enriched library against CD47 Fc, only two titrations were performed, of rounds 2 and 3, to ensure the presence of phages, as seen in **Table 3.3**.

Table 3.3: A table showing the Colony forming unit (CFU/mL) and therefore the phage concentration (PFU/mL) of each round of CD47 Fc phages. *This was calculated with the formula described in Section 2.2.4 using the dilution factor of the enriched library and the number of colonies counted.*

CD47 (Fc)			
Round	**Number of Colonies**	**Dilution Factor**	**Colony Forming Unit (CFU/ml)**
II	62	10^9	1.24×10^{12}
III	28	10^9	5.6×10^{11}

An ELISA was once again performed of the four new rounds of enriched library in five dilutions against bound CD47 fc protein, and the non-target control protein (SARS-Cov2 Spike S1 His-tag), which was kept the same for consistency. A single well containing round 4 of GITR phage

library at a dilution of 1/10 on GITR His-tag was used as a positive control for the assay, while the negative control was the no library well. Despite the changes made to the methodology, biopanning was still unsuccessful, with no statistical significance being observed between rounds 3 and 4 and the negative control. However, contrary to the biopanning against CD47 His-tag, there was also no non-specific binding observed in the four rounds of enriched library. These results may be seen summarised in **Figure 3.4**.

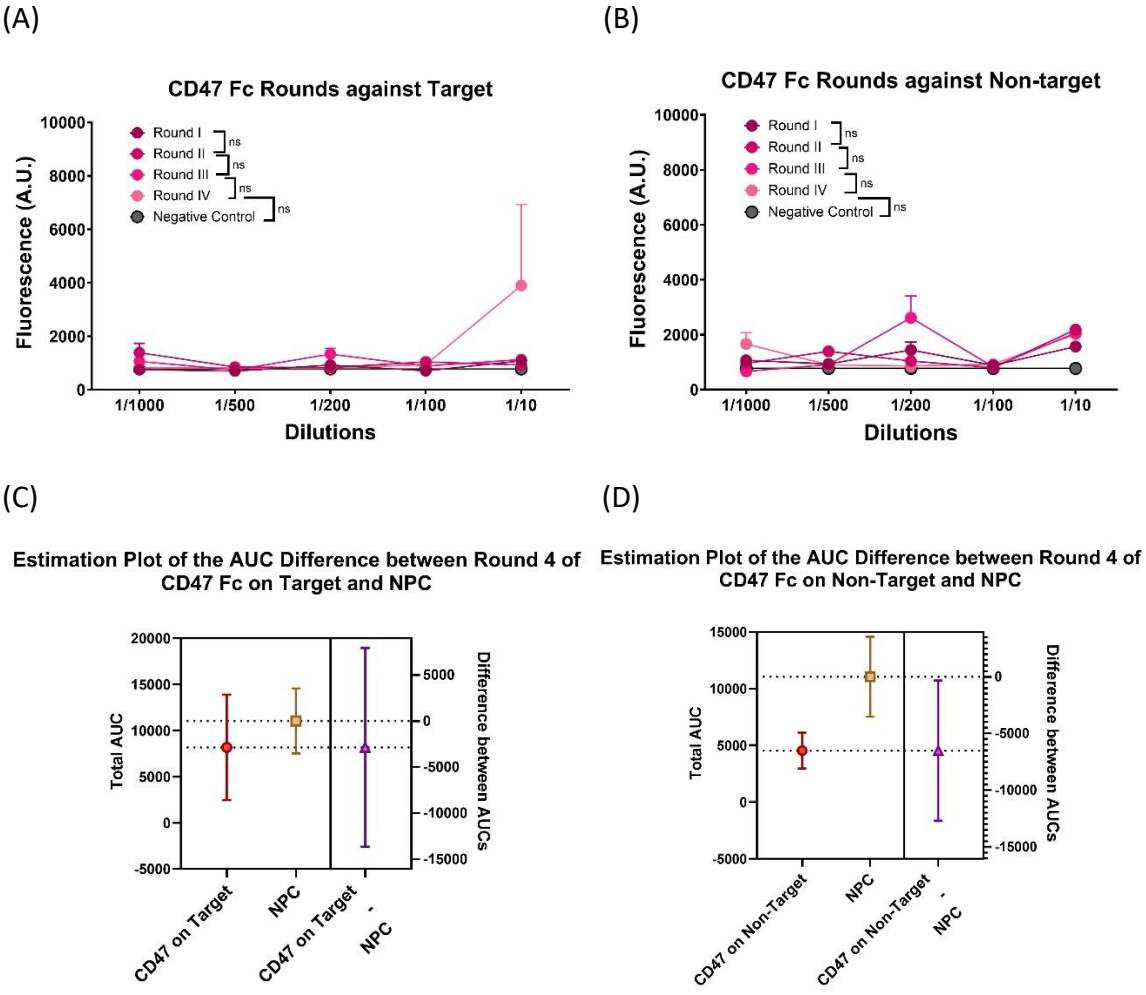

Figure 3.4: A figure showing the graphs of the 5 phage dilutions of rounds 1-4 CD47 Fc against the measured fluorescence in Arbitrary Units (A.U.) of the anti-M13-PE. *Graph (A) shows the four rounds of enriched library bound to CD47 protein, while (B) shows the four rounds on non-target protein. Graphs (C) and (D) show estimation plots comparing the total AUC of round 4 CD47 enriched library and round 4 of the NPC. All fluorescence measurements were performed in 12 replicates for each well. The error bars of each graph show 95% CI.*

From the results it is clear to see that biopanning of CD47 Fc, using Protein G beads completely failed to produce phages with scFv of any affinity. If in future studies biopanning against CD47 is attempted again, it will most likely be using a His-tagged proteins.

3.1.3 TIGIT

TIGIT was the final target of biopanning of this study, and similarly to CD47, was the second not to produce satisfactory results. Biopanning of TIGIT His-tag occurred concurrently with that of GITR His-tag and CD47 His-tag, and the phage titre of the anti-TIGIT phage libraries produced were seen to consistently be above 1×10^{12} PFU/mL. The full calculated phage titres of the enriched TIGIT libraries may be seen in **Table 3.4**.

Table 3.4: A table showing the Colony forming unit (CFU/mL) and therefore the phage concentration (PFU/mL) of each round of TIGIT His-tag phages. *This was calculated with the formula described in Section 2.2.4 using the dilution factor of the enriched library and the number of colonies counted.*

TIGIT (His-Tag)			
Protein	**Number of Colonies**	**Dilution Factor**	**Colony Forming Unit (CFU/ml)**
I	71	10^9	1.42×10^{12}
II	242	10^9	4.84×10^{12}
III	127	10^9	2.54×10^{12}
IV	73	10^9	1.46×10^{12}

The ELISA of the 4 rounds of enriched phage libraries was performed using 5 dilutions of each library against both bound target (TIGIT His-tag) protein and non-target (SARS-Cov2 Spike S1 His-tag) protein. Once again, a no library well was used as a negative control, while GITR round 4 (1/10) was the positive control for the assay. Anti-M13-PE was used to measure the fluorescence (A.U.) levels for each well.

From the ELISA, it was noted that almost no binding of phages occurred against both the target and the non-target protein, due to the lack of statistical significance calculated

between the four rounds. Further estimation plots of the difference between AUCs of round 4 TIGIT and round 4 NPC also showed no statistical significance. This showed that once again, no phages carrying scFv specific to TIGIT target protein were isolated or amplified during biopanning. All graphs of the TIGIT His-tag rounds are shown in **Figure 3.5**.

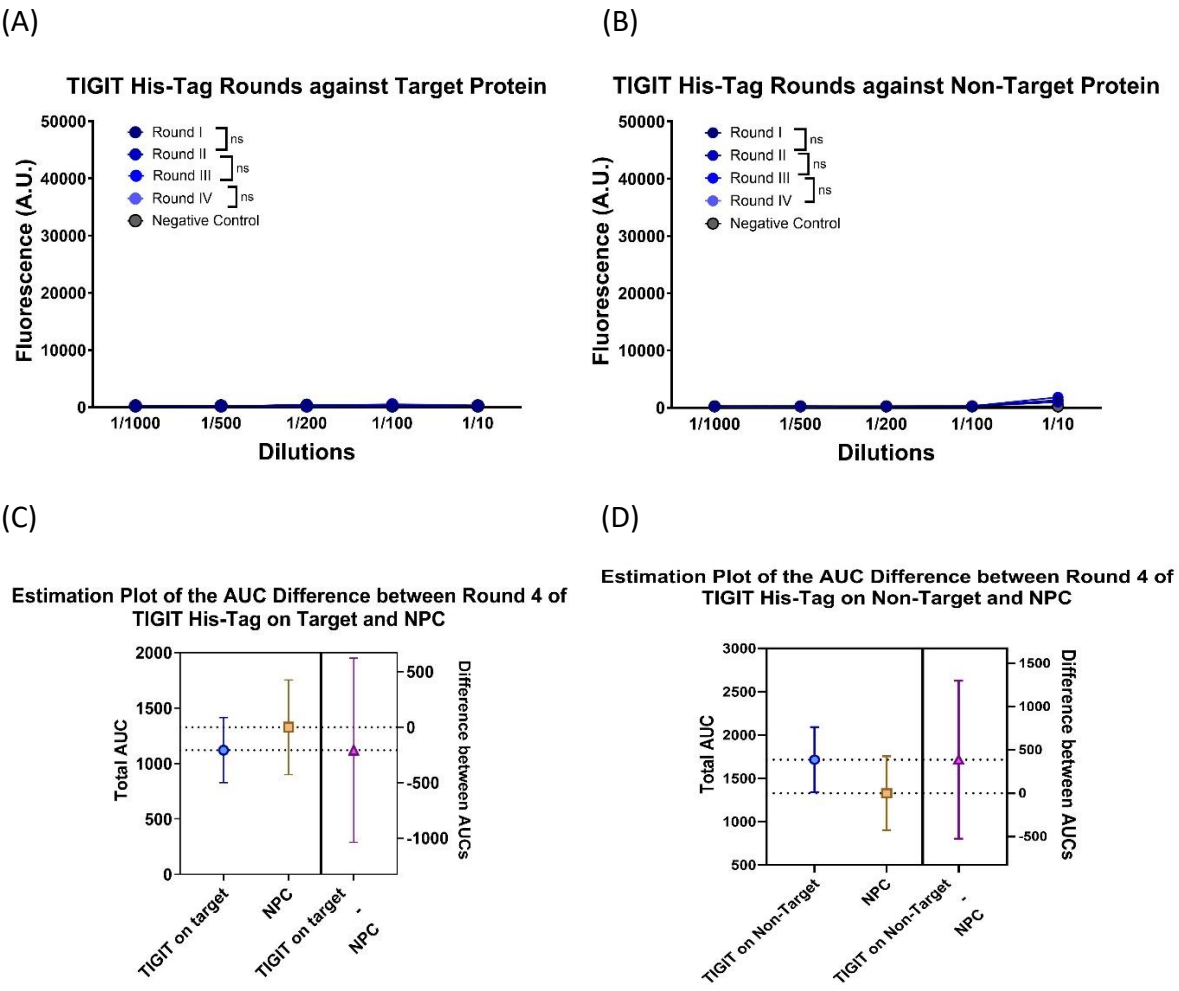

Figure 3.5: A figure showing the graphs of the 5 phage dilutions of rounds 1-4 TIGIT His-tag against the measured fluorescence in Arbitrary Units (A.U.) of the anti-M13-PE. *Graph (A) shows the four rounds of enriched library bound to TIGIT protein, while (B) shows the four rounds on non-target protein. Graphs (C) and (D) show estimation plots comparing the total AUC of round 4 TIGIT enriched library and round 4 of the NPC. All fluorescence measurements were performed in 12 replicates for each well. The error bars of each graph show 95% CI.*

Therefore, similarly to CD47, it was decided to attempt biopanning with TGIT Fc protein on Protein G beads as an attempt to improve yield of specific scFv phages. Biopanning of CD47

Fc and TIGIT Fc was done simultaneously, and phage titration of the TIGIT rounds was only performed twice in the first and final rounds, as summarised in **Table 3.5**.

Table 3.5: A table showing the Colony forming unit (CFU/mL) and therefore the phage concentration (PFU/mL) of each round of TIGIT Fc phages. *This was calculated with the formula described in Section 2.2.4 using the dilution factor of the enriched library and the number of colonies counted.*

TIGIT (Fc)			
Round	**Number of Colonies**	**Dilution Factor**	**Colony Forming Unit (CFU/ml)**
I	36	10^{10}	7.2×10^{12}
IV	57	10^{10}	11.4×10^{12}

An ELISA of the TIGIT Fc rounds was performed simultaneously as that for the CD47 Fc rounds, using the same positive (round 4 GITR) and negative (no library) controls on the plate. Dilutions of all four rounds of TIGIT library against bound target and non-target protein were prepared and fluorescence measured using anti-M13-PE antibody. Unfortunately, once again, biopanning was found to be unsuccessful in the isolation of phages expressing high affinity and high specificity anti-TIGIT scFv. The differences in the AUC between the TIGIT rounds as were not considered statistically significant, on both target and non-target proteins. Furthermore, estimation plots comparing the AUC of round 4 TIGIT Fc and round 4 of the NPC also showed fluorescence levels to be significantly lower for TIGIT than the NPC.

The appropriate graphs of the results of the TIGIT Fc biopanning rounds may be seen in **Figure 3.6**.

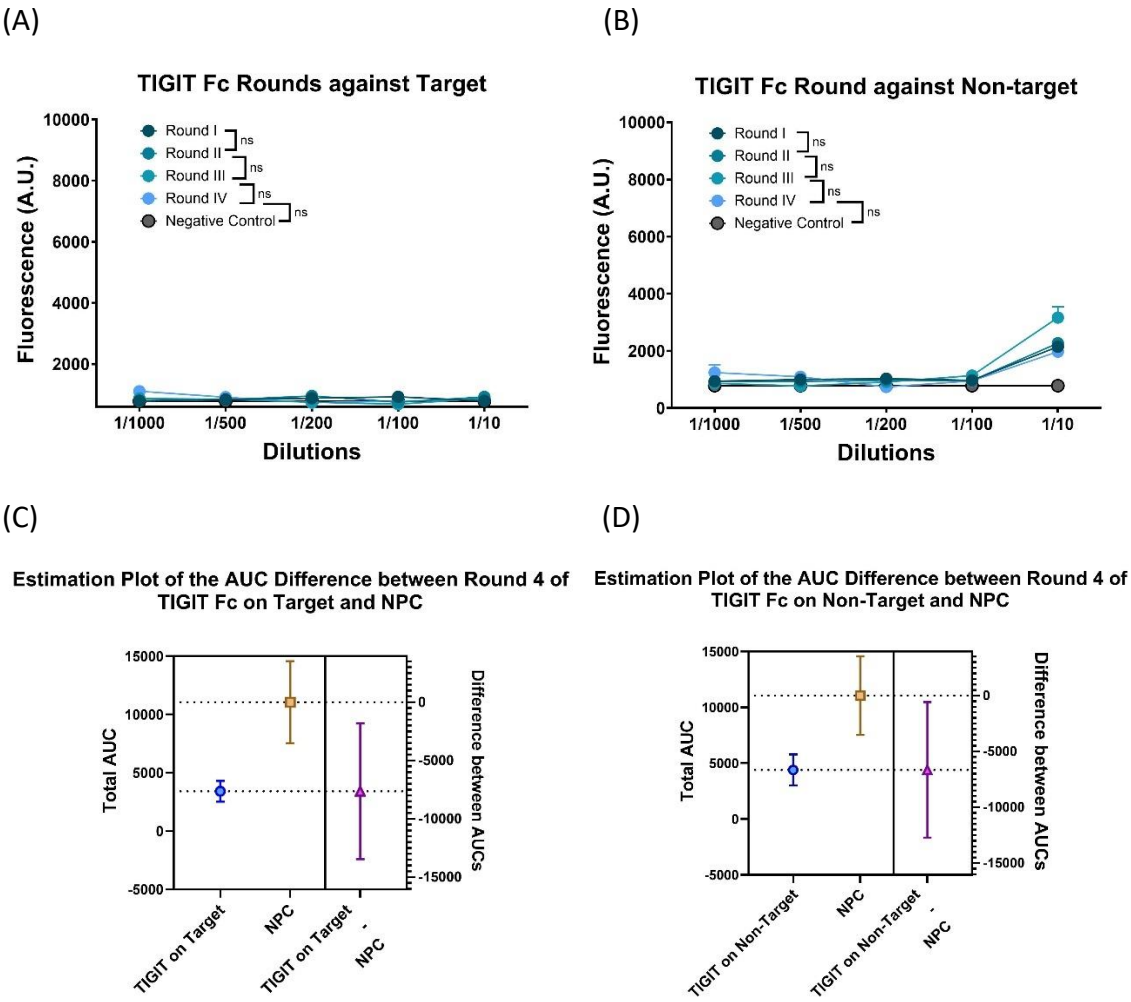

Figure 3.6: A figure showing the graphs of the 5 phage dilutions of rounds 1-4 TIGIT Fc against the measured fluorescence in Arbitrary Units (A.U.) of the anti-M13-PE. *Graph (A) shows the four rounds of enriched library bound to TIGIT protein, while (B) shows the four rounds on non-target protein. Graphs (C) and (D) show estimation plots comparing the total AUC of round 4 TIGIT enriched library and round 4 of the NPC. All fluorescence measurements were performed in 12 replicates for each well. The error bars of each graph show 95% CI.*

At this point in the project, due to time constraints, it was decided not to continue with further biopanning rounds against CD47 and TIGIT target proteins. Further studies are needed in order to fully determine the reasons behind these failures and how they may be overcome in order to successfully produce high affinity scFv antibodies against TIGIT and CD47 using phage display biopanning techniques.

3.2 GITR Monoclonal Analysis

After confirming the successful biopanning of the phage library against GITR target, an analysis of specific monoclones of scFvs with high affinity towards GITR was conducted. From the ELISA of the biopanning rounds, it was determined that the highest amount of affinity to target was seen in round 3. Therefore, 60 clones were selected from LB carbenicillin plates holding the phage titration of Round 3 GITR. This was done by picking 30 well isolated colonies at a time, amplifying and purifying each, and discovering the highest affinity clones using an ELISA measuring each clone against target and non-target protein. As a positive control for the ELISA, the round 3 GITR polyclonal pool was used in a single well, and the negative control consisted of a well coated in target protein with no addition of phages.

The fluorescence was measured with 12 technical replicates, using anti-M13-PE antibody in each well, with the lowest level of fluorescence on each plate expected to be the negative control. While normally, the positive control of the polyclonal phage pool would be considered to have the highest amount of fluorescence exhibited, it should be kept in mind that the round 3 enriched library was produced using M13KO7 helper phage, while the clones were amplified with hyperphage, which has been confirmed to give yields of phages 2-3 times higher than when using helper phage (Rondot, Koch et al. 2001, Breitling, Broders et al. 2010). Therefore, it is not completely surprising that several clones show a higher level of fluorescence than the positive control.

The level of fluorescence (A.U.) of each clone against the target and non-target protein were compared, and those clones which showed a statistically significant amount of preferential binding to the target protein were said to have a high binding affinity. On the graph, a line was drawn based on the highest peak showing non-specific binding, with any peaks falling

below the line being excluded from analysis. Of the 60 clones chosen, only 17 were seen to show a low affinity to the target, while the remaining 43 clones could be classified as having a high affinity towards the GITR target. The graphs showing all 60 clones may be seen in **Figure 3.7**.

Of the isolated clones, the only low affinity clones were the following: 7, 11, 12, 14, 17, 18, 19, 26, 28, 39, 42, 43, 44, 50 54, 55, and 56. Several of these such as clones 11 and 44 showed a higher level of fluorescence towards the non-target bait protein over the target, while clone 7 was seen to have fluorescence levels comparable to the negative control for both proteins, thus showing almost no level of binding to either bait protein. On the other hand, while clones 12, 14, 26, and 28 all showed a higher level of affinity towards the target than the non-target protein, their levels of fluorescence were much lower than that of many of the other high affinity clones, and were seen to be comparable to the fluorescence levels shown by the non-specific clones.

Before these 60 clones were selected, an initial 30 clones of round 3 GITR as well as the NPC were selected and amplified using helper phage rather than hyperphage. The results for these clones are discussed in **Appendix F**.

(A)

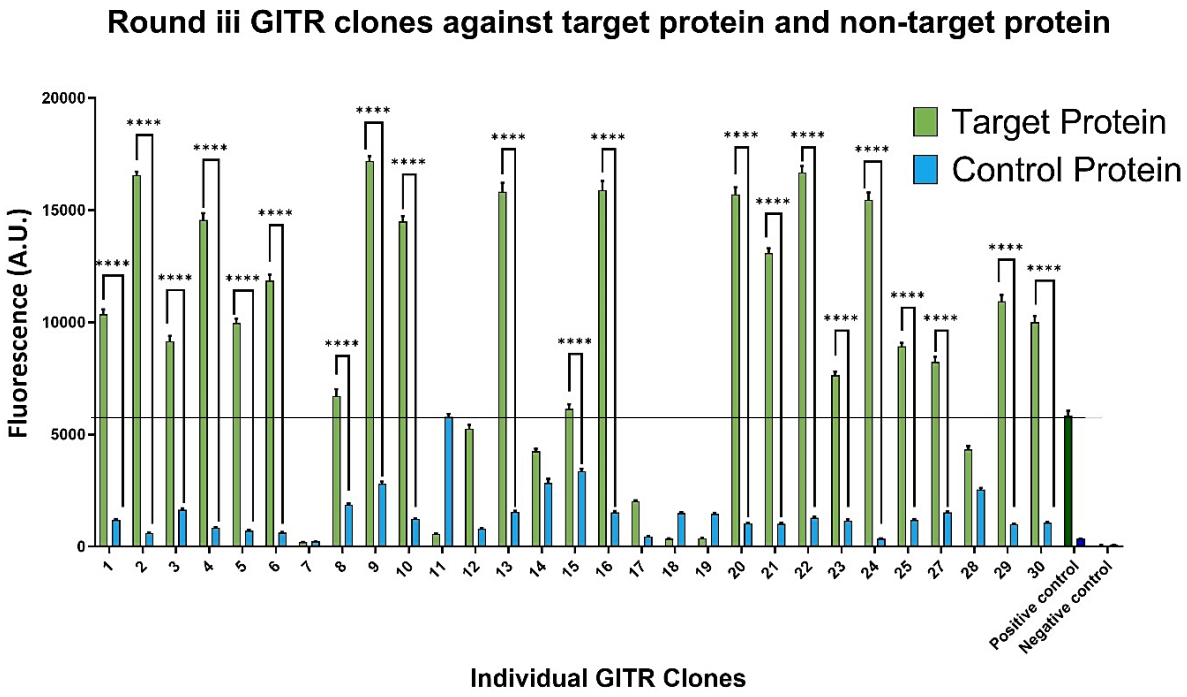

(B)

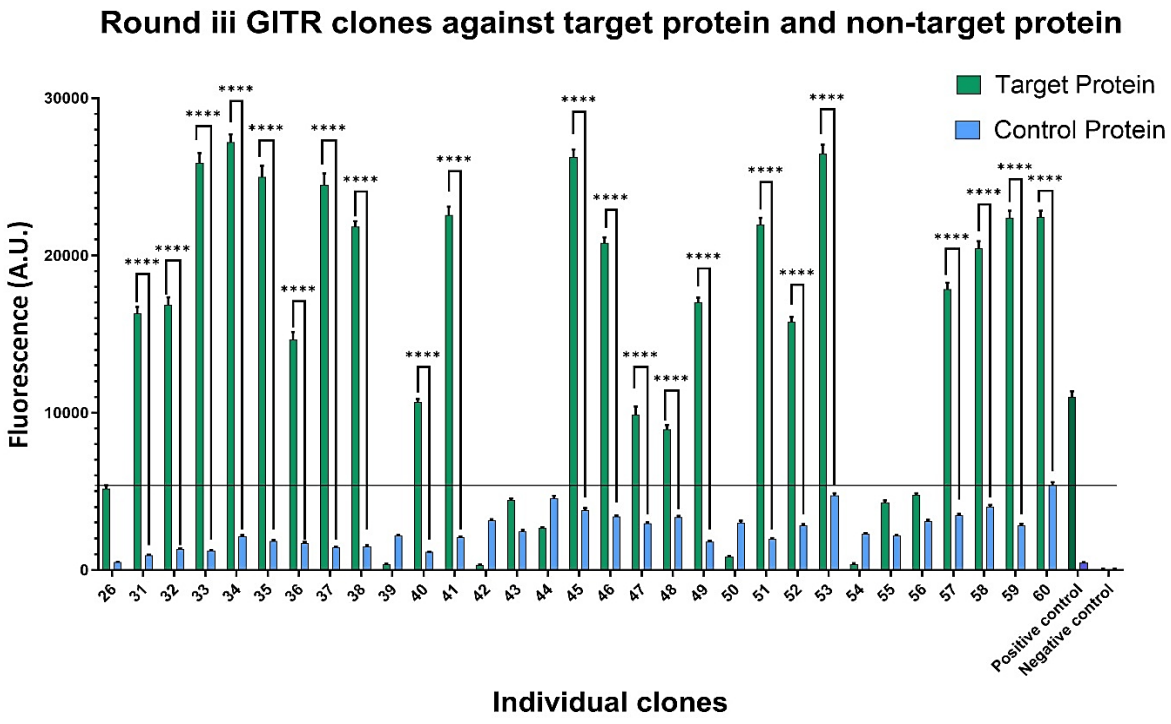

Figure 3.7: Graphs showing the individual monoclones expressing scFv antibodies against GITR His-tag, bound to both the target and the SARS-CoV-2 Spike S1 non-target bait proteins. *Graph (A) shows monoclones 1-30 without 26, while graph (B) shows clones 31-60, with added 26. Clone 26 was added to the second graph due to an error during preparation which gave the need for it to be discarded in the first round of clone picking and thus added into the second. From the levels of fluorescence shown, it can be seen that the majority of clones show a high level of binding affinity and specificity to the target with a few exceptions, although some clones show a much higher affinity than others.*

3.3 Sanger Sequencing and Analysis of Monoclones

After the selection, amplification, and purification of the 60 individual anti-GITR scFv monoclones described in **Section 3.2**, each of these clones were sent abroad to LGC Genomics GmbH in Berlin for sanger sequencing. Extraction of the DNA plasmid of the PC1 culture of each clone was performed, and the level of DNA was determined using the NanoDrop, the results of which may be seen in **Appendix G**.

The program SnapGene [SnapGene By Dotmatics, GSL Biotech LLC, Boston, Massachusetts, US] was used to analyse the data received and determine the exact amino acid sequences of each clone to compare and contrast. The CDRs of the VL and the VH chain of each clone were identified and labelled, and the clones were manually aligned and sorted based on the similarity of CDR3-VH. Of the 60 clones sent for sequencing, the only ones which failed to be sequenced were clone 36, 39 and 42, of which only clone 36 showed good binding affinity. Clones 39 and 42 also showed very low NanoDrop readings, along with a low affinity to the target. Of the other clones, almost all were fully sequenced except for clone 38, which showed a stop codon shortly after the CDR2- VL, although surprisingly, it still showed a high level of affinity to the target protein in the ELISA.

A dendrogram, seen in **Figure 3.8**, was created from a csv file of the CDR3-VH and CDR3-VL of each sequenced clone in order to more easily compare and group the amino acid sequences based on similarity. The software used to generate the dendrogram was designed by Ms. Francesca Chircop specifically for the purposes of this research. From the dendrogram, it can be seen that, while there is some variation in sequence, many of the isolated clones share the same or similar sequence to several others. Of the most common sequence, belonging to the largest group of 24 clones (yellow), most were strong binders, with the exception of clones

14 and 17, which showed a lower affinity. On the other hand, of the second largest group of 18 clones (green), seven were poor binders, while the rest, while showing affinity for GITR, overall exhibited a slightly lower amount of fluorescence than other high-binding scFv clones, based on the height of the peaks observed from the monoclonal ELISA. Also, it should be noted that in this group, clones 18 and 19, which were identified as poor binders, exhibited the same VH CDR sequences of their own group (green), but the VL CDR sequences matched that of the previous group (yellow).

Additionally, two more smaller groups (red) containing 4 and 3 similar clones respectively were also identified, all of which showed high levels of specificity and affinity to GITR.

Finally, the remaining 8 clones were found to have unique sequences mostly unrelated to each other or to other clones. Of these, only two were found to strongly bind to GITR, while some, such as clone 11, showed a high amount of non-specific binding. With help from the dendrogram, the clones were manually aligned based on all three CDRs of the VH and VL regions, which may be seen in **Table 3.5**.

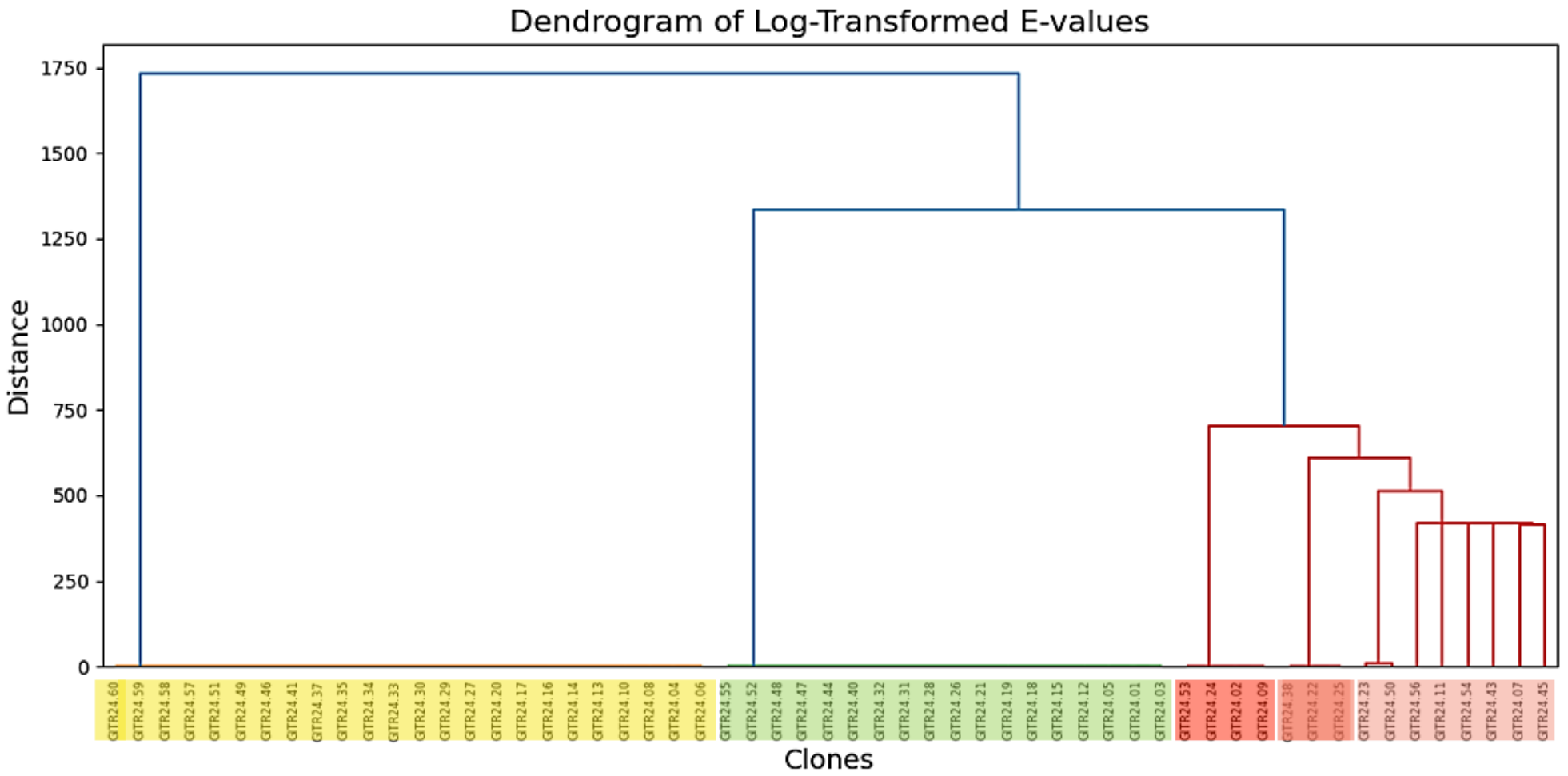

Figure 3.8: A dendrogram showing the position of each clone based on the amino acid sequence of the CDR3-VH and CDR3-VL regions. *From the dendrogram, it can be seen that the clones may be categorised into two larger and two smaller groups of nearly identical CDR3s, with the rest having unique sequences.*

Table 3.6: A table showing the manual alignment of amino acid sequences of all CDRs of the VH and VL chains of the sequenced clones. *Each coloured section represents a different group of clones as sorted by the dendrogram. All non-binding clones from each section are marked with an * symbol for convenience.*

Clone	CDR1-VH	CDR2-VH	CDR3-VH	CDR1-VL	CDR2-VL	CDR3-VL
GITR24.04	SYSMS	GINSGGSSTYYTDAVKG	YPGGGTILPD	TGSSSNIGGNYVG	GNNYRPS	SSWDDSLRGSV
GITR24.06	SYSMS	GINSGGSSTYYTDAVKG	YPGGGTILPD	TGSSSNIGGNYVG	GNNYRPS	SSWDDSLRGSV
GITR24.08	SYSMS	GINSGGSSTYYTDAVKG	YPGGGTILPD	TGSSSNIGGNYVG	GNNYRPS	SSWDDSLRGSV
GITR24.10	SYSMS	GINSGGSSTYYTDAVKG	YPGGGTILPD	TGSSSNIGGNYVG	GNNYRPS	SSWDDSLRGSV
GITR24.13	SYSMS	GINSGGSSTYYTDAVKG	YPGGGTILPD	TGSSSNIGGNYVG	GNNYRPS	SSWDDSLRGSV
GITR24.14*	**SYSMS**	**GINSGGSSTYYTDAVKG**	**YPGGGTILPD**	**TGSSSNIGGNYVG**	**GNNYRPS**	**SSWDDSLRGSV**
GITR24.16	SYSMS	GINSGGSSTYYTDAVKG	YPGGGTILPD	TGSSSNIGGNYVG	GNNYRPS	SSWDDSLRGSV
GITR24.17*	**SYSMS**	**GINSGGSSTYYTDAVKG**	**YPGGGTILPD**	**TGSSSNIGGNYVG**	**GNNYRPS**	**SSWDDSLRGSV**
GITR24.20	SYSMS	GINSGGSSTYYTDAVKG	YPGGGTILPD	TGSSSNIGGNYVG	GNNYRPS	SSWDDSLRGSV
GITR24.27	SYSMS	GINSGGSSTYYTDAVKG	YPGGGTILPD	TGSSSNIGGNYVG	GNNYRPS	SSWDDSLRGSV
GITR24.29	SYSMS	GINSGGSSTYYTDAVKG	YPGGGTILPD	TGSSSNIGGNYVG	GNNYRPS	SSWDDSLRGSV
GITR24.30	SYSMS	GINSGGSSTYYTDAVKG	YPGGGTILPD	TGSSSNIGGNYVG	GNNYRPS	SSWDDSLRGSV
GITR24.33	SYSMS	GINSGGSSTYYTDAVKG	YPGGGTILPD	TGSSSNIGGNYVG	GNNYRPS	SSWDDSLRGSV
GITR24.34	SYSMS	GINSGGSSTYYTDAVKG	YPGGGTILPD	TGSSSNIGGNYVG	GNNYRPS	SSWDDSLRGSV
GITR24.35	SYSMS	GINSGGSSTYYTDAVKG	YPGGGTILPD	TGSSSNIGGNYVG	GNNYRPS	SSWDDSLRGSV
GITR24.37	SYSMS	GINSGGSSTYYTDAVKG	YPGGGTILPD	TGSSSNIGGNYVG	GNNYRPS	SSWDDSLRGSV
GITR24.41	SYSMS	GINSGGSSTYYTDAVKG	YPGGGTILPD	TGSSSNIGGNYVG	GNNYRPS	SSWDDSLRGSV
GITR24.46	SYSMS	GINSGGSSTYYTDAVKG	YPGGGTILPD	TGSSSNIGGNYVG	GNNYRPS	SSWDDSLRGSV
GITR24.49	SYSMS	GINSGGSSTYYTDAVKG	YPGGGTILPD	TGSSSNIGGNYVG	GNNYRPS	SSWDDSLRGSV
GITR24.51	SYSMS	GINSGGSSTYYTDAVKG	YPGGGTILPD	TGSSSNIGGNYVG	GNNYRPS	SSWDDSLRGSV
GITR24.57	SYSMS	GINSGGSSTYYTDAVKG	YPGGGTILPD	TGSSSNIGGNYVG	GNNYRPS	SSWDDSLRGSV
GITR24.58	SYSMS	GINSGGSSTYYTDAVKG	YPGGGTILPD	TGSSSNIGGNYVG	GNNYRPS	SSWDDSLRGSV
GITR24.59	SYSMS	GINSGGSSTYYTDAVKG	YPGGGTILPD	TGSSSNIGGNYVG	GNNYRPS	SSWDDSLRGSV
GITR24.60	SYSMS	GINSGGSSTYYTDAVKG	YPGGGTILPD	TGSSSNIGGNYVG	GNNYRPS	SSWDDSLRGSV
GITR24.18*	**NYAMS**	**DISSSGSTYYADAVRG**	**VPGLDNFDS**	**TGSSSNIGGNYVG**	**GNNYRPS**	**SSWDDSLRGAV**
GITR24.19*	**NYAMS**	**DISSSGSTYYADAVRG**	**VPGLDNFDS**	**TGSSSNIGGNYVG**	**GNNYRPS**	**SSWDDSLRGAV**
GITR24.01	NYAMS	DISSSGSTYYADAVRG	VPGLDNFDS	SGESLNRHYAQ	KDTERPS	GSDVNSGTAYE
GITR24.03	NYAMS	DISSSGSTYYADAVRG	VPGLDNFDS	SGESLNRHYAQ	KDTERPS	GSDVNSGTAYE

Clone	CDR1-VH	CDR2-VH	CDR3-VH	CDR1-VL	CDR2-VL	CDR3-VL
GITR24.05	NYAMS	DISSSGSTYYADAVRG	VPGLDNFDS	SGESLNRHYAQ	KDTERPS	GSDVNSGTAYE
GITR24.12*	**NYAMS**	**DISSSGSTYYADAVRG**	**VPGLDNFDS**	**SGESLNRHYAQ**	**KDTERPS**	**GSDVNSGTAYE**
GITR24.15	NYAMS	DISSSGSTYYADAVRG	VPGLDNFDS	SGESLNRHYAQ	KDTERPS	GSDVNSGTAYE
GITR24.21	NYAMS	DISSSGSTYYADAVRG	VPGLDNFDS	SGESLNRHYAQ	KDTERPS	GSDVNSGTAYE
GITR24.26*	**NYAMS**	**DISSSGSTYYADAVRG**	**VPGLDNFDS**	**SGESLNRHYAQ**	**KDTERPS**	**GSDVNSGTAYE**
GITR24.28*	**NYAMS**	**DISSSGSTYYADAVRG**	**VPGLDNFDS**	**SGESLNRHYAQ**	**KDTERPS**	**GSDVNSGTAYE**
GITR24.31	NYAMS	DISSSGSTYYADAVRG	VPGLDNFDS	SGESLNRHYAQ	KDTERPS	GSDVNSGTAYE
GITR24.32	NYAMS	DISSSGSTYYADAVRG	VPGLDNFDS	SGESLNRHYAQ	KDTERPS	GSDVNSGTAYE
GITR24.40	NYAMS	DISSSGSTYYADAVRG	VPGLDNFDS	SGESLNRHYAQ	KDTERPS	GSDVNSGTAYE
GITR24.44*	**NYAMS**	**DISSSGSTYYADAVRG**	**VPGLDNFDS**	**SGESLNRHYAQ**	**KDTERPS**	**GSDVNSGTAYE**
GITR24.47	NYAMS	DISSSGSTYYADAVRG	VPGLDNFDS	SGESLNRHYAQ	KDTERPS	GSDVNSGTAYE
GITR24.48	NYAMS	DISSSGSTYYADAVRG	VPGLDNFDS	SGESLNRHYAQ	KDTERPS	GSDVNSGTAYE
GITR24.52	NYAMS	DISSSGSTYYADAVRG	VPGLDNFDS	SGESLNRHYAQ	KDTERPS	GSDVNSGTAYE
GITR24.55*	**NYAMS**	**DISSSGSTYYADAVRG**	**VPGLDNFDS**	**SGESLNRHYAQ**	**KDTERPS**	**GSDVNSGTAYE**
GITR24.02	GYYMY	RITSDGSSTYYGDAVKG	EAWNTYGPVY	GGDNIGSKSVH	DDSSRPT	QVWDSSAKASV
GITR24.24	GYYMY	RITSDGSSTYYGDAVKG	EAWNTYGPVY	GGDNIGSKSVH	DDSSRPT	QVWDSSAKASV
GITR24.09	GYYMY	RITSDGSSTYYGDAVKG	EAWNTYGPVY	GGDSIGDKSVQ	GDSYRPS	SSWDNRLRGSV
GITR24.53	GYYMY	RITSDGSSTYYGDAVKG	EAWNTYGPVY	GGDSIGDKSVQ	GDSYRPS	SSWDNRLRGSV
GITR24.22	SYGMT	DITRSGTTYYADAVKD	IAAWKDEY	GGDSIGSKYVQ	KDSNRPT	QVWDGSAKLL
GITR24.25	SYGMT	DITRSGTTYYADAVKD	IAAWKDEY	SGESLSKFYAQ	KDTERPS	ESAVSTDTVV
GITR24.38	SYGMT	DITRSGTTYYADAVKD	IAAWKDEY	SGESLSKFYAQ	KDTERP	n/a
GITR24.07*	**TYGMH**	**SVDSGGRTVYADAVKG**	**DAYSGRGNPEY**	**EGNNIGDKYVH**	**EDTKRPS**	**ESAVSPDAV**
GITR24.11*	**NYGMN**	**GISSSGNTHYADAVKG**	**GPYNGH**	**GGDSIGSKSVH**	**GDLSRPS**	**QIWDRNTKTIV**
GITR24.23	NHYMS	YINSGGDKIYYADAVKG	GVVGTYGDLEY	EGNNIGDKYAY	EDSKRPS	ESIDSTDKAIV
GITR24.43*	**NYSMS**	**GINSGGNTGYADAVKG**	**GSPYYESYES**	**EGDRVGSRNVY**	**DDSSRPS**	**QVGDSNTKHGV**
GITR24.45	TYEMT	QIDSSGNTYYADAVKG	GSSYDRWSGYDMDY	GGDNIGSKTVQ	GDISRPS	QVWDRSAAV
GITR24.50*	**TYGMN**	**GIDSGGNTDYADAVKG**	**PGYYDRYYGELEY**	**TLSSEHSNYIVR**	**VRSDGSYKRGD**	**GADYTISGQHGFV**
GITR24.54*	**SYSMY**	**DINSDGSSTHYTDAVKG**	**ASDRDNLEY**	**TGSSSNIGRYVA**	**DINKRPS**	**SSYDSLSGAV**
GITR24.56*	**NYDMS**	**AIDSGGSNTRYADAVKG**	**RWGAAH**	**SGESLTKYYAQ**	**KDTERPS**	**ESEVKTGTASV**

Therefore, from the above alignment, it can be concluded that not all of the high affinity anti-GITR scFv monoclones identified share the same amino acid sequence. Using SWISS-MODEL, 3D structures of some of the highest and lowest binding scFvs were generated. **Figure 3.9** shows the model and Ramachandran plot of clone 34, one of the highest binding scFv clones of the largest group (yellow).

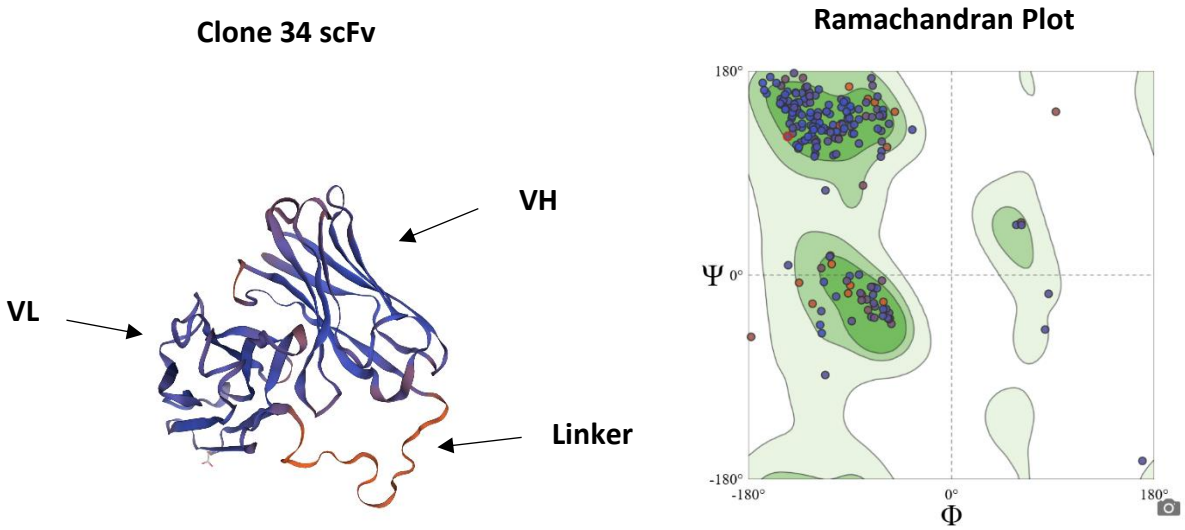

Figure 3.9: The 3D structure of clone 34, composed of the VL and VH, connected by a flexible linker. *The Ramachandran plot (right) compares the phi and psi angles of each amino acid, separated out into alpha-helical (bottom left quadrant) and beta strand (top left quadrant) conformations. The cluster in the upper right quadrant represents turns in the amino acid sequence. Based on the regularity of these clusters, it can be concluded the model generated for this scFv is of a good quality.*

On the other hand, **Figure 3.10** shows the same of clone 11, a unique clone with low binding affinity and the highest levels of non-specific binding. Further such models of other clones may be seen in **Appendix I**.

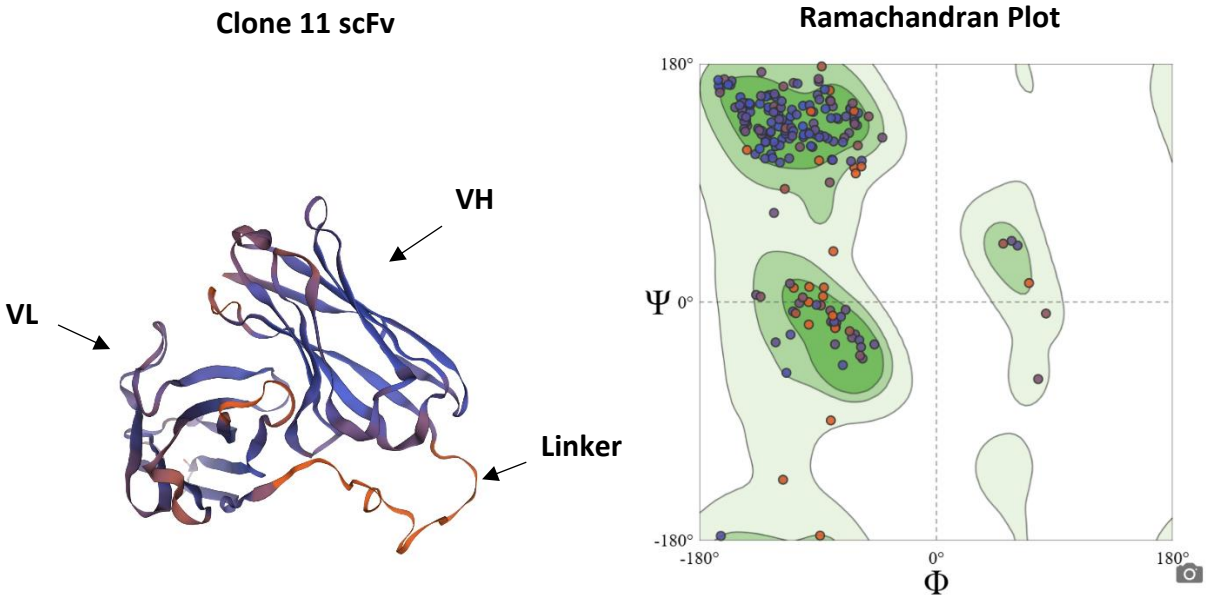

Figure 3.10: The 3D structure of clone 11, composed of the VL and VH, connected by a flexible linker. *The Ramachandran plot (right) compares the phi and psi angles of each amino acid, separated out into alpha-helical (bottom left quadrant) and beta strand (top left quadrant) conformations. The cluster in the upper right quadrant represents turns in the amino acid sequence. Based on the regularity of these clusters, it can be concluded the model generated for this scFv is of a good quality.*

Using the structures obtained from SWISS-MODEL, a protein docking model was also created using the HADDOCK v2.4 online software. The pdb file was obtained for clone 34 directly from SWISS-MODEL, while the crystalline structure and pdb file for GITR were both obtained using the AlphaFold Protein structure database (Tumour necrosis factor receptor superfamily member 18) and UniProtKB (Q9Y5U5 - TNR18_HUMAN). The generated model may be seen in **Figure 3.11**.

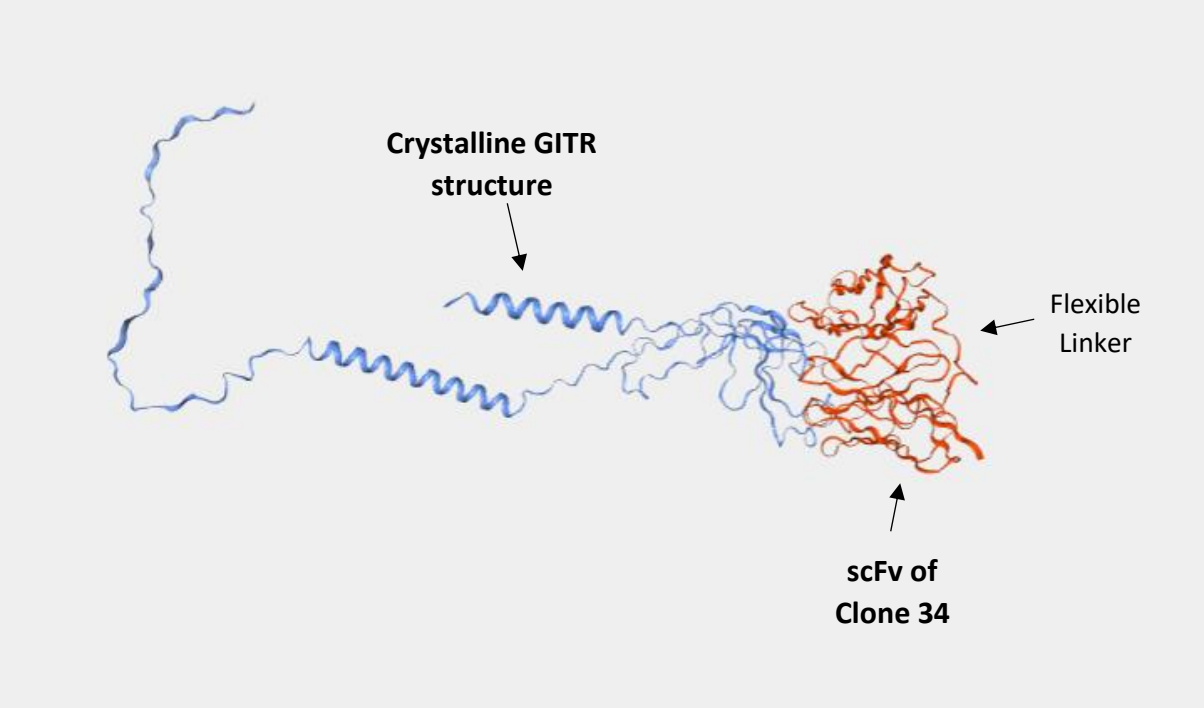

Figure 3.11: A figure showing the protein docking model of clone 34 and GITR, as obtained by HADDOCK 2.4 online software. *The structure represents the best of the top 10 most reliable clusters identified with a HADDOCK score of -11.7 +/- 10.8 and a Z-score of -1.7. The Z-score in this case represents the number of standard deviations of the cluster from the average in terms of overall score, with the more negative it is, the better. While the scores generated by HADDOCK are not perfectly correlated with binding affinity of the proteins, they are still a useful tool in the determination of the possible relationship between the generated scFv antibody fragment and the target protein.*

The HADDOCK program clustered 171 structures into 11 total clusters representing 85 % of the water-refined models generated by HADDOCK. When examining the statistics of the most reliable cluster, a HADDOCK score of -11.7 +/- 10.8 was observed with a Z-score of -1.7. While the Z-score acts as a measure of standard deviations from the average score, the HADDOCK score is a numerical value assigned by HADDOCK as an indication of the quality of the protein-scFv complex. In the case of both Z-scores and HADDOCK scores, a negative value represents a favourable interaction, with the more negative a score is, the more stable the reaction supposedly is (Bonvin 2025b). A full list of all the parameters listed for this cluster may be found in **Appendix J**.

4. Discussion

The main purpose of this study was to utilise the phage display biopanning technique to produce unique scFv antibodies with a high affinity and specificity to immune checkpoint proteins, which could be used to elicit heightened immune responses against malignant cells in humans. The immune checkpoints chosen to be the focus of this study were GITR, CD47, and TIGIT. Anti-GITR scFv antibodies were successfully identified over the course of this study, after carrying out 4 rounds of biopanning, which was confirmed using an ELISA of each enriched library carrying anti-GITR scFv as well as individual anti-GITR clones, against both the target protein, and the unrelated non-target protein SARS-CoV-2 Spike S1. After a review of the available literature, as of the writing of this discussion, it appears that this is one of the first times scFv antibody fragments specific to GITR have been successfully identified using phage display techniques. From the enriched library showing the highest affinity binding, which was achieved by the third round of biopanning, a total of 43 high affinity phage anti-GITR monoclones were identified and sent for sanger sequencing. The data was analysed using SnapGene, and it was determined that the majority of the identified high affinity monoclones shared similarities in the complementarity determining regions of the variable light and variable heavy chains of most of the strongly binding phage clones.

On the other hand, phage display biopanning failed to identify scFv antibodies specific to the CD47 and TIGIT targets, despite carrying out a total of 8 rounds of biopanning in two separate attempts, while making use of different types of bait protein (His-tagged and Fc-tagged). This was surprising due to the aforementioned success of the use of phage display in the identification of anti-GITR scFv, since the process was carried out simultaneously for all three checkpoints, making use of identical reagents and methodology. This result also goes against

some of the more recently available literature, which references the successful application of phage display techniques in the identification of various anti-CD47 and anti-TIGIT antibodies/antibody fragments (Musnier, Corde, et al. 2025, Zeng, Sun, et al. 2016).

In fact, over the course of this study, it was discovered that two different anti-CD47 antibodies generated by phage display have already been approved for use in therapeutic settings, those being Lemzoparlimab and STI−6643. Clinical trial results of Lemzoparlimab monotherapy as well as in combination with Rituximab (anti-CD20) have so far shown a significant level of efficacy against Non-Hodgkin's Lymphoma with minimal adverse effects (Mehta, Harb et al. 2021). Furthermore, while clinical trials of STI−6643 are still on-going, a significantly improved T cell functionality and a decrease in immune cell depletion have been observed both *in vitro* and *in vivo*, as opposed to other similarly studied anti-CD47 clones that have been produced (Thaker, Rivera et al. 2022, *Study of the Safety and Efficacy of STI-6643 in Subjects With Advanced Solid Tumors* 2023-last updated). Additionally, Rilvegostomig, a combined immunotherapy of both anti-TIGIT and anti-PD-1, similarly produced using phage display, has also shown promising results in the treatment of biliary tract tumours during clinical trials (Fan, Bekaii-Saab et al. 2024). A comprehensive analysis was therefore performed of the chosen methods used over the course of this study, as well as available literature of similar studies in order to determine potential causes for this failure to produce high affinity anti-CD47 and anti-TIGIT scFv antibodies, as well as determine ways to mitigate these issues in future studies.

It is clear to see that the use of immune checkpoint specific antibodies in cancer immunotherapy is a highly promising and fast growing field of research (Sharma, Goswami et al. 2023). However, several drawbacks have also been identified with this type of therapy,

such as the emergence of autoimmune symptoms due to non-specific attacks on healthy cells by the immune checkpoint therapy, unsatisfying response rates to malignancies with low mutational burden, as well as a general loss of effectiveness over time due to adaptive resistance of the malignant cells (He, Xu 2020). Therefore, in order to mitigate these disadvantages, the identification of novel immunotherapeutic targets within the tumour microenvironment has become the primary focus of research in this field of study, as well as the successful identification of specific antibodies capable of carrying out the necessary regulatory effects which would lead to a positive clinical outcome (Kamali, Bautista et al. 2023). The three immune checkpoints chosen for the study are only a few of several such emerging attractive targets (Davar and Zappasodi 2023, Yang, Xun et al. 2023, Zhang, Liu et al. 2024). Conversely, phage display has quickly emerged as a powerful tool in the generation of monoclonal antibodies and antibody fragments, improving their binding affinity, as well as discovering new epitopes of tumour antigens, all of which is vital to the advancement of this technology (Bazan, Całkosiński et al. 2012). It has also been shown to be far less costly and time intensive than many of the other most commonly utilised methods to produce IC regulatory antibodies, such as in the use of hybridomas and single B cell sorting. However, it should also be noted that one of the biggest weaknesses of this methodology is the increased potential for the production of lower affinity or low specificity antibodies, when compared to other methods of antibody generation (Istomina, Gorchakov et al. 2024). This was seen first-hand over the course of this study.

One of the first sources of error considered in this study stemmed from the original canine phage library itself. The library chosen for this study was a canine derived library of type III (pIII) phages carrying a wide range of scFv specific to human immune checkpoints. While phage libraries using other types of phages do exist, such as type VIII (pVIII) phages, and have

been successfully used to perform phage display of smaller peptides, it is widely posited, that for the display and amplification of more complex proteins such as scFv, the pIII phage library is preferable (Aripov, Volkova et al. 2024).

One of the largest strengths of a phage library is the sheer diversity of different scFv antibodies that may be expressed and represented on individual phages. However, typically, phage libraries are limited to around 10^{10} to 10^{12} scFv variants, with the naïve library used in this study only having a confirmed 10^{9} scFv variants, which may not be enough to contain all possible binders to a particular protein of interest. Many of the scFvs expressed may also be artificial types that would never have been produced by B cells and thus have unclear affinities (DeKosky, Ippolito et al. 2013). It has been found that some proteins of interest may even interfere directly with phage assembly, making it nearly impossible for those proteins to be fully expressed within the library. Furthermore, due to the nature of phage libraries there is a certain level of expression bias of scFvs that may at first appear to bind strongly to a target, but in actuality, fail *in vivo* due to a lack of full protein folding mechanisms in Eukaryotic cells, that preferentially express some proteins over others. This often leads to the accidental exclusion of strong binders, and thus further limits the display of some antibodies. Finally, it should be noted that there could have been a loss of DNA during library construction due to repetitive purifications, which may have led to a loss of relevant scFvs from the final library (Kerry 2025, Hammers, Stanley 2014).

Apart from the inherent limitations of the library, loss of phages may have occurred due to improper storage and handling of the original phage library during the course of the study. Prior to the first biopanning, the phage library had been stored at -20^{o}C, and had undergone multiple freeze thaw cycles, which may have led to the degradation of some high affinity scFv

phages. This is the reason why for the second biopanning attempt of CD47 and TIGIT, a fresh original library was obtained, aliquoted, and stored at -80^{o}C in order to avoid such errors. Furthermore, a larger volume was used in the initial biopanning round as a way of increasing the chances of including phages carrying scFvs with high affinity to the targets. The continued lack of amplification of high affinity phages for these two targets, shows that the issues likely do not stem from improper handling of library, and may therefore be due to an inherent weakness of the original phage library used (Andre, Moutinho et al. 2022, Baek, Suk 2002).

Sinkjaer, Sloth et al. 2025 also note the high level of heterogenicity and non-uniformity within peptide sequences present in different lots of the same type of original phage library, despite maintaining identical steps within its construction, which may lead to completely different biopanning outcomes, as was seen between the different attempts with CD47 His-tag and Fc-tag target proteins. This conclusion would suggest the need for alternate phage libraries in subsequent biopanning attempts or even contemplating the viability of the construction of an in house original phage library, to ensure all research needs are met (André, Moutinho et al. 2022).

It should be noted that the act of amplification itself, while necessary for increasing the numbers of the identified high affinity phages, also always leads to a loss of diversity of the library. This almost always leads to a loss of some high affinity clones, due to amplification bias of the fastest propagating phage clones, which often outcompete other clones that may have had higher affinity scFv to the target protein (Derda, Tang et al. 2011, Hoen, Jirka et al. 2011).

This phenomenon is another common weakness of the phage display method and may be one of the largest reasons for non-specific binding of enriched phage libraries, as well as the

noted loss of affinity in subsequent biopanning rounds, as was seen between rounds 3 and 4 of GITR, and even within rounds 3 and 4 of the first try of biopanning against CD47. This is also why it was decided that performing more than 4 biopanning rounds against the targets would not be conducive to the selection of a wide diversity of high affinity clones. (Sinkjaer, Sloth et al. 2025, Derda, Tang et al. 2011).

This observed amplification bias may also have been exacerbated due to deficient helper phage during this step. To facilitate amplification, phagemid vectors carrying the gene encoding the pIII-scFv fusion protein are the main method through which infection of the bacterial cells occurs. Since these phagemids often lack the necessary genes encoding for assembly of new phages, the helper phage is vital to providing the necessary components for infection, replication, assembly and budding. The M13KO7 helper phage is the most widely used for this procedure, with all other available helper phages being derivatives of this phage. The helper phage is designed in such a way that it contains a relatively low number of copies of the p15A replication start site, as opposed to the pIII-scFv phagemid, allowing for the phagemid to displace helper phage genome during replication. However, in practice, it has been found that the wild-type pIII encoded by helper phage often outcompetes the pIII-scFv complex encoded by the phagemid, often leading to a large number of phages being produced that do not carry scFv, otherwise known as “bald” phages. One way in which to potentially mitigate this issue is through the use of alternative helper phages (Aripov, Volkova et al. 2024, Kramer 2003).

One such alternative is hyperphage, which was used during the amplification of individual phage clones from round 3 of the anti-GITR scFv enriched library. As stated previously, hyperphage, while expressing a wild type pIII phenotype, allowing for infection through the

F+ pilus of *E. coli*, does not have a functional pIII gene. This counteracts the main limitation of the M13KO7 helper phages, which is the preferential inclusion of the wild-type pIII over the pIII-scFv fusion protein into newly generated phages and therefore ensures the production of a much higher fraction of phages which carry scFv. This has been seen to increase the yield of high affinity phages two-three fold in many similar studies (Rondot, Koch et al. 2001, Breitling, Broders et al. 2010). While in the current study, hyperphage was only used during candidate phage clone preparation, since the M13KO7 helper phage was deemed to give sufficient results in similar phage display experiments, it is possible that the outcome of phage display biopanning for anti-CD47 and anti-TIGIT scFv may have been more favourable if hyperphage had been used instead.

Another possible candidate in consideration for alternative helper phage during biopanning is the CM13. This is a derivative of the M13KO7 helper phage, containing an interference resistance ir3B A->G mutation, which often leads to higher phage yields during biopanning (Stefan, Light et al. 2021). However, the main reason for its consideration over other helper phages is specifically due to its derivative CM13K, a trypsin sensitive helper phage, which, upon exposure to trypsin, loses the N1N2 domain of the pIII, making it impossible to further infect F+ *E. coli* cells, while leaving any pIII-scFv fusion proteins intact. This makes it so that after a time, the only phages capable of infection are those carrying the scFv, thus greatly increasing the yield of high affinity phages, similarly to hyperphage (*CM13K Trypsin-Sensitive Helper Phage INSTRUCTION MANUAL* 2023). This method has also been successfully utilised in phage display using other trypsin-sensitive helper phages, such as AGM13, although CD13K seems to be the most readily available (Gupta, Shrivastava et al. 2013).

Furthermore, another advantage of this method is the introduction of trypsin digestion as an alternate release mode to TEA which was the main mode of elution in this study. One of the largest possible sources of error in phage display is incomplete elution of strongly binding phages from the beads at the end of the biopanning procedure leading to recovery bias. Typically, elution of the phages is carried out through the breaking of the necessary non-covalent bonds between the pIII-scFv fusion protein on the viral surface and the immobilised bait protein using fluctuations in pH, such as with TEA solution (pH 11.3), or when using acid elution. Incomplete elution would therefore lead to a failure to conserve the strongest binding phages and the irreversible loss of the highest affinity scFvs from the first round, with the issue only being exacerbated with continuous rounds (Thota, Puddu et al. 2024). Furthermore, the use of the high pH TEA also runs the risk of potential degradation of displayed scFv, which may occur if the TEA solution is not immediately neutralised to a pH of about 7-8 (Kristensen, Winter 1998, Ward, Clark et al. 1996).

Contrarily, with proteolytic release using trypsin, rather than breaking the bond between the scFv and the bait protein, the scFv is cleaved from the surface of the phage, allowing for full release, irrespective of the binding affinity. This, therefore, has the potential to greatly increase the yield of high affinity phages for subsequent rounds of biopanning. Furthermore, in some cases, an increase of virulence was noted in the phages to have undergone this protein cleavage, in large part thanks to the removal of the scFv from the pIII and thus allowing for easier infection of bacterial cells during amplification. The one major disadvantage to this alternate method, is the need for a modified phage library, making use of a trypsin-sensitive tether to display the scFv. Nevertheless, it is a viable alternative to the traditional methods of phage display that has the potential to greatly increase both the yield

of phages, as well as the affinity of the identified scFv (Thomas, Smith 2010, Duan, Siegumfeldt 2010, Marsh, Witten et al. 2018).

Another important consideration taken from the beginning of the study was the choice of solid medium on which to immobilise target proteins for biopanning. From the start, beads were chosen over plates due to the work of Grima 2022 and Spiteri 2022 who found that biopanning was significantly more effective at isolating phages carrying high affinity scFv when bound to magnetic beads (McConnell, Dinh et al. 1999). Furthermore, His-tag beads were chosen for the first biopanning attempt due to concerns for potential clumping of Protein G beads that was observed for some targets by Grima 2022 and Spiteri 2022. A polyhistidine tag was expressed on the C terminus of each of the proteins of interest, which allowed for the binding of the protein to cobalt (Co^{2+}) beads through interactions of the divalent ions with the imidazole ring of the histidine tag in neutral conditions (*His Tagged Protein Purification*, 2025, Liu, Yu 2016, Hogg, Hilgenfeld 2007). However, a high level of non-specific binding was observed in the enriched libraries of both CD47 and TIGIT despite the satisfactory phage yields calculated with the titrations between rounds, leading to the conclusion that low specificity phages were preferentially binding directly to the beads themselves rather than the target protein, thus leading to a loss of high affinity phages. This could be due to an inaccessible His-tag, a phenomenon that may occur in certain proteins due to their tertiary structures which lead to insufficient coating of the beads in protein and therefore low levels of high affinity phages produced. (*Affinity His-Tag Purification Troubleshooting Guide*, 2019, Pina, Batalha et al. 2014). Another noted disadvantage of the His-tagged beads is the possible presence of metal binding proteins naturally expressed by bacteria, which may also bind to the beads, and thus offer another binding target to the

phages of the enriched libraries (*His-tagged Protein Expression & Purification* 2025, Young, Britton et al. 2012).

In order to avoid this potential problem, for the second attempt, Protein G beads were used. These are super paramagnetic beads covalently coated in recombinant Protein G which is able to bind to an Fc-tag, a protein tag derived from the Fc portion of IgG fused to the C terminus of the target proteins (*Dynabeads™ Protein G package insert* 2025). Flow cytometry was used to ensure adequate coating of the beads with the target proteins, as well as binding in the correct orientation (Liu, Yu 2016). However, despite these considerations, there was no amplification of high affinity phage clones noted when biopanning using Fc-tagged proteins on Protein G beads, with ELISA showing fluorescence levels of the enriched libraries comparable to the NPC. This suggests an even higher level of preferential binding of the phages to the beads than when using His-tag beads.

Another consideration could be the steric hindrance of the phages by the BSA in the blocking buffer. Normally, blocking buffer is meant to play an integral role in the biopanning process, by occupying non-specific binding sites and thus minimising the presence of non-specific phages. However, a study by Yun, Lee et al. (2019) showed a marked improvement in phage binding affinity through the use of a modified method that included two additional negative selection steps against BSA blocking agent. This shows that the level of steric interference of BSA may have been a significant reason for the loss of affinity during phage display on CD47 and TIGIT.

Finally, loss of phages may also occur during precipitation of the phages after the amplification step. The precipitation method chosen for this study was PEG/NaCl precipitation over ice, although alternative methods, such as the use of cesium chloride (CsCl) density

gradients, are also quite common. The purpose of this step is the precipitation and separation of the amplified phages from the bacterial culture, thus providing a concentrated and pure phage sample, as well as removing any bacterial proteins that may affect stability of the phages. However, a study by Carrol-Portillo, Coffman et al. (2021) suggests that this step often leads to a stark reduction of both phage population size as well as diversity. While precipitation using PEG/NaCl was found to be far less detrimental than CsCl density gradient centrifugation, a significant loss of phage activity was still noted, with greater losses observed when using PEG with higher molecular weight. This was noted to be especially detrimental in the heterogenous enriched phage libraries, where such a loss of phages could have led to the irreversible loss of unique high affinity phage clones (Kunisch, Wagemans et al. 2023).

However, precipitation of phages, despite the noted disadvantages, is still considered an important step in the purification of phages, as it ensures separation from bacterial debris and nucleic acids that may interfere in further analysis as well as lead to a degradation of scFvs from the surfaces of phages through bacterial proteases over time. This would eventually lead to a loss of functionality of those scFvs, and therefore unintentionally lead to their exclusion in further biopanning steps, thus also leading to loss of overall affinity of the enriched library (Lakowitz, Krull et al. 2017, Fouladvand, Bemani et al. 2020, Yamamoto, Alberts et al. 1970). Therefore, it is important to find a balance in the methodology used in order to successfully carry out these processes with the lowest possible loss of phages.

Briefly, the omission of the amplification step from the process was also considered in order to minimise many of these disadvantages, such as suggested by Derda, Tang et al. (2011). However, while this amplification-free procedure does help maintain the diversity of the library, as well as reduces the loss of phages through amplification bias and PEG precipitation,

it ultimately also lead to a much higher population of phages binding to pluripotent cells, and therefore a much reduced fraction of binders to non-binders, as opposed to this study, which produced 43 high affinity anti-GITR clones out of only 60 selected (Derda, Mussah et al. 2010, Orner, Derda et al. 2004).

Unfortunately, further consideration needs to be taken regarding the generation of scFv for CD47 and TIGIT before phage display may be attempted again in future studies. However, despite the failures observed for two of the targets, high affinity scFv phages were successfully identified for GITR by round 3 of biopanning with His-tag beads. Due to the observable loss of affinity by round 4, likely due to an underrepresentation of high affinity clones, either through recovery bias or preferential amplification, it was decided that individual clones would be chosen from round 3. This would also increase the chances of selecting a larger variety of clone sequences, as each amplification step leads to a loss of diversity of the enriched library (Derda, Tang et al. 2011, Hoen, Jirka et al. 2011). The phage titre of this round also indicated a satisfactory amount of phages present at 3.04×10^{12} PFU/mL.

A total of 60 clones were successfully selected and sequenced, 43 of which showed a high affinity to GITR. While several unique phage clones were identified within this cohort, the majority of the strong binders showed nearly identical CDR sequences. Several studies suggest the direct sequencing of the original phage libraries in order to counteract this loss of diversity from phage display amplification and monoclone preparation, and gain a better understanding of the exact sequence composition of the available phages. While this method cannot be used to generate specific high affinity scFv, it appears to be a useful tool for the analysis of different lots of original library, as well as for performing comparisons of the

sequence composition between amplified libraries and the original naïve library, to gain a better understanding of amplification rates of different high and low affinity scFv phages (Sinkjaer, Sloth et al. 2025).

As has been stated, the scFv expressed by phages is in the form of a fusion to the protein pIII which is responsible for *E. coli* infection. Within the cDNA phagemid genome, the VL-linker-VH sequence may be found in-between a myc tag sequence, connected via the NotI 3' of the VL and a pelB linker sequence connected to the NcoI 5' of the VH (Klangprapan, Weng et al. 2021). The myc tag epitope may be fused with either the N or C terminus of the protein of interest through a short spacer sequence of three Alanine residues, and is one of the most widely used epitopes for signal development and protein stability of target antibodies and antibody fragments (Bahara, Tye et al. 2013, De Inés, Cochlovius et al. 2000, Lima, Hajdu et al. 2024). Past the myc tag, an amber codon may be found which allows for the fusion of the scFv to the pIII sequence (Ossysek, Uchański et al. 2015, Pansri, Jaruseranee et al. 2009). On the other hand, the pelB leader sequence is a hybrid between a bacterial pelB leader and human Kappa leader, with the function of driving the production of scFv as well as properly directing them towards the bacterial periplasm for correct protein folding, while also preventing aggregation within the cytoplasm (*scFv Conversion Into scFv-Fc* 2015, Chen, Wu et al. 2020). Within this phagemid, the gene coding for Ampicillin resistance is also present.

The scFv itself is the smallest active unit of an immunoglobulin, consisting of only the VH and VL fragments connected by a flexible linker sequence, allowing for the two segments to be covalently bound as opposed to the use of disulphide bonds. The nature of this linker is also considered an important factor in the efficacy of the scFv produced. The flexibility of the linker heavily depends on its length and amino acid sequence. Studies suggest that the linker chosen

should ideally have a length of 5 to 35 amino acids and should consist of a hydrophilic sequence to ensure correct peptide folding as well as prevent steric interference of the variable scFv domains (Pansri, Jaruseranee et al. 2009, Li, Zettlitz et al. 2015). Most commonly, flexibility is granted through repeated Glycine (Gly, G) and Serine (Ser, S) residues, while charged residues such as Glutamic acid (Glu, E), and Lysine (Lys, K) provide the necessary level of solubility (Arslan, Karadag et al. 2022, Ahmad, Yeap et al. 2012). The linker length has also been linked to aggregation of produced soluble scFv. Linkers shorter than 12 residues have been seen to be unable to functionally fold the V domains and instead forms a bivalent dimer, or diabody through interactions with a second scFv. This can be further restricted through the joining of VH and VL domains without the use of a linker and leading to the formation of a triabody through the association of three separate scFv (Atwell, Breheney et al. 1999, Carmichael, Power et al. 2003). These multivalent recombinant fragments have often been found to have a higher avidity and specificity than single scFv due to the ability to bind to and cross-link different adjacent surface receptors, as well as show a slower clearance from the tumour microenvironment due to their relatively larger size (Todorovska, Roovers et al. 2001, Hudson, Kortt 1999, Miller, Demarest et al. 2010). However, since the goal of this study was in the identification of single specific scFv antibody fragments, a linker of 15 amino acid residues was used to avoid this aggregation, with the amino acid sequence "EGKSSGASGESKVDD".

The VH and VL domains of the scFv each consisted of 3 highly variable Complementarity Determining Regions (CDR), joined together by four Framework (FR) regions. The FRs showed little variation between the different scFv clones and acted as a structural framework allowing for the correct folding and conformation of the CDRs, while also affecting the stability of the scFv as a whole. While not normally directly involved with protein signalling, the structure of

the FRs can have an effect on the conformation of the CDRs and thus on the affinity of the scFv (Sarén, Saronio et al. 2023, Luo, Mah et al. 1995). While some variation was observed in the FR regions between anti-GITR scFv clones, they were far fewer than in the CDRs and normally consisted of only one of two amino acid differences.

The clones which were observed to have the most variation in the FR sequences included clones 7, 11, 23, 43, 45, 50, 54, 55, and 56. Of these only clones 23 and 45 showed a high level of affinity to GITR. Furthermore, while most of the mentioned clones also exhibited several major variations within their CDR sequences when compared to many of the other clones, the CDRs of clone 55 were found to match exactly to those of several other high binding clones that had been grouped together based on similarities in CDR3 (green group). This could therefore be potential evidence to the effect of severe variability within the FR regions on scFv affinity. Apart from these aforementioned clones, there were several common substitutions of amino acids that occurred frequently within the other clones that do not appear to have severely affected the affinity of the clones.

On the other hand, the CDR regions are the most variable segments of the scFv and directly responsible for the formation of the antigen binding site. Of these three regions, CDR3, of both the VH and the VL consistently show the highest level of variability and play a significant role in the fusion and rearrangement of the Variable (V) and Diversity (D), of the VH, and the Joining (J) of the VL during V(D)J recombination, a process vital to the activity of an antibody (*Antibody Variable Regions: Structure, Function, and Applications* 2025). Small variations in the CDR sequences can often lead to massive changes to both the affinity and the stability of the generated scFv, as well as the specific epitopes of the target protein on which they preferentially bind, which is the main reason why these regions were the focus of sequence

comparisons carried out between separate clones (Fennell, Mcdonnell et al. 2013). However, the contributions of the different CDRs of the scFv are variable, with the CDR3-VH found to be responsible for contributing up to 29% of total binding specificity of the scFv, while the CDR3-VL contributes only 4%. This difference is also the reason why a quickly emerging field of research in cancer treatment is the use of camelid single domain antibodies (sdAbs) composed solely of a VHH nanobody lacking the VL entirely, which has also been shown to provide improved response to treatment over mAbs, as well as have a higher solubility and stability to scFv along with a relatively lower production cost (Li, Hoefnagel et al. 2023, Dizicheh, Chen et al. 2023, *Most Popular Antibody Fragment: Single Domain Antibody vs. ScFv* 2023). This difference in contribution would also explain how clone number 38 was seen to be a strongly binding scFv, despite having a stop codon after its CDR2-VL, thus cutting the VL chain short and completely eliminating CDR3-VL along with FR3-VL and FR4-VL. This is further evident with clones 22 and 25, which share the same three CDR-VH sequences as clone 38 yet show a great deal of variability in the sequences of the three CDR-VLs, and yet still showed a high level of affinity. Similarly, the clones 2, 9, 24, and 53 were also seen to share identical sequences for all three CDRs of the VH, while showing some variability in the sequences of the VL CDRs, and yet all showed comparable levels of fluorescence in the ELISA. This therefore emphasises the importance of the VH, and more specifically, CDR3-VH when determining scFv affinity. The presence of the stop codon of clone 38 itself is likely a product of the various diversity generating processes that occur during preparation of the naïve library (Jaroszewicz, Morcinek-Orłowska et al. 2022, Sloth, Bakhshinejad et al. 2022).

When examining the CDRs of all clones as a whole, it was clear to see that the majority of the clones fell within two major groups showing near identical sequences to each other. This was likely the result of amplification bias of these particular scFvs from the previous rounds, which

lead to an overexpression of these scFvs, as well as a general loss of diversity in the enriched library (Derda, Tang et al. 2011). The majority of the clones belonging to these groups showed high levels of affinity to the target protein with a few exceptions.

Of all of the clones examined, the CDR sequences shown by clones 18 and 19 were some of the most interesting. While these clones were shown to be poor binders during the ELISA, when checking their respective amino acid sequences, it was noted that while the CDRs of the VH chain matched perfectly to one group of high affinity clones (green), the CDRs of the VL matched with those of another identified large group of clones (yellow). Normally, clones that had been aligned based on the CDR3-VH were also found to be near perfectly aligned based on all CDR sequences, with few exceptions. Therefore, to have identified two clones composed of a VH and VL that seem to derive from two completely separate scFv lines was quite interesting. These clones are likely a case of a random VH-VL recombination that occurred during the *in vitro* library preparation which led to the production of a non-functioning artificial scFv. This VH-VL combination would likely never have been naturally produced by B cells *in vivo*. Encountering scFvs such as these from the phage library is unfortunately one of the many drawbacks of the phage display method (Lai, Lim 2020, Chen, Lipes et al. 2008).

On the other hand, when examining the sequences for clones 12, 14, 17, 26 and 28, it was noted that while all CDRs seemed identical to other high affinity clones, the levels of fluorescence observed from the ELISA of these scFv on immobilised GITR were not particularly high. While they were seen to show some level of preferential binding to GITR over the control protein, it was not to the extent of other high binding clones. Upon examination of the FR regions of these clones, no particular variations were observed that differed greatly from

other clones. Therefore, the reasons for their reduced levels of signalling may have been due to errors performed during the ELISA itself, such as insufficient levels of protein coating in those wells, or other such pipetting errors.

Special attention should also be placed on clones 23 and 45, which showed very few similarities in the sequences of the CDRs and the FRs to other clones, or even to each other, yet showed a high level of affinity in the ELISA, especially in regard to clone 45, which was shown to be one of the strongest binders. These two unique clones are a prime example of the effects of amplification bias of some scFvs over others that occurs during phage display, regardless of their affinity levels to the target protein. This is also the main reason why there is a visible overexpression of only two or three unique high affinity scFvs within the round 3 enriched library. Most likely, even more of this diversity was lost by round 4 (Derda, Tang et al. 2011).

Finally, it should be stated that while 60 clones were selected, only 57 of them were successfully sequenced, with the unsequenced clones being 36, 39, and 42. While 36 and 39 were not sequenced at all, clone 42 only showed a short non-sense sequence of 30 base pairs. Of the three, only clone 36 showed a high level of affinity in the ELISA, while clones 39 and 42 showed stronger levels of fluorescence to the control protein. Upon checking the nanopore measurements showcasing DNA concentration of each clone eluate, clone 36 showed DNA levels comparable to several of the other clones at 125.6 ng/µL, which leads to the conclusion that the failed sequencing was most likely due to damage of the sample during transit. However, it was seen that the nanopore results for both clones 39 and 42 showed a measurement of 30.2 ng/µL and 30 ng/µL respectively, which is far lower than all other selected clones. This could be a result of the phenomenon known as “bald” phages, or phages

which do not display the scFv-pIII fusion protein on their surfaces, due to displacement of the gene by wild-type pIII coming from the helper phage that had been preferentially enclosed during amplification. These phages often bind non-specifically during biopanning, and if present in a large majority, may easily outcompete scFv carrying phages during amplification steps, thus leading to a general loss of diversity. As has already been stated, the presence of these “bald” phages may be mitigated through the use of alternative helper phages such as hyperphage over the classically used M13KO7 (Aripov, Volkova et al. 2024, Kramer 2003). The potential presence of such phages in round 3 of the anti-GITR biopanning rounds also offers another clue into the potential reason for the drop of affinity noted by the fourth round.

A group of the best and worst binding clones was selected to undergo protein modelling using SWISS-model in order to visualise the structure of the scFv produced, compare them to structures of similar molecules, as well as produce Ramachandran plots to evaluate the quality of the models (Jumper, Evans et al. 2021, Varadi, Bertoni et al. 2024). Focus was placed on clone 34, as one of the highest affinity clones belonging to the largest group of similar clones, as well as clone 11 for an example of a low affinity clone. Clone 11 was also the clone which showed the highest level of non-specific binding and was seen to have very little similarities in its CDR sequences to other clones (Martz 2016, Ho and Brasseur 2005). The Ramachandran plots of both of these clones were highly regular, with clear clustering of the residues within the favoured regions, showing that both clone models were of good quality. Further models of other clones may also be seen in **Appendix I**.

Other methods could also potentially be used to more accurately compare structures and binding sites of the isolated clones. One such method is the use of hydrogen deuterium exchange mass spectrometry, which is a technique that may be used to effectively map the

structure and action of a protein through observing the exchange of hydrogen atoms with deuterium atoms while the protein has been placed in a deuterated solution. This is a technique that has become quite commonplace in the study of protein structure and interaction and can be quite useful in the mapping of protein targets that may otherwise be difficult to examine (Knight, Woolley et al. 2020, Ozohanics, Ambrus 2020, Konermann, Scrosati 2024).

Docking studies were also performed using the obtained models of these scFvs, as well as a model of the target protein GITR which was obtained from the UniProt online database. Focus was placed on clone 34 as an example of a high affinity clone. Both the Z-score as well as the overall HADDOCK score were negative values, giving more credence to the stability of the scFv-GITR complex. However, it is not generally recommended to rely solely on the HADDOCK score when trying to determine the level of interaction between two different proteins. Firstly, this scoring is most useful when it is able to be compared to similar reference structures, as well as to already available biological knowledge of the particular interaction. In many instances it has been found that the HADDOCK score may not perfectly correlate to protein affinity. Therefore, while it is a useful tool for visualisation of different protein-ligand interactions, as well as comparisons between ligands, on its own, it does not give definitive proof of affinity (Honorato, Trellet et al. 2024, Bonvin 2025c, Bonvin 2025d).

Alternative approaches to protein docking that may provide more robust results than the modelling obtained through the HADDOCK software also include the amplified luminescent proximity homogenous (AlphaLISA) assay. This is a homogenous, chemiluminescent, no wash immunoassay making use of beads, in order to effectively study protein interaction. This is a widely emerging assay which offers several advantages to alternative assays like ELISA, such

as its increased throughput, sensitivity, and decreased assay time. This technique makes use of donor and acceptor beads coated in immobilised proteins of interest, which are able to interact with each other through the target analyte, thus producing a chemiluminescent signal that can then be measured and quantified, thus providing an adequate measure of protein interaction (Hunt, Vögeli et al. 2023, Beaudet, Rodriguez-Suarez et al. 2008, *AlphaLISA Immunoassay Kits* 2025).

There are several possible avenues of research available that may be undertaken upon the completion of this project. One such example is in the reformatting of the generated scFv into full length IgG, a commonly performed technique for engineering of antibodies produced through phage display. There are several advantages to carrying out this process, including stabilising the antibody to allow for longer circulation time, as well as improving solubility through the prevention of clumping of the smaller scFv. Anti-tumour effectiveness may also be improved from the bivalent nature of IgGs, allowing for binding to occur to two different epitopes present in close proximity on the cell membrane, as well as allowing for further engagement of the immune system through interactions with the Fc region of the antibody, a region which is naturally absent from scFvs. These differences are the main reasons why the majority of available immunotherapeutic pharmaceuticals present on the market are predominantly IgG (Bujak, Matasci et al. 2014, Wörn, Maur et al. 2000). While there is research showing the successful creation of fragment antigen binding antibodies (Fab) from phage derived scFv using type IIS restriction enzymes, the process most commonly used in order to reformat scFv into IgG is one-step emulsion PCR (Sanmark, Houvinen et al. 2015, Liu, Gu et al. 2018). This is a high-throughput procedure making use of a relatively simple technique of dilution and compartmentalization of molecular templates inside the individual water droplets of an oil emulsion (Kanagal-Shamanna 2016). This technique is often used in

the production of IgG from scFv after screening to determine the highest affinity scFvs beforehand, in order to preserve the unique pairings of the VH-VL in each individual scFv. However, a study by Xiao, Douthwaite et al. (2017) suggests a modification to this method wherein reformatting into IgG is performed prior to screening in order to maintain antibody diversity, as well as improve throughput. Modifications such as these are therefore vital to the driving of this area of research and the development of novel strategies for the efficient screening and selection of potentially therapeutic antibodies and antibody fragments (Reader, Workman et al. 2019, Xiao, Chen et al. 2015).

Finally, attention should be drawn towards another area of potential future research, with that being whole cell biopanning. This is a technique that involves the incubation of a phage display library against cells expressing the protein of interest on their cell membrane. This process shares many similarities with phage display biopanning using protein coated beads, with the major difference being that target proteins are expressed on the surface of cultured cells instead. The main advantage of this method over bead or plate based biopanning is the easier identification of biologically relevant scFv, through the selection of antibody fragments which specifically recognise the target protein in a cellular context. Often times, scFvs selected through solid phase biopanning may appear to show high affinity for the target protein in practice but fail when tested *in vivo*. This is largely due to the vast diversity of the naïve phage library that may contain phages carrying scFv specific to sections of the target protein that are not involved with cell signalling. Therefore, cell biopanning may offer a more stringent selection of scFvs with a higher level of relevance and functionality to clinical applications (Panagides, Zacchi et al. 2022, Alfaleh, Jones et al. 2017, Wu, Liu et al. 2016). However, there are also currently many disadvantages to this method as well, such as the time-consuming preparation of the cells, as well as the increased possibility of non-specific

binding due to absorption of the phage into the cell membrane through other coat proteins. The level of background from non-target proteins also tends to be much higher than the target during whole cell biopanning (Jones, Alfaleh et al. 2016). Nevertheless, this methodology remains as a useful next avenue of research to confirm the potential for generation of high affinity scFv from an original phage library that may provide effective anti-tumour activity in a clinical environment.

To conclude, this study was successful in the generation of high affinity monoclonal scFv clones specific to the GITR immune checkpoint target and appears to be one of the first to have done so. This could, therefore, potentially lead to the development novel diagnostic and therapeutic techniques against malignancies, both as a monotherapy and in combination with other immunotherapeutic agents. While effective scFv could not be produced for the two other targets of interest of this study, those being CD47 and TIGIT, there are still many potential avenues that may be taken in future studies that would allow for the successful biopanning of these targets.

References

A Guide for Choosing Between Commonly Used Antibiotics, 2025. [Gold Biotechnology], [Online] Available: https://goldbio.com/articles/article/a-guide-for-choosing-between-commonly-used-antibiotics?srsltid=AfmBOoqOCxvwpWgvzplydlpwqfMMz2zSWJgvW0q0m8Q-4twNXQhdxXvx. [Mar 18, 2025].

Affinity His-Tag Purification Troubleshooting Guide, 2019. [Gold Biotechnology], [Online], Available: https://goldbio.com/documents/1013/Affinity%20His-Tag%20Purification%20Troubleshooting.pdf?srsltid=AfmBOoqpdK_hAZ87LLspevXVPayI9_0BdRldghzUm6FTMClGGTNQsdzs. [Jun 5, 2025].

AHAMADI-FESHARAKI, R., FATEH, A., VAZIRI, F., SOLGI, G., SIADAT, S. D., MAHBOUDI, F. and RAHIMI-JAMNANI, F., 2019. Single-chain variable fragment-based bispecific antibodies: Hitting two targets with one sophisticated arrow, *Molecular Therapy - Oncolytics*, 14, pp. 38–56, doi: 10.1016/j.omto.2019.02.004.

AHMAD, S., DA COSTA GONZALES, L. J., BOWLER-BARNETT, E. H., RICE, D. L., KIM, M., WIJERATHNE, S., LUCIANI, A., KANDASAAMY, S., LUO, J., WATKINS, X., TURNER, E., MARTIN, M. J., BATEMAN, A., MARTIN, M., and the UniProt Consortium, 2025. The UniProt website API: facilitating programmatic access to protein knowledge, *Nucleic Acids Research*, 53(W1), pp. W547-W553, doi: 10.1093/nar/gkaf394

AHMAD, Z. A., YEAP, S. K., ALI, A. M., HO, W. Y., ALITHEEN, N. B. M., and HAMID, M., 2012. SCFV Antibody: principles and clinical application. *Clinical and Developmental Immunology*, *2012*, pp. 1–15. doi: 10.1155/2012/980250.

ALBANDAR, H. J., FUQUA, J., ALBANDAR, J. M., SAFI, S., MERRILL, S. A. and MA, P. C., 2021. Immune-related adverse events (IRAE) in cancer immune checkpoint inhibitors (ICI) and survival outcomes correlation: To Rechallenge or not?, *Cancers*, 13(5), p. 989, doi: 10.3390/cancers13050989.

ALFALEH, M. A., ALSAAB, H. O., MAHMOUD, A. B., ALKAYYAL, A. A., JONES, M. L., MAHLER, S. M. and HASHEM, A. M., 2020. Phage display derived monoclonal antibodies: From bench to bedside, *Frontiers in Immunology*, 11, doi: 10.3389/fimmu.2020.01986.

ALFALEH, M. A., JONES, M. L., HOWARD, C. B., and MAHLER, S. M., 2017. Strategies for Selecting Membrane Protein-Specific Antibodies using Phage Display with Cell-Based Panning. *Antibodies*, *6*(3), p. 10. doi: 10.3390/antib6030010.

AlphaFold Protein Structure Database, 2025. [Google DeepMind and EMBL-EBI], [Online], Available: https://alphafold.ebi.ac.uk/ [May 18, 2025].

AlphaLISA Immunoassay Kits, 2025. [Revvity], [Online], Available: https://www.revvity.com/ask/alphalisa-immunoassay-kits [Jun 15, 2025].

American Cancer Society, 2022. Cancer Facts & Figures 2022, [Atlanta: American Cancer Society (ACS)], [Online] Available: https://www.cancer.org/latest-news/facts-and-figures-2022.htmL [April 3, 2023].

ANDERSON, A. C., JOLLER, N., and KUCHROO, V. K., 2016. LAG-3, tim-3, and TIGIT: Co-inhibitory receptors with specialized functions in immune regulation, *Immunity*, 44(5), pp. 989–1004, doi: 10.1016/j.immuni.2016.05.001.

ANDERSON, N. M., and SIMON, M. C., 2020. The tumor microenvironment*, Current Biology,* 30(16), pp. 921–925*,* doi:10.1016/j.cub.2020.06.081.

ANDRÉ, A. S., MOUTINHO, I., DIAS, J. N. R., and AIRES-DA-SILVA, F., 2022. In vivo Phage Display: A promising selection strategy for the improvement of antibody targeting and drug delivery properties. *Frontiers in Microbiology*, *13*. doi: 10.3389/fmicb.2022.962124.

ANDREWS, M. C. and WARGO, J. A., 2017. Cancer evolution during immunotherapy, *Cell*, 171(4), pp. 740–742, doi: 10.1016/j.cell.2017.10.027.

ANNESE, T., TAMMA, R. and RIBATTI, D., 2022. Update in TIGIT immune-checkpoint role in cancer, *Frontiers in Oncology*, 12, doi: 10.3389/fonc.2022.871085.

Antibody CDR annotation, 2025. [NovoPro labs], [Online]. Available: https://www.novoprolabs.com/tools/cdr [Mar 28, 2025].

Antibody Variable regions: Structure, function, and applications, 2025. [Creative Proteomics], [Online], Available: https://www.creative-proteomics.com/proteinseq/resource/antibody-variable-regions-structure-function-applications.htm [Jun 12, 2025].

ARIPOV, V. S., VOLKOVA, N. V., ILYICHEV, A. A., and SHCHERBAKOV, D. N., 2024. Problems of creating antibody phage libraries and their solutions. *Vavilov Journal of Genetics and Breeding*, *28*(2), pp. 249–257. doi: 10.18699/vjgb-24-29.

ARSLAN, M., KARADAG, M., ONAL, E., GELINCI, E., CAKAN-AKDOGAN, G., and KALYONCU, S., 2022. Effect of non-repetitive linker on in vitro and in vivo properties of an anti-VEGF scFv. *Scientific Reports*, *12*(1). doi: 10.1038/s41598-022-09324-4.

ATWELL, J. L., BREHENEY, K. A., LAWRENCE, L. J., MCCOY, A. J., KORTT, A. A., and HUDSON, P. J., 1999. scFv multimers of the anti-neuraminidase antibody NC10: length of the linker between VH and VL domains dictates precisely the transition between diabodies and triabodies. *Protein Engineering Design and Selection*, *12*(7), pp. 597–604. doi: 10.1093/protein/12.7.597.

AVOGADRI, F., YUAN, J., YANG, A., SCHAER, D. and WOLCHOK, J. D., 2010. Modulation of CTLA-4 and GITR for cancer immunotherapy, *Current Topics in Microbiology and Immunology*, 344, pp. 211–244, doi: 10.1007/82_2010_49.

BAGHBAN, R., ROSHANGAR, L., JAHANBAN-ESFAHLAN, R., SEIDI, K., EBRAHIMI-KALAN, A., JAYMAND, M., KOLAHIAN, S., JAVAHERI, T., and ZARE, P., 2020. Tumor microenvironment complexity and therapeutic implications at a glance. *Cell Communication and Signaling*. 18 (59), doi: 10.1186/s12964-020-0530-4.

BAHARA, N. H. H., TYE, G. J., CHOONG, Y. S., ONG, E. B. B., ISMAIL, A., and LIM, T. S., 2013. Phage display antibodies for diagnostic applications. *Biologicals*, *41*(4), pp. 209–216. doi: 10.1016/j.biologicals.2013.04.001.

BASHIR, S., and PAESHUYSE, J., 2020. Construction of antibody phage libraries and their application in veterinary immunovirology, *Antibodies*, 9(2), p. 21, doi:10.3390/antib9020021.

BASRAN, A., 2019. Identification and characterisation of Affimer proteins that are able to bind and agonise human co-stimulatory cell surface targets, *Cancer Research*, 79(13), doi: 10.1158/1538-7445.am2019-4155.

BAZAN, J., CAŁKOSIŃSKI, I. and GAMIAN, A., 2012. Phage display—a powerful technique for immunotherapy, *Human Vaccines & Immunotherapeutics*, 8(12), pp. 1817–1828, doi: 10.4161/hv.21703.

BEAUDET, L., RODRIGUEZ-SUAREZ, R., VENNE, M., CARON, M., BÉDARD, J., BRECHLER, V., PARENT, S., and BIELEFELD-SÉVIGNY, M., 2008. AlphaLISA immunoassays: the no-wash alternative to ELISAs for research and drug discovery. *Nature Methods*, *5*(12), pp. an8–an9. doi: 10.1038/nmeth.f.230.

BIENERT, S., WATERHOUSE, A., DE BEER, T.A.P., TAURIELLO, G., STUDER, G., BORDOLI, L., and SCHWEDE, T., 2017. The SWISS-MODEL Repository - new features and functionality. *Nucleic Acids Res*. 45, pp. 313-319.

BLAKE, S. J., DOUGALL, W. C., MILES, J. J., TENG, M. W. L. and SMYTH, M. J., 2016. Molecular pathways: Targeting CD96 and TIGIT for cancer immunotherapy, *Clinical Cancer Research*, 22(21), pp. 5183–5188, doi: 10.1158/1078-0432.ccr-16-0933.

BONVIN, A., 2025a. HADDOCK basic protein-protein docking tutorial, [Bonvin Lab], [Online]. Available: https://www.bonvinlab.org/education/HADDOCK-protein-protein-basic/ [May 30, 2025].

BONVIN, A., 2025b. Haddock2.4 scoring function, [Bonvin Lab], [Online]. Available: https://www.bonvinlab.org/software/haddock2.4/scoring/ [Apr 18, 2025].

BONVIN, A., 2025c. How to analyse docking results from Haddock or refine models?, [Bonvin Lab], [Online]. Available: https://www.bonvinlab.org/software/bpg/analysis/ [Apr 18, 2025].

BONVIN, A., 2025d. HADDOCK2.4 manual – Analysis, [Bonvin Lab], [Online], Available: https://www.bonvinlab.org/software/haddock2.4/analysis/ [Jun 2, 2025].Bovine Serum Albumin (BSA Protein), 2025. NMR Chemical Shifts of Impurities, *Sigma Aldrich* [Merck], [Online] Available: https://www.sigmaaldrich.com/MT/en/products/cell-culture-and-analysis/cell-culture-supplements-and-reagents/albumins-and-transport-proteins/bovine-serum-albumin [Mar 19, 2025].

BOŻYK, A., WOJAS-KRAWCZYK, K., KRAWCZYK, P., and MILANOWSKI, J., 2022. Tumor microenvironment—a short review of cellular and interaction diversity. *Biology*. 11 (6), p. 929, doi: 10.3390/biology11060929.

BREITLING, F., BRODERS, O., HELMSING, S., HUST, M., and DÜBEL, S., 2010. Improving Phage Display Throughput by Using Hyperphage, Miniaturized Titration and pVIII (g8p) ELISA. *Antibody Engineering*, pp.197–206. doi: 10.1007/978-3-642-01144-3_14.

BUCHBINDER, E. I., and DESAI, A., 2016. CTLA-4 and PD-1 Pathways: Similarities, Differences, and Implications of Their Inhibition, *American Journal of Clinical Oncology*, 39(1), pp. 98–106. doi: 10.1097/coc.0000000000000239.

BUJAK, E., MATASCI, M., NERI, D., and WULHFARD, S., 2014. Reformatting of scFv Antibodies into the scFv-Fc Format and Their Downstream Purification. *Methods in Molecular Biology*, pp. 315–334. doi: 10.1007/978-1-62703-992-5_20.

BUZZATTI, G., DELLEPIANE, C., and DEL MASTRO, L., 2019. New emerging targets in cancer immunotherapy: The role of GITR, *ESMO Open*, 4(3), doi: 10.1136/esmoopen-2020-000738.

BYUN, D. J., WOLCHOK, J. D., ROSENBERG, L. M., and GIROTRA, M., 2017. Cancer immunotherapy — immune checkpoint blockade and associated endocrinopathies, *Nature Reviews Endocrinology*, 13(4), pp. 195–207, doi: 10.1038/nrendo.2016.205.

Can carbenicillin be substituted for ampicillin when selecting for the pGEM Vectors, 2025. [Promega], [Online], Available: https://worldwide.promega.com/resources/pubhub/enotes/can-carbenicillin-be-substituted-for-ampicillin-when-selecting-for-the-pgem-vectors/. [Mar 18, 2025].

Cancer Research UK, 2021. Types of cancer immunotherapy, [Cancer Research UK], [Online], Available: https://www.cancerresearchuk.org/about-cancer/treatment/immunotherapy/types [3 Apr, 2023].

Cancer Research UK, 2022. Checkpoint inhibitors, [Cancer Research UK], [Online], Available: https://www.cancerresearchuk.org/about-cancer/treatment/immunotherapy/types/checkpoint-inhibitors [3 Apr, 2023].

CARME PONS ROYO, M., and JUNGBAUER, A., 2025. Polyethylene glycol precipitation: fundamentals and recent advances. *Preparative Biochemistry & Biotechnology*, pp.1–20. doi: 10.1080/10826068.2025.2470220.

CARMICHAEL, J. A., POWER, B. E., GARRETT, T. P., YAZAKI, P. J., SHIVELY, J. E., RAUBISCHEK, A. A., WU, A. M., and HUDSON, P. J., 2003. The Crystal Structure of an Anti-CEA scFv Diabody Assembled from T84.66 scFvs in VL-to-VH Orientation: Implications for Diabody Flexibility. *Journal of Molecular Biology*, *326*(2), pp. 341–351. doi: 10.1016/s0022-2836(02)01428-6.

CARROLL-PORTILLO, A., COFFMAN, C. N., VARGA, M. G., ALCOCK, J., SINGH, S. B., and LIN, H. C., 2021. Standard bacteriophage purification procedures cause loss in numbers and activity. *Viruses*, *13*(2), p. 328. doi: 10.3390/v13020328.

CHATTOPADHYAY, K., RAMAGOPAL, U. A., MUKHOPADHAYA, A., MALASHKEVICH, V. N., DILORENZO, T. P., BRENOWITZ, M., NATHENSON, S. G., and ALMO, S. C., 2007. Assembly and structural properties of glucocorticoid-induced TNF receptor ligand: Implications for function, *Proceedings of the National Academy of Sciences*, 104(49), pp. 19452–19457, doi: 10.1073/pnas.0709264104.

CHAUVIN, J.-M., and ZAROUR, H. M., 2020. TIGIT in cancer immunotherapy, *Journal for ImmunoTherapy of Cancer*, 8(2), doi: 10.1136/jitc-2020-000957.

CHEN, W., WU, J., CHEN, W., HU, P., and WANG, X., 2020. An approach to achieve highly soluble bioactive ScFv antibody against staphylococcal enterotoxin A in E.coli with pelB leader. *IOP Conference Series Earth and Environmental Science*, *512*(1), p. 012077. doi: 10.1088/1755-1315/512/1/012077.

CHEN, Y., LIPES, B. D., KENAN, D. J., STAATS, H. F., and GUNN, M. D., 2008. Identification of recombinant antibodies against multiple distinct toll-like receptors by homolog mining a single immune scFv phage library. *Journal of Immunological Methods*, *340*(2), pp. 144–153. doi: 10.1016/j.jim.2008.10.013.

CM13K Trypsin-Sensitive Helper Phage Instruction Manual, 2023. In *Antibody Design Labs*, [Online]. Available: https://www.abdesignlabs.com/content/manuals/CM13K%20manual.pdf. [May 17, 2025].

COE, D., BEGOM, S., ADDEY, C., WHITE, M., DYSON, J., and CHAI, J.-G., 2010. Depletion of regulatory T cells by anti-GITR Mab as a novel mechanism for cancer immunotherapy, *Cancer Immunology, Immunotherapy*, 59(9), pp. 1367–1377, doi: 10.1007/s00262-010-0866-5.

CUSABIO, 2023. The overview of phage display: Protocol, Classification, Application and FAQs, [CUSABIO], [Online], Available: https://www.cusabio.com/c-20680.htmL [7 April 2023].

DAS, S., and JOHNSON, D. B., 2019. Immune-related adverse events and anti-tumor efficacy of immune checkpoint inhibitors, *Journal for ImmunoTherapy of Cancer*, 7(1), doi: 10.1186/s40425-019-0805-8.

DAVAR, D., and ZAPPASODI, R., 2023. Targeting GITR in cancer immunotherapy - there is no perfect knowledge. *Oncotarget*, *14*(1), pp. 614–621. doi: 10.18632/oncotarget.28461.

DE INÉS, C., COCHLOVIUS, B., SCHMIDT, S., and LITTLE, M., 2000. A cell surface-displayed anti-c-myc single-chain antibody: new perspectives for the genetic improvement of cellular tumor vaccines. *Cancer Gene Therapy*, *7*(9), pp. 1257–1262. doi: 10.1038/sj.cgt.7700230.

DE SOUSA LINHARES, A., LEITNER, J., GRABMEIER-PFISTERSHAMMER, K., and STEINBERGER, P., 2018. Not all immune checkpoints are created equal. *Frontiers in Immunology*, 9, doi: 10.3389/fimmu.2018.01909.

DE VRIES, S.J., VAN DIJK, M., and BONVIN, A.M.J.J., 2010. The HADDOCK web server for data-driven biomolecular docking. *Nature Protocols*, 5, pp. 883-897.

DEKOSKY, B. J., IPPOLITO, G. C., DESCHNER, R. P., LAVINDER, J. J., WINE, Y., RAWLINGS, B. M., VARADARAJAN, N., GIESECKE, C., DÖRNER, T., ANDREWS, S. F., WILSON, P. C., HUNICKE-SMITH, S. P., WILLSON, C. G., ELLINGTON, A. D., and GEORGIOU, G., 2013. High-throughput sequencing of the paired human immunoglobulin heavy and light chain repertoire. *Nature Biotechnology*, *31*(2), pp. 166–169. doi: 10.1038/nbt.2492.

DERDA, R., MUSAH, S., ORNER, B. P., KLIM, J. R., LI, L., and KIESSLING, L. L., 2010. High-Throughput discovery of synthetic surfaces that support proliferation of pluripotent cells. *Journal of the American Chemical Society*, *132*(4), pp. 1289–1295. doi: 10.1021/ja906089g.

DERDA, R., TANG, S.K.Y., LI, S.C., NG, S., MATOCHKO, W., and JAFARI, M.R., 2011. Diversity of Phage Displayed Libraries of Peptides during Panning and Amplification. *Molecules*, 16(2), pp. 1776-1803. doi: 10.3390/molecules16021776.

DIZICHEH, Z. B., CHEN, I., and KOENIG, P., 2023. VHH CDR-H3 conformation is determined by VH germline usage. *Communications Biology*, *6*(1). doi: 10.1038/s42003-023-05241-y.

DONG, Y., MENG, F., WANG, Z., YU, T., CHEN, A., XU, S., WANG, J., YIN, M., TANG, L., HU, C., WANG, H. and CAI, J., 2020. Construction and application of a human scfv phage display library based on CRE-LoxP recombination for anti-PCSK9 antibody selection, *International Journal of Molecular Medicine*, 47(2), pp. 708–718, doi: 10.3892/ijmm.2020.4822.

DOUGALL, W. C., KURTULUS, S., SMYTH, M. J., and ANDERSON, A. C., 2017. TIGIT and CD96: New checkpoint receptor targets for cancer immunotherapy, *Immunological Reviews*, 276(1), pp. 112–120, doi: 10.1111/imr.12518.

DUAN, Z., and SIEGUMFELDT, H., 2010. An efficient method for isolating antibody fragments against small peptides by antibody phage display. *Combinatorial Chemistry & High Throughput Screening*, *999*(999), pp. 1–11. doi: 10.2174/1386210206151942073.

DYBA, T., RAND,I G., BRAY, F., MARTOS, C., GIUSTI, F., NICHOLSON, N., GAVIN, A., FLEGO, M., NEAMTIU, L., DIMITROVA, N., NEGRÃO CARVALHO, R., FERLAY, J., and BETTIO, M., 2021. The European cancer burden in 2020: Incidence and mortality estimates for 40 countries and 25 major cancers, *European Journal of Cancer*, 157, pp. 308–347, doi: 10.1016/j.ejca.2021.07.039.

Dynabeads™ His-Tag Isolation & Pulldown package insert, Publication No. MAN0017121. Invitrogen, California, United States, 5/17. [Online]. Available: https://tools.thermofisher.com/content/sfs/manuals/DynabeadsHisTagIsolationPulldown_man.pdf [Mar 21, 2025].

Dynabeads™ Protein G package insert, Publication No. MAN0015809. Invitrogen, California, United States, 3/16. [Online]. Available: https://www.veritastk.co.jp/products/pdf/100.03D04D_Dynabeads_Protein_G_%28rev005%29.pdf [Mar 21, 2025].

EL OSTA, B., HU, F., SADEK, R., CHINTALAPALLY, R., and TANG, S.-C., 2017. Not all immune-checkpoint inhibitors are created equal: Meta-analysis and systematic review of immune-related adverse events in cancer trials, *Critical Reviews in Oncology/Hematology*, 119, pp. 1–12, doi: 10.1016/j.critrevonc.2017.09.002.

ELADL, E., TREMBLAY-LEMAY, R., RASTGOO, N., MUSANI, R., CHEN, W., LIU, A., and CHANG, H., 2020. Role of CD47 in hematological malignancies, *Journal of Hematology & Oncology*, 13(96), doi: 10.1186/s13045-020-00930-1.

EL-MESERY, M., TREBING, J., SCHÄFER, V., WEISENBERGER, D., SIEGMUND, D., and WAJANT, H., 2013. CD40-directed scfv-trail fusion proteins induce CD40-restricted tumor cell death and activate dendritic cells, *Cell Death & Disease*, 4(11), doi: 10.1038/cddis.2013.402.

European Cancer Information System, 2023-last update. European Cancer Information System, Cancer burden statistics and trends across Europe, [European Union], [Online] Available: https://ecis.jrc.ec.europa.eu/ [April 3, 2023].

EUROSTAT, 2022-last update. Cancer statistics, Statistics Explained, [Eurostat], [Online]. Available: https://ec.europa.eu/eurostat/statistics-explained/index.php [April 3, 2023].

FAN, J., BEKAII-SAAB, T. S., ALDRIGHETTI, L. A., BRIDGEWATER, J. A., FERRONE, C. R., HARDING, J. J., IKEDA, M., KNOX, J. J., WANG, J., KAYHANIAN, H., CHEN, X., BAI, S. Y., DRACHSLER, M. W., and OH, D., 2024. A phase 3, randomized study of adjuvant rilvegostomig plus chemotherapy in resected biliary tract cancer: ARTEMIDE-Biliary01. *Journal of Clinical Oncology*, *42*(16_suppl), TPS4199. doi: 10.1200/jco.2024.42.16_suppl.tps4199.

FELLERMEIER, S., BEHA, N., MEYER, J.-E., RING, S., BADER, S., KONTERMANN, R. E., and MÜLLER, D. 2016. Advancing targeted co-stimulation with antibody-fusion proteins by introducing TNF superfamily members in a single-chain format, *OncoImmunology*, 5(11), doi: 10.1080/2162402x.2016.1238540.

FENALTI, G., VILLANUEVA, N., GRIFFITH, M., PAGARIGAN, B., LAKKARAJU, S. K., HUANG, R. Y., LADYGINA, N., SHARMA, A., MIKOLON, D., ABBASIAN, M., JOHNSON, J., HADJIVASSILIOU, H., ZHU, D., CHAMBERLAIN, P. P., CHO, H., and HARIHARAN, K., 2021. Structure of the human marker of self 5-transmembrane receptor CD47. *Nature Communications*, *12*(1). doi: 10.1038/s41467-021-25475-w.

FENNELL, B. J., MCDONNELL, B., TAM, A. S. P., CHANG, L., STEVEN, J., BROADBENT, I. D., GAO, H., KIERAS, E., ALLEY, J., LUXENBERG, D., EDMONDS, J., FITZ, L. J., MIAO, W., WHITTERS, M. J., MEDLEY, Q. G., GUO, Y. J., DARMANIN-SHEEHAN, A., AUTIN, B., SHÚILLEABHÁIN, D. N., . . . CUNNINGHAM, O., 2013. CDR-restricted engineering of native human scFvs creates highly stable and soluble bifunctional antibodies for subcutaneous delivery. *mAbs*, *5*(6), pp. 882–895. doi: 10.4161/mabs.26201.

FERMIN, G., RAMPERSAD, S., and TENNANT, P., 2018. Viruses as tools of biotechnology, *Viruses, Molecular Biology, Host Interactions and Applications to Biotechnology*, pp. 291–316, doi: 10.1016/b978-0-12-811257-1.00012-7.

FlowJo™ Software (for Windows), 2023. Version v10.10. Ashland, OR: Becton, Dickinson and Company.

FOULADVAND, F., BEMANI, P., MOHAMMADI, M., AMINI, R., and JALILIAN, F. A., 2020. A review of the methods for concentrating M13 phage. *Journal of Applied Biotechnology Reports*, *7*(1), pp. 7–15. doi: 10.30491/jabr.2020.105916.

FRENTZAS, S., MENIAWY, T., KAO, S. C.-H., WANG, R., ZUO, Y., ZHENG, H., and TAN, W., 2021. Advantig-105: Phase 1 dose-escalation study of anti-TIGIT monoclonal antibody ociperlimab (BGB-A1217) in combination with tislelizumab in patients with advanced solid tumors., *Journal of Clinical Oncology*, 39(15), pp. 2583–2583, doi: 10.1200/jco.2021.39.15_suppl.2583.

GE, Z., PEPPELENBOSCH, M. P., SPRENGERS, D., and KWEKKEBOOM, J., 2021. TIGIT, the next step towards successful combination immune checkpoint therapy in cancer, *Frontiers in Immunology*, 12, doi: 10.3389/fimmu.2021.699895.

GRIMA, M., 2022. Development of Recombinant Antibodies Targeting T Cell Co-Inhibitory Protein TIM-3. BSc Thesis, Malta: University of Malta.

GRIMA, M., 2024. Development of Monoclonal Antibodies Targeting T Cell Co Inhibitory Proteins TIM-3 and TIM-4. MSc Thesis, Malta: University of Malta.

GUEX, N., PEITSCH, M.C., and SCHWEDE, T., 2009. Automated comparative protein structure modeling with SWISS-MODEL and Swiss-PdbViewer: A historical perspective. *Electrophoresis* 30, pp. 162-173.

GUPTA, A., SHRIVASTAVA, N., GROVER, P., SINGH, A., MATHUR, K., VERMA, V., KAUR, C., and CHAUDHARY, V. K., 2013. A novel Helper Phage enabling construction of Genome-Scale ORF-Enriched Phage display libraries. *PLoS ONE*, *8*(9), p. e75212. doi: 10.1371/journal.pone.0075212.

HAANEN, J., ERNSTOFF, M. S., WANG, Y., MENZIES, A. M., PUZANOV, I., GRIVAS, P., LARKIN, J., PETERS, S., THOMPSON, J. A., and OBEID, M., 2020. Autoimmune diseases and immune-checkpoint inhibitors for cancer therapy: Review of the literature and personalized risk-based prevention strategy, *Annals of Oncology*, 31(6), pp. 724–744, doi: 10.1016/j.annonc.2020.03.285.

HADDOCK 2.4, 2025. *Rascar science*, [Bovinlab], [Online]. Available: https://rascar.science.uu.nl/haddock2.4/ [May 18, 2025].

HALL, B. L., BOROUGHS, J., and KOBRIN, B. J., 1998. A novel tumor-specific human single-chain FV selected from an active specific immunotherapy phage display library, *Immunotechnology*, 4(2), pp. 127–140, doi: 10.1016/s1380-2933(98)00016-5.

HAMMERS, C. M., and STANLEY, J. R., 2014. Antibody phage Display: technique and applications. *Journal of Investigative Dermatology*, *134*(2), pp. 1–5. doi: 10.1038/jid.2013.521.

HAN, D., XU, Y., ZHAO, X., MAO, Y., KANG, Q., WEN, W., YU, X., XU, L., LIU, F., ZHANG, M., CUI, J., WANG, Z., YANG, Z., DU, P., and QIN, W., 2021. A novel human anti-TIGIT monoclonal antibody with excellent function in eliciting NK cell-mediated antitumor immunity. *Biochemical and Biophysical Research Communications*, 534, pp. 134–140, doi: 10.1016/j.bbrc.2020.12.013.

HE, C., MANIYAR, R. R., AVRAHAM, Y., ZAPPASODI, R., RUSINOVA, R., NEWMAN, W., HEATH, H., WOLCHOK, J. D., DAHAN, R., MERGHOUB, T., and MEYERSON, J. R., 2022. Therapeutic antibody activation of the glucocorticoid-induced TNF receptor by a clustering mechanism. *Science Advances*, *8*(8). doi: 10.1126/sciadv.abm4552

HE, X., and XU, C., 2020. Immune checkpoint signaling and cancer immunotherapy. *Cell Research*, *30*(8), pp. 660–669. doi: 10.1038/s41422-020-0343-4.

His Tagged Protein Purification, 2025. [SinoBiological], [Online], Available: https://www.sinobiological.com/resource/protein-review/poly-his-tag-protein-expression [Jun 4, 2025].

His-tagged Protein Expression & Purification, 2025. NEB, [New England Biolabs], [Online], Available: https://www.neb.com/en/applications/protein-purification/affinity-purification-and-expression-tags/his-tagged-protein-expression [Jun 5, 2025].

HO, B. K., and BRASSEUR, R., 2005. The Ramachandran plots of glycine and pre-proline. *BMC Structural Biology*, *5*(1). doi: 10.1186/1472-6807-5-14.

HOEN, P. A. ’., JIRKA, S. M., BROEKE, B. R. T., SCHULTES, E. A., AGUILERA, B., PANG, K. H., HEEMSKERK, H., AARTSMA-RUS, A., VAN OMMEN, G. J., and DUNNEN, J. T. D., 2011. Phage display screening without repetitious selection rounds. *Analytical Biochemistry*, *421*(2), pp. 622–631. doi: 10.1016/j.ab.2011.11.005.

HOGG, T., and HILGENFELD, R., 2007. Protein crystallography in drug discovery. In *Elsevier eBooks*, pp. 875–900. doi:10.1016/b0-08-045044-x/00111-5.

HONORATO, R.V., KOUKOS, P.I., JIMÉNEZ-GARCÍA, B., TSAREGORODTSEV, A., VERLATO, M., GIACHETTI, A., ROSATO, A., and BONVIN, A.M.J.J., 2021. Structural biology in the clouds: The WENMR-EOSC ecosystem, *Frontiers in molecular biosciences*. 8:729513. doi: 10.3389/fmolb.2021.729513.

HONORATO, R.V., TRELLET, M.E., JIMÉNEZ-GARCÍA, B., SCHAARSCHMIDT, J.J., GIULINI, M., REYS, V., KOUKOS, P.I., RODRIGUES, J.P.G.L.M., KARACA, E., VAN ZUNDERT, G.C.P., ROEL-TOURIS, J., VAN NOORT, C.W., JANDOVÁ, Z., MELQUIOND, A.S.J., and BONVIN, A.M.J.J., 2024. The HADDOCK2.4 web server for Integrative Modeling of Biomolecular Complexes. *Nature protocols*. **19**(11), pp. 3219-3241. doi: 10.1038/s41596-024-01011-0.

HUDSON, P. J., and KORTT, A. A., 1999. High avidity scFv multimers; diabodies and triabodies. *Journal of Immunological Methods*, *231*(1–2), pp. 177–189. doi: 10.1016/s0022-1759(99)00157-x.

HUNT, A. C., VÖGELI, B., HASSAN, A. O., GUERRERO, L., KIGHTLINGER, W., YOESEP, D. J., KRÜGER, A., DEWINTER, M., DIAMOND, M. S., KARIM, A. S., and JEWETT, M. C., 2023. A rapid cell-free expression and screening platform for antibody discovery. *Nature Communications*, *14*(1). doi: 10.1038/s41467-023-38965-w.

Informational Affinity His-Tag Purification Troubleshooting Guide, 2019-last update. [Gold Biotechnology], [Online]. Available: https://goldbio.com/documents/1013/Affinity%20His-Tag%20Purification%20Troubleshooting.pdf?srsltid=AfmBOorj_RH3GDEnXY-tNb2hzzfdi202-gZotFrRpcQt7aSR4FpAH4pc. [Mar 23, 2025].

ISTOMINA, P. V., GORCHAKOV, A. A., PAOIN, C., and YAMABHAI, M., 2024. Phage display for discovery of anticancer antibodies. *New Biotechnology*, *83*, pp. 205–218. doi: 10.1016/j.nbt.2024.08.506.

JACOBSON, A., 1972. Role of F Pili in the Penetration of Bacteriophage fl. *Journal of Virology*, 10(4), pp.835–843. doi: 10.1128/jvi.10.4.835-843.1972.

JAROSZEWICZ, W., MORCINEK-ORŁOWSKA, J., PIERZYNOWSKA, K., GAFFKE, L., and WĘGRZYN, G., 2022. Phage display and other peptide display technologies. *FEMS microbiology reviews*, 46(2), doi: 10.1093/femsre/fuab052.

JEONG, B.-S., NAM, H., LEE, J., PARK, H.-Y., CHO, K. J., SHEEN, J. H., SONG, E., OH, M., LEE, S., CHOI, H., YANG, J.-E., KIM, M., and OH, B.-H., 2022. Structural and functional characterization of a monoclonal antibody blocking TIGIT, *MAbs*, 14(1), doi: 10.1080/19420862.2021.2013750.

JIA, X., YAN, B., TIAN, X., LIU, Q., JIN, J., SHI, J., and HOU, Y., 2021. CD47/SIRPA pathway mediates cancer immune escape and immunotherapy, *International Journal of Biological Sciences*, 17(13), pp. 3281–3287, doi: 10.7150/ijbs.60782.

JIANG, Z., SUN, H., YU, J., TIAN, W., and SONG, Y., 2021. Targeting CD47 for cancer immunotherapy, *Journal of Hematology & Oncology*, 14(180), doi: 10.1186/s13045-021-01197-w.

JOLLER, N., and KUCHROO, V. K., 2017. Tim-3, LAG-3, and TIGIT, *Current Topics in Microbiology and Immunology*, 410, pp. 127–156, doi: 10.1007/82_2017_62.

JONES, M. L., ALFALEH, M. A., KUMBLE, S., ZHANG, S., OSBORNE, G. W., YEH, M., ARORA, N., HOU, J. J. C., HOWARD, C. B., CHIN, D. Y., and MAHLER, S. M., 2016. Targeting membrane proteins for antibody discovery using phage display. *Scientific Reports*, *6*(1). doi: 10.1038/srep26240.

JUMPER, J., EVANS, R., PRITZEL, A., GREEN, T., FIGURNOV, M., RONNEBERGER, O., TUNYASUVUNAKOOL, K., BATES, R., ŽÍDEK, A., POTAPENKO, A., BRIDGLAND, A., MEYER, C., KOHL, S.A.A., J BALLARD, A.J., COWIE, A., ROMERA-PAREDES, B., NIKOLOV, S., JAIN, R., ADLER, J., BACK, T., PETERSEN, S., REIMAN, D., CLANCY, E., ZIELINSKI, M., STEINEGGER, M., PACHOLSKA, M., BERGHAMMER, T., BODENSTEIN, S., SILVER, D., VINYALS, O., SENIOR, A.W., KAVUKCUOGLU, K., KOHLI, P., and HASSABIS, D., 2021. Highly accurate protein structure prediction with alphafold, *Nature*, 596(7873), pp. 583–589. doi: 10.1038/s41586-021-03819-2.

KAMALI, A. N., BAUTISTA, J. M., EISENHUT, M., and HAMEDIFAR, H., 2023. Immune checkpoints and cancer immunotherapies: insights into newly potential receptors and ligands. *Therapeutic Advances in Vaccines and Immunotherapy*, *11*. doi: 10.1177/25151355231192043.

KANAGAL-SHAMANNA, R., 2016. Emulsion PCR: Techniques and applications. *Methods in Molecular Biology*, pp. 33–42. doi: 10.1007/978-1-4939-3360-0_4.

KARAMITOPOULOU, E., 2019. Tumour microenvironment of pancreatic cancer: Immune landscape is dictated by molecular and histopathological features. *British Journal of Cancer*. 121 (1), pp. 5–14, doi: 10.1038/s41416-019-0479-5.

KERRY, J., 2025, January 2. Phage display antibody discovery, [Rapid Novor], Available: https://www.rapidnovor.com/phage-display-antibody-discovery/. [May 25, 2025].

KHAN, M., MAKER, A.V., and JAIN, S., 2021. The Evolution of Cancer Immunotherapy, *Vaccines*, 9(6), p.614, doi: 10.3390/vaccines9060614.

KIGUCHI, Y., OYAMA, H., MORITA, I., MORIKAWA, M., NAKANO, A., FUJIHARA, W., INOUE, Y., SASAKI, M., SAIJO, Y., KANEMOTO, Y., MURAYAMA, K., BABA, Y., TAKEUCHI, A., and KOBAYASHI, N., 2020. Clonal array profiling of scfv-displaying phages for high-throughput discovery of affinity-matured antibody mutants, *Scientific Reports*, 10, doi: 10.1038/s41598-020-71037-3.

KLANGPRAPAN, S., WENG, C., HUANG, W., LI, Y., and CHOOWONGKOMON, K., 2021. Selection and Characterization of a Single-Chain Variable Fragment against Porcine Circovirus Type 2 Capsid and Impedimetric Immunosensor Development. *ACS Omega*, *6*(37), pp. 24233–24243. doi: 10.1021/acsomega.1c03894.

KNEE, D. A., HEWES, B., and BROGDON, J. L., 2016. Rationale for anti-GITR cancer immunotherapy, *European Journal of Cancer*, 67, pp. 1–10, doi: 10.1016/j.ejca.2016.06.028.

KNIGHT, M.J., WOOLLEY, R.E., KWOK, A., PARSONS, S., JONES, H.B.L., GULÁCSY, C.E., PHAAL, P., KASSAAR, O., DAWKINS, K., RODRIGUEZ, E., MARQUES, A., BOWSHER, L., WELLS, S.A., WATTS, A., VAN DEN ELSEN, J.M.H., TURNER, A., O'HARA, J., and PUDNEY, C.R., 2020. Monoclonal antibody stability can be usefully monitored using the excitation-energy-

dependent fluorescence edge-shift. *Biochemical journal*, 477(18), pp. 3599-3612. doi: 10.1042/BCJ20200580.

KONERMANN, L., and SCROSATI, P. M., 2024. Hydrogen/Deuterium Exchange Mass Spectrometry: fundamentals, limitations, and opportunities. *Molecular and Cellular Proteomics*, *23*(11), p. 100853. doi: 10.1016/j.mcpro.2024.100853.

KORAIMANN, G., 2018. Spread and persistence of virulence and antibiotic resistance genes: A ride on the F plasmid conjugation module. *EcoSal Plus*, *8*(1). doi: 10.1128/ecosalplus.esp-0003-2018.

KRAMER, R. A., 2003. A novel helper phage that improves phage display selection efficiency by preventing the amplification of phages without recombinant protein. *Nucleic Acids Research*, *31*(11), pp. 59e–559. doi: 10.1093/nar/gng058.

KRISTENSEN, P., and WINTER, G., 1998. Proteolytic selection for protein folding using filamentous bacteriophages. *Folding & design*, 3(5), pp. 321-328. doi: 10.1016/S1359-0278(98)00044-3.

KUNISCH, F., WAGEMANS, J., and MORENO, M. G., 2023. Bacteriophage Precipitation with Polyethylene Glycol (PEG). *Research Square (Research Square)*. doi: 10.21203/rs.3.pex-1956/v1.

LAI, J. Y., and LIM, T. S., 2020. Infectious disease antibodies for biomedical applications: A mini review of immune antibody phage library repertoire. *International Journal of Biological Macromolecules*, *163*, pp. 640–648. doi: 10.1016/j.ijbiomac.2020.06.268.

LAKOWITZ, A., KRULL, R., and BIEDENDIECK, R., 2017. Recombinant production of the antibody fragment D1.3 scFv with different Bacillus strains. *Microbial Cell Factories*, *16*(1). doi: 10.1186/s12934-017-0625-9.

LAPLANE, L., DULUC, D., BIKFALVI, A., LARMONIER, N., and PRADEU, T., 2019. Beyond the tumour microenvironment. *International Journal of Cancer*. 145 (10), pp. 2611–2618, doi: 10.1002/ijc.32343.

LEDSGAARD, L., LJUNGARS, A., RIMBAULT, C., SØRENSEN, C.V., TULIKA, T., WADE, J., WOUTERS, Y., MCCAFFERTY, J., and LAUSTSEN, A.H., 2022. Advances in antibody phage

display technology. *Drug Discovery Today*. 27 (8), pp. 2151–2169, doi: 10.1016/j.drudis.2022.05.002.

LI, K., ZETTLITZ, K. A., LIPIANSKAYA, J., ZHOU, Y., MARKS, J. D., MALLICK, P., REITER, R. E., and WU, A. M., 2015. A fully human scFv phage display library for rapid antibody fragment reformatting. *Protein Engineering Design and Selection*, *28*(10), pp. 307–316. doi: 10.1093/protein/gzv024.

LI, S., HOEFNAGEL, S. J. M., and KRISHNADATH, K. K., 2023. Single domain Camelid antibody fragments for molecular imaging and therapy of cancer. *Frontiers in Oncology*, *13*. doi: 10.3389/fonc.2023.1257175.

LIMA, A. J. F., HAJDU, K. L., ABDO, L., BATISTA-SILVA, L. R., DE OLIVEIRA ANDRADE, C., CORREIA, E. M., ARAGÃO, E. A. A., BONAMINO, M. H., and LOURENZONI, M. R., 2024. In silico and in vivo analysis reveal impact of c-Myc tag in FMC63 scFv-CD19 protein interface and CAR-T cell efficacy. *Computational and Structural Biotechnology Journal*, *23*, pp. 2375–2387. doi: 10.1016/j.csbj.2024.05.032.

LIN, C., REN, W., LUO, Y., LI, S., CHANG, Y., LI, L., XIONG, D., HUANG, X., XU, Z., YU, Z., WANG, Y., ZHANG, J., HUANG, C., and XIA, N., 2020. Intratumoral delivery of a PD-1–blocking scfv encoded in oncolytic HSV-1 promotes antitumor immunity and synergizes with TIGIT blockade, *Cancer Immunology Research*, 8(5), pp. 632–647, doi: 10.1158/2326-6066.cir-19-0628.

LISOWSKA, M., WORRALL, E. G., ZAVADIL-KOKAS, F., CHARLTON, K., MURRAY, E., MOHTAR, M. A., KREJCIR, R., HRABAL, V., BRYDON, J., URIONABARRENETXEA, A. G., SALIBA, D. G., GRIMA, M., KALATHIYA, U., MULLER, P., KREJCI, A., VOJTESEK, B., BALL, K. L., FAHRAEUS, R., ARGYLE, D. J., . . . HUPP, T. R., 2025. The development of a canine single-chain phage antibody library to isolate recombinant antibodies for use in translational cancer research. *Cell Reports Methods*, *5*(3), p. 101008. doi: 10.1016/j.crmeth.2025.101008.

LIU, Y., and YU, J., 2016. Oriented immobilization of proteins on solid supports for use in biosensors and biochips: a review. *Microchimica Acta*, 183(1), pp. 1-19. doi: 10.1007/s00604-015-1623-4.

LIU, Y., GU, M., WU, Y., WANG, W., WANG, R., DU, M., MA, P., ZHOU, X., WANG, Y., CAO, Y., and ZHANG, H., 2018. High-throughput reformatting of phage-displayed antibody fragments to IgGs by one-step emulsion PCR. *Protein Engineering Design and Selection*, *31*(11), pp. 427–436. doi: 10.1093/protein/gzz004.

LUKE, J., 2023. Immunomodulators: Checkpoint Inhibitors, Cytokines, Agonists, and Adjuvants, [Cancer Research Institute], [Online], Available: https://www.cancerresearch.org/immunotherapy-by-treatment-types/immunomodulators [3 Apr, 2023].

LUO, D., MAH, N., KRANTZ, M., WILDE, K., WISHART, D., ZHANG, Y., JACOBS, F., and MARTIN, L., 1995. VI-Linker-VH Orientation-Dependent expression of single chain FV containing an engineered Disulfide-Stabilized bond in the framework Regions1. *The Journal of Biochemistry*, *118*(4), pp. 825–831. doi: 10.1093/oxfordjournals.jbchem.a124986.

MALMBORG, A.-C., SÖDERLIND, E., FROST, L., and BORREBAECK, C.A.K., 1997. Selective phage infection mediated by epitope expression on F pilus. *Journal of Molecular Biology*, 273(3), pp.544–551. doi: 10.1006/jmbi.1997.1332.

MARSH, W., WITTEN, A., and STABENFELDT, S. E., 2018. Exploiting phage display for development of novel cellular targeting strategies. *Methods in Molecular Biology*, pp. 71–94. doi: 10.1007/978-1-4939-8661-3_7.

MARTZ, E., 2016-last updated. Tutorial: Ramachandran principle and phi psi angles: The Ramachandran Principle - Phi (ϕ) and Psi (ψ) Angles in Proteins, [Proteopedia], [Online], Available: https://proteopedia.org/wiki/index.php/Tutorial:Ramachandran_principle_and_phi_psi_angles [Mar 15, 2025].

MCCONNELL, S. J., DINH, T., LE, M., and SPINELLA, D. G., 1999. Biopanning phage display libraries using magnetic beads vs. polystyrene plates. *BioTechniques*, *26*(2), pp. 208–214. doi: 10.2144/99262bm06.

MCDOWELL, S., 2018. What is cancer control? [American Cancer Society], [Online]. Available: https://www.cancer.org/latest-news/what-is-cancer-control.htmL [3 Ap, 2023].

MEHTA, A., HARB, W., XU, C., MENG, Y., LEE, L., YUAN, V., WANG, Z., SONG, P., SHEN, J. H., and GOPAL, A. K., 2021. Lemzoparlimab, a Differentiated Anti-CD47 Antibody in Combination with Rituximab in Relapsed and Refractory Non-Hodgkin's Lymphoma: Initial Clinical Results. *Blood*, *138*(Supplement 1), p. 3542. doi: 10.1182/blood-2021-150606.

Method 1643: Male-specific (F+) and Somatic Coliphage in Secondary (No Disinfection) Wastewater by the Single Agar Layer (SAL) Procedure, 2018. *EPA*. Environmental Protection Agency, [Online]. Available: https://www.epa.gov/sites/default/files/2018-09/documents/method_1643_draft_2018.pdf [Mar 18, 2025].

MILLER, B. R., DEMAREST, S. J., LUGOVSKOY, A., HUANG, F., WU, X., SNYDER, W. B., CRONER, L. J., WANG, N., AMATUCCI, A., MICHAELSON, J. S., and GLASER, S. M., 2010. Stability engineering of scFvs for the development of bispecific and multivalent antibodies. *Protein Engineering Design and Selection*, *23*(7), pp. 549–557. doi: 10.1093/protein/gzq028.

MILLER, T. W., KAUR, S., IVINS-O'KEEFE, K., and ROBERTS, D. D., 2013. Thrombospondin-1 is a CD47-dependent endogenous inhibitor of hydrogen sulfide signaling in T cell activation, *Matrix Biology*, 32(6), pp. 316–324, doi: 10.1016/j.matbio.2013.02.009.

Monarch® Plasmid Miniprep Kit Instruction Manual, 9/2021. version 3.1, *New England BioLabs Inc.*, Massachusetts, United States, [Online]. Available: https://www.neb.com/monarch/-/media/73e527a1f8014c1189567f2ec1ff833e.ashx [Apr 15, 2025].

Most Popular Antibody Fragment: Single Domain Antibody vs. ScFv, 2023, April 14. Single Domain Antibody Blog, [Creative Biolabs], [Online], Available: https://www.creative-biolabs.com/blog/sdab/biological-knowledge/most-popular-antibody-fragment-single-domain-antibody-vs-scfv/ [Jun 11, 2025].

MUSNIER, A., CORDE, Y., VERDIER, A., CORTES, M., PALLANDRE, J., DUMET, C., BOUARD, A., KESKES, A., OMAHDI, Z., PUARD, V., POUPON, A., and BOURQUARD, T., 2025. AI-enhanced profiling of phage-display-identified anti-TIM3 and anti-TIGIT novel antibodies. *Frontiers in Immunology*, *16*. doi: 10.3389/fimmu.2025.1499810.

NAGANO, K., and TSUTSUMI, Y., 2021. Phage display technology as a powerful platform for antibody drug discovery, *Viruses*, 13(2), p. 178, doi: 10.3390/v13020178.

NATH, P. R., PAL-NATH, D., KAUR, S., GANGAPLARA, A., MEYER, T. J., CAM, M. C., and ROBERTS, D. D., 2022. Loss of CD47 alters CD8+ T cell activation in vitro and immunodynamics in mice, *OncoImmunology*, 11(1), doi: 10.1080/2162402x.2022.2111909.

National Cancer Institute, 2019. Immunotherapy for cancer, [National Cancer Institute], [Online]. Available: https://www.cancer.gov/about-cancer/treatment/types/immunotherapy [3 Apr, 2023].

NIU, J., MAURICE-DROR, C., LEE, D. H., KIM, D.-W., NAGRIAL, A., VOSKOBOYNIK, M., CHUNG, H. C., MILEHAM, K., VAISHAMPAYAN, U., RASCO, D., GOLAN, T., BAUER, T. M., JIMENO, A., CHUNG, V., CHARTASH, E., LALA, M., CHEN, Q., HEALY, J. A., and AHN, M.-J., 2022. First-in-human phase 1 study of the anti-TIGIT antibody vibostolimab as monotherapy or with pembrolizumab for advanced solid tumors, including non-small-cell lung cancer, *Annals of Oncology*, 33(2), pp. 169–180, doi: 10.1016/j.annonc.2021.11.002.

NOCENTINI, G., and RICCARDI, C., 2009. Gitr: A modulator of immune response and inflammation, *Advances in Experimental Medicine and Biology, Therapeutic Targets of the TNF Superfamily* , 647, pp. 156–173, doi: 10.1007/978-0-387-89520-8_11.

NOCENTINI, G., RONCHETTI, S., PETRILLO, M. G., and RICCARDI, C., 2012. Pharmacological modulation of GITRL/GITR system: Therapeutic perspectives, *British Journal of Pharmacology*, 165(7), pp. 2089–2099, doi: 10.1111/j.1476-5381.2011.01753.x.

NOVOTNY, C.P., and FIVES-TAYLOR, P., 1974. Retraction of F Pili. *Journal of Bacteriology*, 117(3), pp.1306–1311. doi: 10.1128/jb.117.3.1306-1311.1974.

O'CALLAGHAN, R., BRADLEY, R., and PARANCHYCH, W., 1973. The effect of M13 phage infection upon the F pili of E. coli. *Virology*, 54(1), pp.220–229. doi: 10.1016/0042-6822(73)90131-1.

ORNER, B. P., DERDA, R., LEWIS, R. L., THOMSON, J. A., and KIESSLING, L. L., 2004. Arrays for the combinatorial exploration of cell adhesion. *Journal of the American Chemical Society*, *126*(35), pp. 10808–10809. doi: 10.1021/ja0474291.

OSSYSEK, K., UCHAŃSKI, T., KULESZA, M., BZOWSKA, M., KLAUS, T., WOŚ, K., MADEJ, M., and BERETA, J., 2015. A new expression vector facilitating production and functional analysis of

scFv antibody fragments selected from Tomlinson I + J phagemid libraries. *Immunology Letters*, *167*(2), pp. 95–102. doi: 10.1016/j.imlet.2015.07.005.

OZOHANICS, O., and AMBRUS, A., 2020. Hydrogen-Deuterium Exchange Mass spectrometry: a novel structural biology approach to structure, dynamics and interactions of proteins and their complexes. *Life*, *10*(11), p. 286. doi: 10.3390/life10110286.

PANAGIDES, N., ZACCHI, L. F., DE SOUZA, M. J., MORALES, R. A. V., KARNOWSKI, A., LIDDAMENT, M. T., OWCZAREK, C. M., MAHLER, S. M., PANOUSIS, C., JONES, M. L., and FERCHER, C., 2022. Evaluation of phage display biopanning strategies for the selection of Anti-Cell surface receptor antibodies. *International Journal of Molecular Sciences*, *23*(15), p. 8470. doi: 10.3390/ijms23158470.

PANSRI, P., JARUSERANEE, N., RANGNOI, K., KRISTENSEN, P., and YAMABHAI, M., 2009. A compact phage display human scfv library for selection of antibodies to a wide variety of antigens, *BMC Biotechnology*, 9(6), doi: 10.1186/1472-6750-9-6.

Ph.D. Phage Display Libraries Instruction Manual, 2020. version 5.0_8/20. *New England BioLabs Inc.*, Massachusetts, United States, [Online]. Available: https://www.neb.com/en/-/media/nebus/files/manuals/manuale8100_e8101_e8110_e8111_e8120.pdf [Feb 02, 2025].

PINA, A. S., BATALHA, Í. L., and ROQUE, A. C. A., 2014. Affinity Tags in Protein Purification and Peptide Enrichment: An Overview. *Methods in Molecular Biology*, pp. 147–168. doi: 10.1007/978-1-62703-977-2_14.

QI, H., LU, H., QIU, H., PETRENKO, V., and LIU, A., 2012. Phagemid Vectors for Phage Display: Properties, Characteristics and Construction. *Journal of Molecular Biology*, *417*(3), pp. 129–143. doi: 10.1016/j.jmb.2012.01.038.

READER, R. H., WORKMAN, R. G., MADDISON, B. C., and GOUGH, K. C., 2019. Advances in the production and batch reformatting of phage antibody libraries. *Molecular Biotechnology*, *61*(11), pp. 801–815. doi: 10.1007/s12033-019-00207-0.

Recombinant Human CD47 Protein (ECD, hFc Tag), HPLC-verified Package Insert. R&D Systems, Minnesota, United States, [Online]. Available: https://www.sinobiological.com/recombinant-proteins/human-cd47-12283-h02h [Jul 14, 2024].

Recombinant Human CD47 Protein (ECD, His Tag), HPLC-verified, High activity Package Insert. R&D Systems, Minnesota, United States, [Online]. Available: https://www.sinobiological.com/recombinant-proteins/human-cd47-12283-h08h [Sep 12, 2023].

Recombinant Human GITR/TNFRSF18/AITR Protein (ECD, His Tag), HPLC-verified Package Insert. R&D Systems, Minnesota, United States, [Online]. Available: https://www.sinobiological.com/recombinant-proteins/human-gitr-13643-h08h [Sep 12, 2023].

Recombinant Human TIGIT Protein (Dimer, ECD, His Tag), HPLC-verified Package Insert. R&D Systems, Minnesota, United States, [Online]. Available: https://www.sinobiological.com/recombinant-proteins/human-tigit-10917-h08h3 [Sep 12, 2023].

Recombinant Human TIGIT Protein (ECD, hFc Tag), HPLC-verified Package Insert. R&D Systems, Minnesota, United States, [Online]. Available: https://www.sinobiological.com/recombinant-proteins/human-tigit-10917-h02h [Jul 14, 2024].

REZAEI, G., HABIBI-ANBOUHI, M., MAHMOUDI, M., AZADMANESH, K., MORADI-KALBOLANDI, S., BEHDANI, M., GHAZIZADEH, L., ABOLHASSANI, M., and SHOKRGOZAR, M. A., 2017. Development of anti-CD47 single-chain variable fragment targeted magnetic nanoparticles for treatment of human bladder cancer, *Nanomedicine*, 12(6), pp. 597–613, doi: 10.2217/nnm-2016-0302.

RIAZ, N., HAVEL, J. J., MAKAROV, V., DESRICHARD, A., URBA, W. J., SIMS, J. S., HODI, F. S., MARTÍN-ALGARRA, S., MANDAL, R., SHARFMAN, W. H., BHATIA, S., HWU, W.-J., GAJEWSKI, T. F., SLINGLUFF, C. L., CHOWELL, D., KENDALL, S. M., CHANG, H., SHAH, R., KUO, F., MORRIS, L. G. T., SIDHOM, J.-W., SCHNECK, J. P., HORAK, C. E., WEINHOLD, N., and CHAN, T. A., 2017. Tumor and microenvironment evolution during immunotherapy with nivolumab, *Cell*, 171(4), doi: 10.1016/j.cell.2017.09.028.

RODRIGUEZ-ABREU, D., JOHNSON, M. L., HUSSEIN, M. A., COBO, M., PATEL, A. J., SECEN, N. M., LEE, K. H., MASSUTI, B., HIRET, S., YANG, J. C.-H., BARLESI, F., LEE, D. H., PAZ-ARES, L. G.,

HSIEH, R. W., MILLER, K., PATIL, N., TWOMEY, P., KAPP, A. V., MENG, R., and CHO, B. C., 2020. Primary analysis of a randomized, double-blind, phase II study of the anti-TIGIT antibody tiragolumab (TIRA) plus atezolizumab (atezo) versus placebo plus Atezo as first-line (1L) treatment in patients with PD-L1-selected NSCLC (Cityscape)., *Journal of Clinical Oncology*, 38(15), pp. 9503–9503, doi: 10.1200/jco.2020.38.15_suppl.9503.

RONDOT, S., KOCH, J., BREITLING, F., and DÜBEL, S., 2001. A helper phage to improve single-chain antibody presentation in phage display. *Nature Biotechnology*, 19(1), pp.75–78. doi: 10.1038/83567.

ROTH, K. D., WENZEL, E. V., RUSCHIG, M., STEINKE, S., LANGREDER, N., HEINE, P. A., SCHNEIDER, K.-T., BALLMANN, R., FÜHNER, V., KUHN, P., SCHIRRMANN, T., FRENZEL, A., DÜBEL, S., SCHUBERT, M., MOREIRA, G. M., BERTOGLIO, F., RUSSO, G., and HUST, M., 2021. Developing recombinant antibodies by phage display against infectious diseases and toxins for diagnostics and therapy, *Frontiers in Cellular and Infection Microbiology*, 11, doi: 10.3389/fcimb.2021.697876.

ROTTE, A., 2019. Combination of CTLA-4 and PD-1 blockers for treatment of cancer, *Journal of Experimental & Clinical Cancer Research*, 38(255), doi: 10.1186/s13046-019-1259-z.

ROTTE, A., SAHASRANAMAN, S., and BUDHA, N., 2021. Targeting TIGIT for immunotherapy of cancer: Update on clinical development, *Biomedicines*, 9(9), p. 1277, doi: 10.3390/biomedicines9091277.

SANMARK, H., HUOVINEN, T., MATIKKA, T., PETTERSSON, T., LAHTI, M., and LAMMINMÄKI, U., 2015. Fast conversion of scFv to Fab antibodies using type IIs restriction enzymes. *Journal of Immunological Methods*, *426*, pp. 134–139. doi: 10.1016/j.jim.2015.08.005.

SARÉN, T., SARONIO, G., TORRELL, P. M., ZHU, X., THELANDER, J., ANDERSSON, Y., HOFSTRÖM, C., NESTOR, M., DIMBERG, A., PERSSON, H., RAMACHANDRAN, M., YU, D., and ESSAND, M., 2023. Complementarity-determining region clustering may cause CAR-T cell dysfunction. *Nature Communications*, *14*(1). doi: 10.1038/s41467-023-40303-z.

SAW, P. E., and SONG, E.-W., 2019. Phage display screening of therapeutic peptide for cancer targeting and therapy, *Protein & Cell*, 10(11), pp. 787–807, doi: 10.1007/s13238-019-0639-7.

scFv Conversion into scFv-Fc, 2015. Antibody Design Labs, [ABD], [Online], Available: https://www.abdesignlabs.com/technical-resources/scfv-fc-conversion/ [Jun 7, 2025].

SHARMA, P., GOSWAMI, S., RAYCHAUDHURI, D., SIDDIQUI, B. A., SINGH, P., NAGARAJAN, A., LIU, J., SUBUDHI, S. K., POON, C., GANT, K. L., HERBRICH, S. M., ANANDHAN, S., ISLAM, S., AMIT, M., ANANDAPPA, G., and ALLISON, J. P., 2023. Immune checkpoint therapy—current perspectives and Future Directions, *Cell*, 186(8), pp. 1652–1669, doi: 10.1016/j.cell.2023.03.006.

SHERBET, G. V., 2017. Notable approaches to cancer immunotherapy, *Molecular Approach to Cancer Management*, pp. 223–244, doi: 10.1016/b978-0-12-812896-1.00026-x.

SINKJAER, A. W., SLOTH, A. B., ANDERSEN, A. O., JENSEN, M., BAKHSHINEJAD, B., and KJAER, A., 2025. A comparative analysis of sequence composition in different lots of a phage display peptide library during amplification. *Virology Journal*, *22*(1). doi: 10.1186/s12985-024-02600-x.

SLOTH, A.B., BAKHSHINEJAD, B., JENSEN, M., STAVNSBJERG, C., LIISBERG, M.B., ROSSING, M., and KJAER, A., 2022. Analysis of Compositional Bias in a Commercial Phage Display Peptide Library by Next Generation Sequencing. *Viruses*, 14(11), pp. 2402. doi: 10.3390/v14112402.

SMITH, G. P., 1985. Filamentous fusion phage: Novel expression vectors that display cloned antigens on the virion surface, *Science*, 228(4705), pp. 1315–1317, doi: 10.1126/science.4001944.

SMYTH, M.J., NGIOW, S.F., RIBAS, A., and TENG, M.W., 2015. Combination cancer immunotherapies tailored to the tumour microenvironment. *Nature Reviews Clinical Oncology*. 13 (3), pp. 143–158, doi: 10.1038/nrclinonc.2015.209.

SOTO-PANTOJA, D. R., KAUR, S., and ROBERTS, D. D., 2015. CD47 signaling pathways controlling cellular differentiation and responses to stress, *Critical Reviews in Biochemistry and Molecular Biology*, 50(3), pp. 212–230, doi: 10.3109/10409238.2015.1014024.

SPITERI, J., 2022. Development of Recombinant Antibodies Targeting T Cell Co-Inhibitory Molecule VISTA. BSc Thesis, Malta: University of Malta.

SPITZER, M.H., CARMI, Y., RETICKER-FLYNN, N.E., KWEK, S.S., MADHIREDDY, D., MARTINS, M.M., GHERARDINI, P.F., PRESTWOOD, T.R., CHABON, J., BENDALL, S.C., FONG, L., NOLAN, G.P., and ENGLEMAN, E.G., 2017. Systemic immunity is required for effective cancer immunotherapy. *Cell*. 168 (3), pp. 487-502, doi:10.1016/j.cell.2016.12.022.

STEFAN, M. A., LIGHT, Y. K., SCHWEDLER, J. L., MCILROY, P. R., COURTNEY, C. M., SAADA, E. A., THATCHER, C. E., PHILLIPS, A. M., BOURGUET, F. A., MAGEENEY, C. M., MCCLOY, S. A., COLLETTE, N. M., NEGRETE, O. A., SCHOENIGER, J. S., WEILHAMMER, D. R., and HARMON, B., 2021. Development of potent and effective synthetic SARS-CoV-2 neutralizing nanobodies. *mAbs*, *13*(1). doi: 10.1080/19420862.2021.1958663.

STENGEL, K. F., HARDEN-BOWLES, K., YU, X., ROUGE, L., YIN, J., COMPS-AGRAR, L., WIESMANN, C., BAZAN, J. F., EATON, D. L., and GROGAN, J. L., 2012. Structure of TIGIT immunoreceptor bound to poliovirus receptor reveals a cell–cell adhesion and signaling mechanism that requires cis-trans receptor clustering, *Proceedings of the National Academy of Sciences*, 109(14), pp. 5399–5404, doi: 10.1073/pnas.1120606109.

Study of the Safety and Efficacy of STI-6643 in Subjects With Advanced Solid Tumors, 2023-last updated. *ClinicalTrials*. [National Library of Medicine], [Online]. Available: https://clinicaltrials.gov/study/NCT04900519?tab=history. [Mar 30, 2025].

SWISS-MODEL Repository, 2025. *Swissmodel.expasy*. [Swiss Institute of Bioinformatics and Biozentrum], [ELIXIR], [Online]. Available: https://swissmodel.expasy.org/ [May 18. 2025].

TAKKENKAMP, T.J., JALVING, M., HOOGWATER, F.J., and WALENKAMP, A.M., 2020. The immune tumour microenvironment of neuroendocrine tumours and its implications for immune checkpoint inhibitors. *Endocrine-Related Cancer*. 27 (9), doi: 10.1530/ERC-20-0113.

THAKER, Y. R., RIVERA, I., PEDROS, C., SINGH, A. R., RIVERO-NAVA, L., ZHOU, H., SWANSON, B. A., KERWIN, L., ZHANG, Y., GRAY, J. D., KAUFMANN, G. F., JI, H., ALLEN, R. D., and BRESSON, D., 2022. A novel affinity engineered Anti-CD47 antibody with improved therapeutic index that preserves erythrocytes and normal immune cells. *Frontiers in Oncology*, *12*. doi: 10.3389/fonc.2022.884196.

The Ultimate Guide to ANOVA, 2025. [GraphPad] [Online]. Available: https://www.graphpad.com/guides/the-ultimate-guide-to-anova [Mar 29, 2025].

THOMAS, W. D., and SMITH, G. P., 2010. The case for Trypsin release of Affinity-Selected phages. *BioTechniques*, *49*(3), pp. 651–654. doi: 10.2144/000113489.

THOTA, V., PUDDU, V., and PERRY, C. C., 2024. Phage display panning on silica: Optimization of elution conditions for selection of strong binders. *Langmuir*. doi: 10.1021/acs.langmuir.4c01108.

TODOROVSKA, A., ROOVERS, R. C., DOLEZAL, O., KORTT, A. A., HOOGENBOOM, H. R., and HUDSON, P. J., 2001. Design and application of diabodies, triabodies and tetrabodies for cancer targeting. *Journal of Immunological Methods*, *248*(1–2), pp. 47–66. doi: 10.1016/s0022-1759(00)00342-2.

UniProtKB, 2025. *Q9Y5U5 · TNR18_HUMAN*. [EMBL-EBI], [Online]. Available: https://www.uniprot.org/uniprotkb/Q9Y5U5/entry [May 18 2025].

VANNEMAN, M., and DRANOFF, G., 2012. Combining immunotherapy and targeted therapies in cancer treatment, *Nature Reviews Cancer*, 12(4), pp.237-51, doi: 10.1038/nrc3237.

VARADI, M., BERTONI, D., MAGANA, P., PARAMVAL, U., PIDRUCHNA, I., RADHAKRISHNAN, M., TSENKOV, M., NAIR, S., MIRDITA, M., YEO, J., KOVALEVSKIY, O., TUNYASUVUNAKOOL, K., LAYDON, A., ŽÍDEK, A., TOMLINSON, H., HARIHARAN, D., ABRAHAMSON, J., GREEN, T., JUMPER, J., BIRNEY, E., STEINEGGER, M., HASSABIS, D., and VELANKAR, S., 2024. AlphaFold Protein Structure Database in 2024: providing structure coverage for over 214 million protein sequences. *Nucleic Acids Res*. 5;52(D1), pp. D368-D375. doi: 10.1093/nar/gkad1011.

VEILLETTE, A., and CHEN, J., 2018. SIRPA–CD47 immune checkpoint blockade in anticancer therapy, *Trends in Immunology*, 39(3), pp. 173–184, doi: 10.1016/j.it.2017.12.005.

WANG, B., ZHANG, W., JANKOVIC, V., GOLUBOV, J., POON, P., OSWALD, E. M., GURER, C., WEI, J., RAMOS, I., WU, Q., WAITE, J., NI, M., ADLER, C., WEI, Y., MACDONALD, L., ROWLANDS, T., BRYDGES, S., SIAO, J., POUEYMIROU, W., MACDONALD, D., YANCOPOULOS, G. D., SLEEMAN, M. A., MURPHY, A. J., and SKOKOS, D., 2018. Combination cancer immunotherapy targeting PD-1 and GITR can rescue CD8+ T cell dysfunction and maintain memory phenotype, *Science Immunology*, 3(29), doi: 10.1126/sciimmunol.aat7061.

VAN ZUNDERT, G.C.P., RODRIGUES, J.P.G.L.M., TRELLET, M., SCHMITZ, C., KASTRITIS, P.L., KARACA, E., MELQUIOND, A.S.J., VAN DIJK, M., DE VRIES, S.J., and BONVIN, A.M.J.J., 2015. The

HADDOCK2.2 webserver: User-friendly integrative modeling of biomolecular complexes. *Journal of Molecular Biology, 428*, pp. 720-725.

WANG, F., CHAU, B., WEST, S. M., KIMBERLIN, C. R., CAO, F., SCHWARZ, F., AGUILAR, B., HAN, M., MORISHIGE, W., BEE, C., DOLLINGER, G., RAJPAL, A., and STROP, P., 2021. Structures of mouse and human GITR–GITRL complexes reveal unique TNF superfamily interactions, *Nature Communications*, 12(1378), doi: 10.1038/s41467-021-21563-z.

WANG, M., BU, J., ZHOU, M., SIDO, J., LIN, Y., LIU, G., LIN, Q., XU, X., LEAVENWORTH, J. W., and SHEN, E., 2018. CD8 + T cells expressing both PD-1 and TIGIT but not CD226 are dysfunctional in acute myeloid leukemia (AML) patients, *Clinical Immunology*, 190, pp. 64–73, doi: 10.1016/j.clim.2017.08.021.

WANG, Y., GAO, S., LV, J., LIN, Y., ZHOU, L., and HAN, L., 2019. Phage display technology and its applications in cancer immunotherapy, *Anti-Cancer Agents in Medicinal Chemistry*, 19(2), pp. 229–235, doi: 10.2174/1871520618666181029140814.

WARD, R.L., CLARK, M.A., LEES, J., and HAWKINS, N.J., 1996. Retrieval of human antibodies from phage display libraries using enzymatic cleavage. *Journal of immunological methods*, 189(1), pp. 73-82. doi: 10.1016/0022-1759(95)00231-6.

WATERHOUSE, A., BERTONI, M., BIENERT, S., STUDER, G., TAURIELLO, G., GUMIENNY, R., HEER, F.T., DE BEER, T.A.P., REMPFER, C., BORDOLI, L., LEPORE, R., and SCHWEDE, T., 2018. SWISS-MODEL: homology modelling of protein structures and complexes. *Nucleic Acids Res*. 46(W1), pp. 296-303.

WEISKOPF, K., JAHCHAN, N. S., SCHNORR, P. J., CRISTEA, S., RING, A. M., MAUTE, R. L., VOLKMER, A. K., VOLKMER, J.-P., LIU, J., LIM, J. S., YANG, D., SEITZ, G., NGUYEN, T., WU, D., JUDE, K., GUERSTON, H., BARKAL, A., TRAPANI, F., GEORGE, J., POIRIER, J. T., GARDNER, E. E., MILES, L. A., DE STANCHINA, E., LOFGREN, S. M., VOGEL, H., WINSLOW, M. M., DIVE, C., THOMAS, R. K., RUDIN, C. M., VAN DE RIJN, M., MAJETI, R., GARCIA, K. C., WEISSMAN, I. L., and SAGE, J., 2016. CD47-blocking immunotherapies stimulate macrophage-mediated destruction of small-cell lung cancer, *Journal of Clinical Investigation*, 126(7), pp. 2610–2620, doi: 10.1172/jci81603.

WEN, J., MAO, X., CHENG, Q., LIU, Z., and LIU, F.,2021. A pan-cancer analysis revealing the role of TIGIT in tumor microenvironment, *Scientific Reports*, 11, doi: 10.1038/s41598-021-01933-9.

What is the meaning of * or ** or *** in reports of statistical significance from prism or instat?, 2025. *Dotmatics*, [GraphPad], [Online]. Available: https://www.graphpad.com/support/faq/what-is-the-meaning-of--or--or--in-reports-of-statistical-significance-from-prism-or-instat/ [Mar 28, 2025].

Working with Helper Phages, 2024. [Antibody Design Labs.], [Online]. Available: https://www.abdesignlabs.com/technical-resources/helper-phages/ [Mar 22, 2025].

WÖRN, A., MAUR, A. A. D., ESCHER, D., HONEGGER, A., BARBERIS, A., and PLÜCKTHUN, A., 2000. Correlation between in Vitro Stability and in Vivo Performance of Anti-GCN4 Intrabodies as Cytoplasmic Inhibitors. *Journal of Biological Chemistry*, *275*(4), pp. 2795–2803. doi: 10.1074/jbc.275.4.2795.

WU, C., LIU, I., LU, R., and WU, H., 2016. Advancement and applications of peptide phage display technology in biomedical science. *Journal of Biomedical Science*, *23*(1). doi: 10.1186/s12929-016-0223-x.

XIAO, X., CHEN, Y., MUGABE, S., GAO, C., TKACZYK, C., MAZOR, Y., PAVLIK, P., WU, H., DALL'ACQUA, W., and CHOWDHURY, P. S., 2015. A Novel Dual Expression Platform for High Throughput Functional Screening of Phage Libraries in Product like Format. *PLoS ONE*, *10*(10), p. e0140691. doi: 10.1371/journal.pone.0140691.

XIAO, X., DOUTHWAITE, J. A., CHEN, Y., KEMP, B., KIDD, S., PERCIVAL-ALWYN, J., SMITH, A., GOODE, K., SWERDLOW, B., LOWE, D., WU, H., DALL'ACQUA, W. F., and CHOWDHURY, P. S., 2017. A high-throughput platform for population reformatting and mammalian expression of phage display libraries to enable functional screening as full-length IgG. *mAbs*, *9*(6), pp. 996–1006. doi: 10.1080/19420862.2017.1337617.

YAMAMOTO, K. R., ALBERTS, B. M., BENZINGER, R., LAWHORNE, L., and TREIBER, G., 1970. Rapid bacteriophage sedimentation in the presence of polyethylene glycol and its application to large-scale virus purification. *Virology*, *40*(3), pp. 734–744. doi: 10.1016/0042-6822(70)90218-7.

YANG, H., XUN, Y., and YOU, H., 2023. The landscape overview of CD47-based immunotherapy for hematological malignancies, *Biomarker Research*, 11(15), doi: 10.1186/s40364-023-00456-x.

YANG, Y., YANG, Z., and YANG, Y., 2021. Potential role of CD47-directed bispecific antibodies in cancer immunotherapy, *Frontiers in Immunology*, 12, doi: 10.3389/fimmu.2021.686031.

YOUNG, C. L., BRITTON, Z. T., and ROBINSON, A. S., 2012. Recombinant protein expression and purification: A comprehensive review of affinity tags and microbial applications. *Biotechnology Journal*, *7*(5), pp. 620–634. doi: 10.1002/biot.201100155.

YUN, S., LEE, S., PARK, J. P., CHOO, J., and LEE, E, 2019. Modification of phage display technique for improved screening of high-affinity binding peptides. *Journal of Biotechnology*, *289*, pp. 88–92. doi: 10.1016/j.jbiotec.2018.11.020.

ZAPPASODI, R., SIRARD, C., LI, Y., BUDHU, S., ABU-AKEEL, M., LIU, C., YANG, X., ZHONG, H., NEWMAN, W., QI, J., WONG, P., SCHAER, D., KOON, H., VELCHETI, V., HELLMANN, M. D., POSTOW, M. A., CALLAHAN, M. K., WOLCHOK, J. D., and MERGHOUB, T., 2019. Rational design of anti-GITR-based combination immunotherapy, *Nature Medicine*, 25(5), pp. 759–766, doi: 10.1038/s41591-019-0420-8.

ZENG, D., SUN, Q., CHEN, A., FAN, J., YANG, X., XU, L., DU, P., QIU, W., ZHANG, W., WANG, S., and SUN, Z., 2016. A fully human anti-CD47 blocking antibody with therapeutic potential for cancer. *Oncotarget*, *7*(50), pp. 83040–83050. doi: 10.18632/oncotarget.13349.

ZHANG, P., LIU, X., GU, Z., JIANG, Z., ZHAO, S., SONG, Y., and YU, J., 2024. Targeting TIGIT for cancer immunotherapy: recent advances and future directions. *Biomarker Research*, *12*(1). doi: 10.1186/s40364-023-00543-z.

ZHANG, Y., and ZHENG, J., 2020. Functions of immune checkpoint molecules beyond immune evasion, *Regulation of Cancer Immune Checkpoints, Advances in Experimental Medicine and Biology*, 1248, pp. 201–226, doi: 10.1007/978-981-15-3266-5_9.

ZHOU, Z., TONE, Y., SONG, X., FURUUCHI, K., LEAR, J. D., WALDMANN, H., TONE, M., GREENE, M. I., and MURALI, R., 2008. Structural basis for ligand-mediated mouse GITR activation, *Proceedings of the National Academy of Sciences*, 105(2), pp. 641–645, doi: 10.1073/pnas.0711206105.

ZUO, S., WEI, M., XU, T., KONG, L., HE, B., WANG, SHIQUN, WANG, SHIBING, WU, J., DONG, J., and WEI, J., 2021. An engineered oncolytic vaccinia virus encoding a single-chain variable fragment against Tigit induces effective antitumor immunity and synergizes with PD-1 or LAG-3 blockade, *Journal for ImmunoTherapy of Cancer*, 9(12), doi: 10.1136/jitc-2021-002843.

Appendix

A. Titration Plates of the Biopanning Rounds

The following figures show examples of some of the LB/Ampicillin and LB/Carbenicillin phage titre plates used to calculate the amount of phages in each round of enriched library.

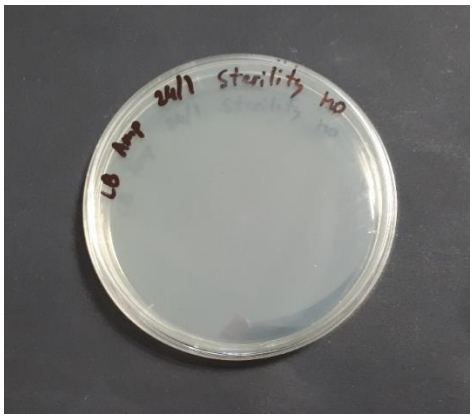

Figure A.1: An image showing an example of a successful sterility plate. *The plate in question was an LB/Ampicillin plate used during the phage titration of round 4 of the original His-tag protein rounds. A volume of 200 µL of the overnight mid-log ER2738 bacterial culture was spread and incubated overnight. Only bacteria infected by phages would carry ampicillin resistance, therefore, no growth had occurred, confirming sterility during the procedure.*

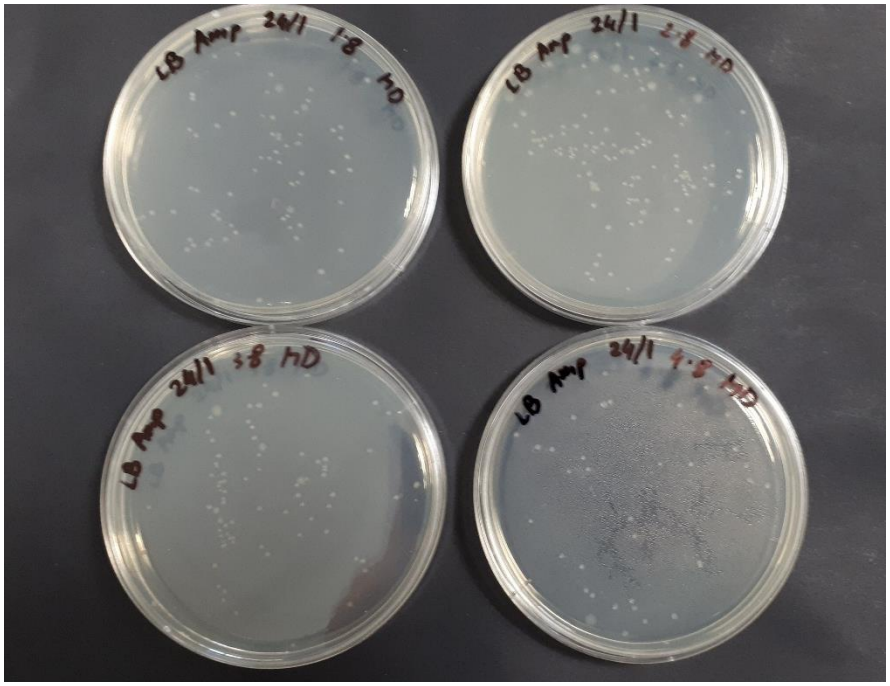

Figure A.2: An image showing the LB/Ampicillin phage titre plates of all four enriched libraries of the round 4 His-tag rounds. *In order, the plates show the NPC (top left), CD47 (top right), TIGIT (bottom left), and GITR (bottom right), at a dilution factor of 10^9. Distinct colonies could be seen and counted on each plate, confirming the presence of phages.*

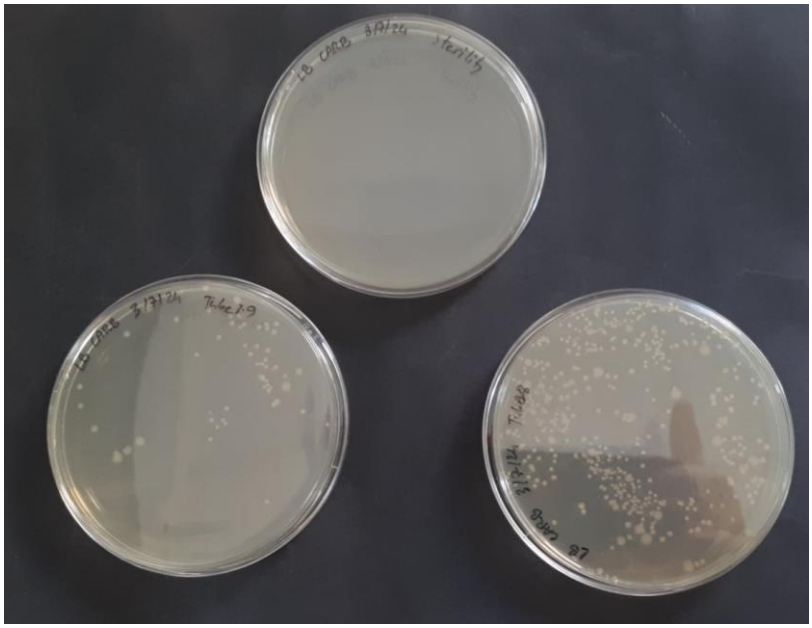

Figure A.3: An image showing an example of the LB/Carbenicillin phage titre plates used during the titration of the Fc rounds. *The above image specifically shows the phage titration of round 4 TIGIT Fc with the sterility plate (top), the 10^{10} dilution (bottom left), and the 10^{9} dilution (bottom right). The sterility plate exhibited no growth. The plate used to calculate the phage titre of the round was the 10^{10} dilution plate.*

B. No Protein Control Rounds

The following section shows the graphs of the full no protein control rounds carried out during biopanning against both His-tagged and Fc-tagged proteins. These were used as the negative control during biopanning, as only non-specific phages would have been isolated.

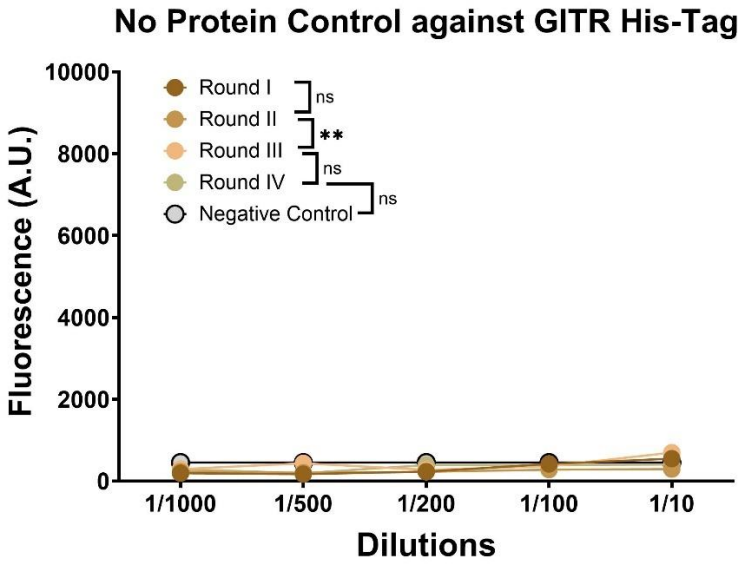

Figure B.1: A graph showing the ELISA results of all 5 dilutions of each of the NPC rounds carried out during biopanning with the His-tag proteins. *GITR His-tag was used as the bait in this particular ELISA, showing nearly no affinity of the phages. The NPC was tested against only one of the targets in order to save on materials and time.*

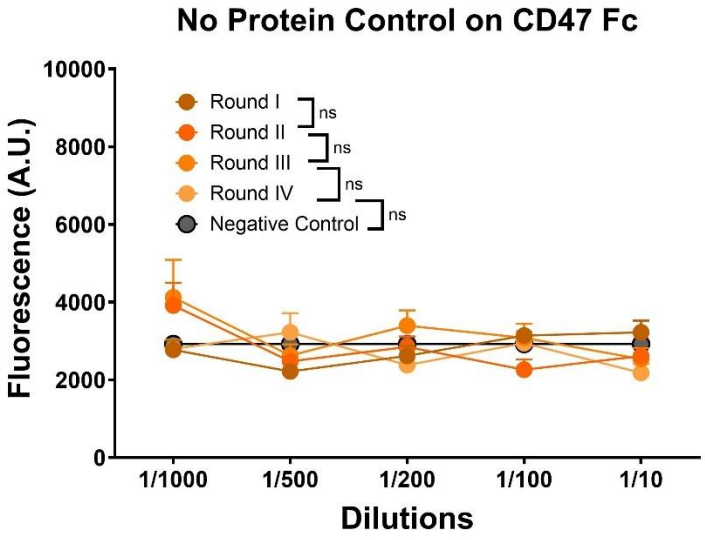

Figure B.2: A graph showing the ELISA results of all 5 dilutions of each of the NPC rounds carried out during biopanning with the Fc proteins. *CD47 Fc was used as the bait in this particular ELISA, showing nearly no affinity of the phages. The NPC was tested against only one of the targets in order to save on materials and time.*

C. Flow Cytometry Results

The following figures show the results of the flow cytometry performed of the Protein G magnetic beads coated with CD47 Fc and TIGIT Fc proteins. Fluorescence was measured using anti-CD47-PE antibody and anti-TIGIT/anti-mouse IgG-PE antibodies.

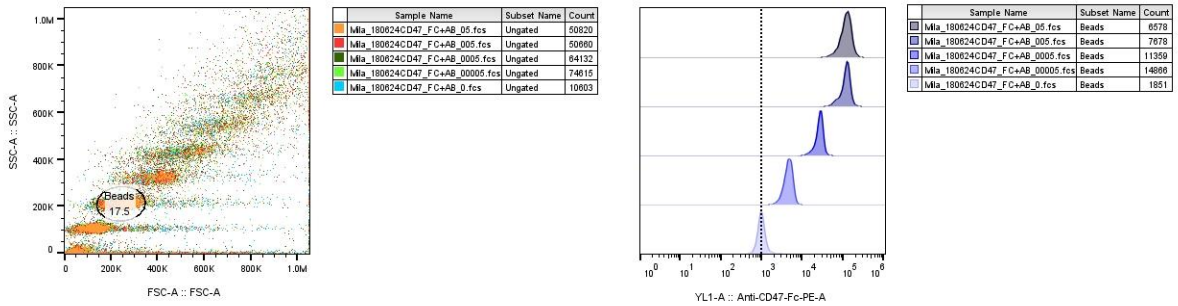

Sample Name	Subset Name	Count
Mla_180624CD47_FC+AB_05.fcs	Ungated	50820
Mla_180624CD47_FC+AB_005.fcs	Ungated	50660
Mla_180624CD47_FC+AB_0005.fcs	Ungated	64132
Mla_180624CD47_FC+AB_00005.fcs	Ungated	74615
Mla_180624CD47_FC+AB_0.fcs	Ungated	10603

Sample Name	Subset Name	Count
Mla_180624CD47_FC+AB_05.fcs	Beads	6578
Mla_180624CD47_FC+AB_005.fcs	Beads	7678
Mla_180624CD47_FC+AB_0005.fcs	Beads	11359
Mla_180624CD47_FC+AB_00005.fcs	Beads	14866
Mla_180624CD47_FC+AB_0.fcs	Beads	1851

Figure C.1: Graphs showing the flow cytometry results of protein G beads coated with the five different dilutions of CD47 Fc protein. *The background fluorescence was determined using beads coated with no protein. From the results, an increase of fluorescence based on the concentration of protein used can be observed, with full saturation of the beads occurring with 0.05 µg/mL of protein.*

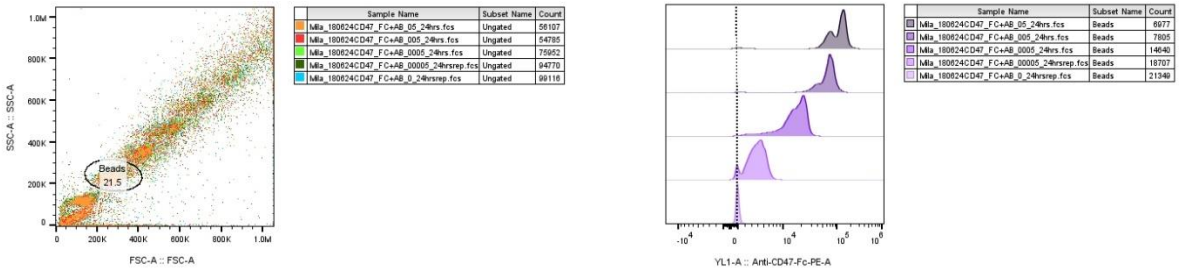

Sample Name	Subset Name	Count
Mla_180624CD47_FC+AB_05_24hrs.fcs	Ungated	56197
Mla_180624CD47_FC+AB_005_24hrs.fcs	Ungated	54785
Mla_180624CD47_FC+AB_0005_24hrs.fcs	Ungated	75952
Mla_180624CD47_FC+AB_00005_24hrsrep.fcs	Ungated	94770
Mla_180624CD47_FC+AB_0_24hrsrep.fcs	Ungated	99116

Sample Name	Subset Name	Count
Mla_180624CD47_FC+AB_05_24hrs.fcs	Beads	6977
Mla_180624CD47_FC+AB_005_24hrs.fcs	Beads	7805
Mla_180624CD47_FC+AB_0005_24hrs.fcs	Beads	14640
Mla_180624CD47_FC+AB_00005_24hrsrep.fcs	Beads	18707
Mla_180624CD47_FC+AB_0_24hrsrep.fcs	Beads	21349

Figure C.2: Graphs showing the flow cytometry results of protein G beads coated with the five different dilutions of CD47 Fc protein, with an added overnight blocking step. *The background fluorescence was determined using beads coated with no protein. These beads were incubated overnight, rather than 1 hour after the addition of the protein, in order to determine if it lead to any significant changes to the amount of fluorescence observed. From the results, an increase of fluorescence based on the concentration of protein used can be observed, with full saturation of the beads occurring with 0.05 µg/mL of protein. The difference between the overnight and 1 hour blocking steps was not considered significant.*

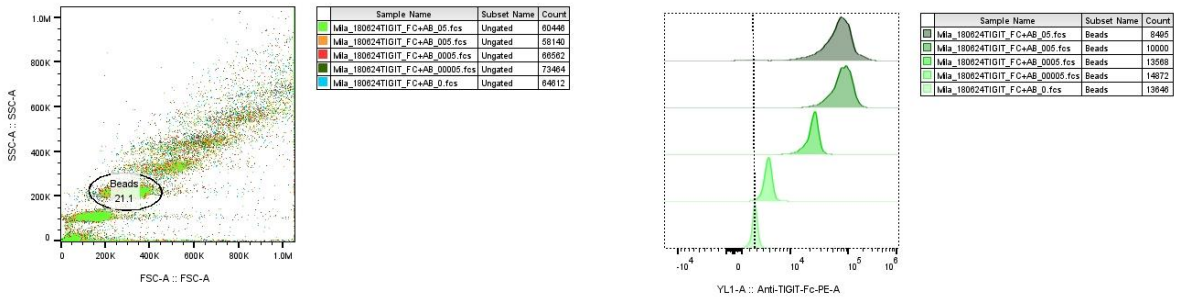

Sample Name	Subset Name	Count
Mla_180624TIGIT_FC+AB_05.fcs	Ungated	60446
Mla_180624TIGIT_FC+AB_005.fcs	Ungated	58140
Mla_180624TIGIT_FC+AB_0005.fcs	Ungated	66562
Mla_180624TIGIT_FC+AB_00005.fcs	Ungated	73464
Mla_180624TIGIT_FC+AB_0.fcs	Ungated	64612

Sample Name	Subset Name	Count
Mla_180624TIGIT_FC+AB_05.fcs	Beads	8495
Mla_180624TIGIT_FC+AB_005.fcs	Beads	10000
Mla_180624TIGIT_FC+AB_0005.fcs	Beads	13568
Mla_180624TIGIT_FC+AB_00005.fcs	Beads	14872
Mla_180624TIGIT_FC+AB_0.fcs	Beads	13646

Figure C.3: Graphs showing the flow cytometry results of protein G beads coated with the five different dilutions of TIGIT Fc protein. *The background fluorescence was determined using beads coated with no protein. From the results, an increase of fluorescence based on the concentration of protein used can be observed, with full saturation of the beads occurring with 0.05 µg/mL of protein.*

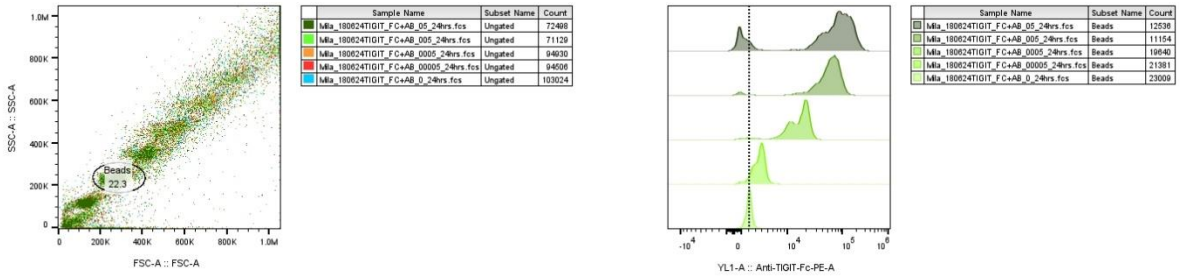

Figure C.4: Graphs showing the flow cytometry results of protein G beads coated with the five different dilutions of TIGIT Fc protein, with an added overnight blocking step. *The background fluorescence was determined using beads coated with no protein. These beads were incubated overnight, rather than 1 hour after the addition of the protein, in order to determine if it lead to any significant changes to the amount of fluorescence observed. From the results, an increase of fluorescence based on the concentration of protein used can be observed, with full saturation of the beads occurring with 0.05 µg/mL of protein. The difference between the overnight and 1 hour blocking steps was not considered significant, despite the observation of a slight split peak at the highest protein concentration .*

D. ELISA Settings

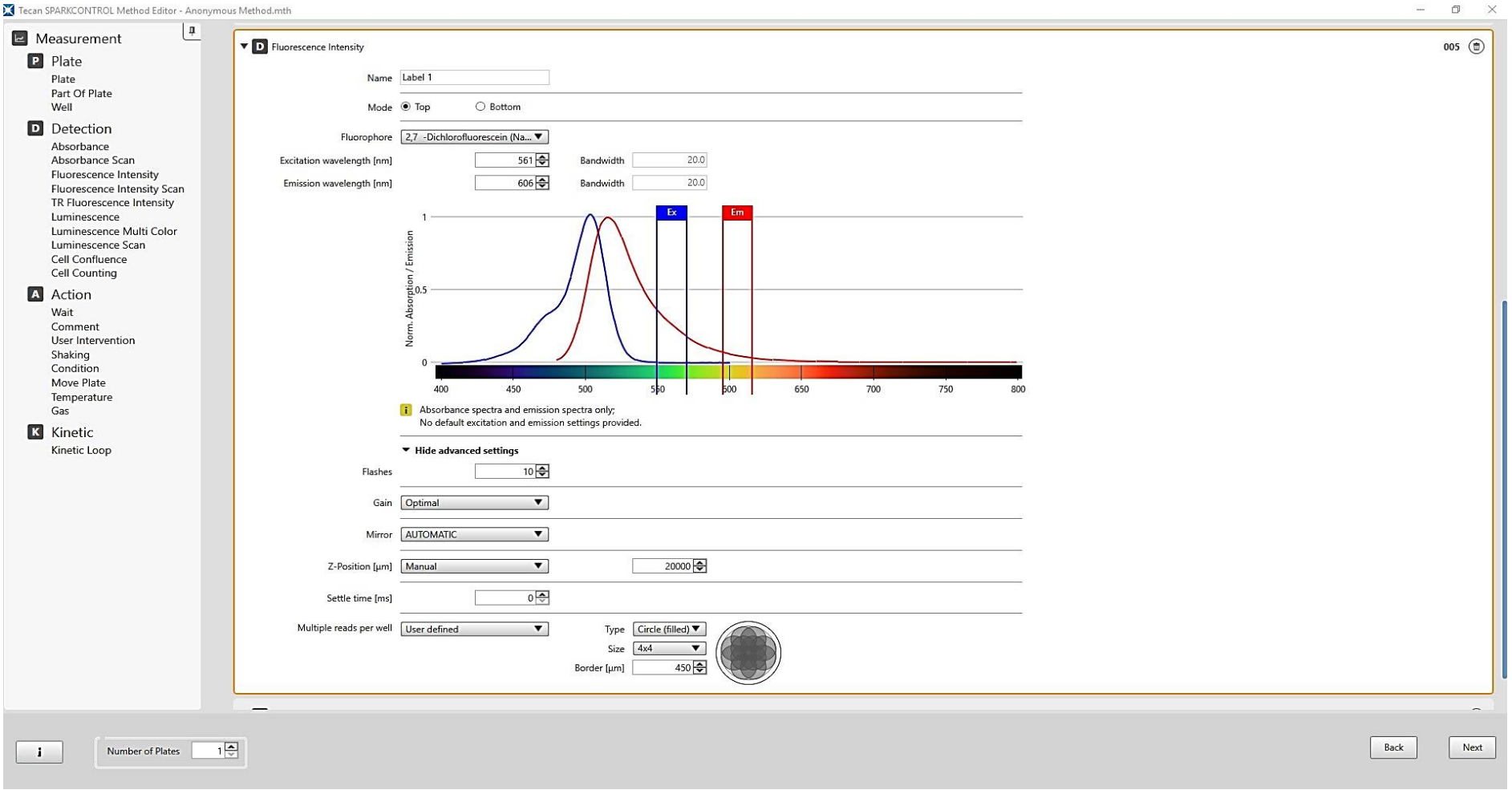

Figure D.1: A screenshot showing the exact fluorescence settings chosen for the various ELISAs performed during the course of the study. *The excitation wavelength used was set as 561, while the emission wavelength was 606. Optimal gain was chosen as the default setting most of the time, although this was changed to enhanced dynamic range in the case of wells that showed overflow. Each well was read a total of 12 times, forming 12 technical replicates of fluorescence*

E. First Simplified ELISAs of His-Tag and Fc Rounds

Prior to the full ELISAs used to obtain the results outlined in **Chapter 3**, an initial simplified ELISA was performed of each round. The methodology used was identical to what was described in **Section 2.2.5**, with the exception of the plate layout, as seen in **Figure E.1**. This primary ELISA only used 2 dilutions per round and tested only round 4 of each target against the control protein. This was done in order to get a preliminary idea of the results of biopanning, before completing the full ELISA for data analysis. Two wells labelled no library control were used as the negative control in this ELISA. Rounds were denoted by R with a roman numeral, as well as a number denoting each target (2 for CD47, 3 for TIGIT, and 4 for GITR). This labelling scheme was kept consistent throughout the study. The results obtained matched exactly to those previously described in **Chapter 3**.

	CD47	TIGIT	GITR	
	1	2	3	4
A	Ri2 1/10 CD47	Ri3 1/10 TIGIT	Ri4 1/10 GITR	No library +CD47
B	Ri2 1/10 CD470	Ri3 1/100 TIGIT	Ri4 1/100 GITR	No library +GITR
C	Rii2 1/10 CD47	Rii3 1/10 TIGIT	Rii4 1/10 GITR	Control prot +Riv2 1/10
D	Rii2 1/100 CD47	Rii3 1/100 TIGIT	Rii4 1/100 GITR	Control prot +Riv2 1/100
E	Riii2 1/10 CD47	Riii3 1/10 TIGIT	Riii4 1/10 GITR	Control prot +Riv3 1/10
F	Riii2 1/100 CD47	Riii3 1/100 TIGIT	Riii4 1/100 GITR	Control prot +Riv3 1/100
G	Riv2 1/10 CD47	Riv3 1/10 TIGIT	Riv4 1/10 GITR	Control prot +Riv 4 1/10
H	Riv2 1/100 CD47	Riv3 1/100 TIGIT	Riv4 1/100 GITR	Control prot +Riv4 1/100

Figure E.1: A figure showing the full plate layout of the first ELISA performed of the His-tag rounds. *Each round of enriched library was diluted twice and the fluorescence of each on their respective target proteins was measured using anti-M13-PE antibody. Only round 4 enriched libraries were measured against the non-target control protein. The wells labelled as no library served as the negative control for this ELISA.*

A similar ELISA was also carried out for the Fc biopanning rounds as well, with the plate layout used shown in **Figure E.2**. Apart from the no library negative control, the first ELISA of the Fc rounds also included a positive control for the ELISA in the form of Round 4 TIM-3 (T cell immunoglobulin mucin 3) enriched phage library, a library produced by Grima (2024) that was proven to have successfully undergone biopanning. A further positive control included was two wells coated in CD47 Fc and TIGIT Fc bait proteins and measured using anti-CD47-PE antibody, and anti-TIGIT/anti-mouse IgG-PE antibodies, which were used to ensure that the bait proteins were successfully immobilised in the ELISA plate wells. Finally, to the wells labelled as no protein, a dilution of round 3 and 4 of each enriched library was added and blocked with blocking buffer overnight, allowing any phages present to bind directly to the well. This was done to ensure the presence of phages at all within the enriched libraries. All of these extra controls were deemed necessary due to the previous failure in the biopanning of those target proteins. High fluorescence readings were observed with all positive controls, including the no protein library controls, proving the success of the ELISA method, and thus confirming that the low fluorescence observed in the enriched libraries and bait protein wells were due to the lack of high affinity phages and not other outlying factors.

	1	2	3	4	5
A	Ri2 1/10 CD47	Ri3 1/10 TIGIT	CD47 no library	Riv Tim-3 and Tim 3 1/10	Riii2 1/10 no protein
B	Ri2 1/100 CD47	Ri3 1/100 TIGIT	TIGIT no library	Riv Tim-3 and Tim 3 1/100	Riv2 1/10 no protein
C	Rii2 1/10 CD47	Rii3 1/10 TIGIT	CP Riv2 1/10	Riv Tim-3 and Tim 3 1/1000	Riii3 1/10 no protein
D	Rii2 1/100 CD47	Rii3 1/100 TIGIT	CP Riv2 1/100	Riv Tim-3 and CP 1/10	Riv3 1/10 no protein
E	Riii2 1/10 CD47	Riii3 1/10 TIGIT	CP Riv3 1/10	Riv Tim-3 and CP 1/100	Riv Tim-3 1/10 no protein
F	Riii2 1/100 CD47	Riii3 1/100 TIGIT	CP Riv3 1/100	Riv Tim-3 and CP 1/1000	
G	Riv2 1/10 CD47	Riv3 1/10 TIGIT	anti-CD47 + CD47		
H	Riv2 1/100 CD47	Riv3 1/100 TIGIT	anti-TIGIT + TIGIT		

Figure E.2: A figure showing the full plate layout of the first ELISA performed of the Fc rounds. *Each round of enriched library was diluted twice and the fluorescence of each on their respective target protein was measured using anti-M13-PE antibody. No anti-M13-PE antibody was added to the two wells labelled anti-CD47 and anti-TIGIT. Only round 3 and round 4 enriched libraries were measured against the non-target control protein (CP). Three dilutions were prepared of round 4 TIM-3 enriched library for the positive control due to the known high phage titre present in those rounds. The wells labelled as no library served as the negative control for this ELISA.*

F. Sequencing of Initial GITR and No Protein Control Clones

Similarly to the initial ELISA of the biopanning rounds, there was also an initial selection of 30 clones from round 3 GITR enriched library, before the 60 clones described in **Chapter 3**. Similarly, 30 clones from round 3 of the NPC were also chosen at this time. However, it was ultimately decided not to use the results of these clones in the final presentation of this study due to differences in the preparation method. Firstly, during amplification of these clones, M13KO7 helper phage was used rather than hyperphage. Furthermore, in the blocking steps, a 1% BSA blocking buffer was used instead of the 3% BSA blocking buffer described in **Chapter 2**. Finally, during the purification and PEG precipitation steps, these clones underwent one less centrifugation cycle than the final 60 clones later isolated. Because of these reasons, it is believed that many high affinity clones were lost during the amplification and purification processes. However, these results are still valuable for the optimisation of the phage clone preparation method, and thus the success of isolating several high affinity clones later on. The plate layouts used to read the fluorescence of these clones, against bound target and non-target protein may be seen in **Figure F.1**. Histograms showing the results of these initial 30 isolated clones may also be seen in **Figure F.2,** and **Figure F.3**.

Plate 1	1	2	3	4	5	6	7	8	9	10	11
A	G1 GITR	G9 GITR	G17 GITR	G25 GITR	G1 CP	G9 CP	G17 CP	G25 CP		Riii GITR 1/10 on GITR	No library GITR
B	G2 GITR	G10 GITR	G18 GITR	G26 GITR	G2 CP	G10 CP	G18 CP	G26 CP		Riii GITR 1/100 on GITR	No library GITR
C	G3 GITR	G11 GITR	G19 GITR	G27 GITR	G3 CP	G11 CP	G19 CP	G27 CP		Riii GITR 1/10 on CP	No library CP
D	G4 GITR	G12 GITR	G20 GITR	G28 GITR	G4 CP	G12 CP	G20 CP	G28 CP		Riii GITR 1/100 on CP	No library CP
E	G5 GITR	G13 GITR	G21 GITR	G29 GITR	G5 CP	G13 CP	G21 CP	G29 CP			
F	G6 GITR	G14 GITR	G22 GITR	G30 GITR	G6 CP	G14 CP	G22 CP	G30 CP			
G	G7 GITR	G15 GITR	G23 GITR		G7 CP	G15 CP	G23 CP				
H	G8 GITR	G16 GITR	G24 GITR		G8 CP	G16 CP	G24 CP				

Plate 2	1	2	3	4	5	6	7	8	9	10	11
a	NP1 GITR	NP9 GITR	NP17 GITR	NP25 GITR	NP1 CP	NP9 CP	NP17 CP	NP25 CP		Riii GITR 1/10 on GITR	No library GITR
b	NP2 GITR	NP10 GITR	NP18 GITR	NP26 GITR	NP2 CP	NP10 CP	NP18 CP	NP26 CP		Riii GITR 1/100 on GITR	No library GITR
c	NP3 GITR	NP11 GITR	NP19 GITR	NP27 GITR	NP3 CP	NP11 CP	NP19 CP	NP27 CP		Riii GITR 1/10 on CP	No library CP
d	NP4 GITR	NP12 GITR	NP20 GITR	NP28 GITR	NP4 CP	NP12 CP	NP20 CP	NP28 CP		Riii GITR 1/100 on CP	No library CP
e	NP5 GITR	NP13 GITR	NP21 GITR	NP29 GITR	NP5 CP	NP13 CP	NP21 CP	NP29 CP			
f	NP6 GITR	NP14 GITR	NP22 GITR	NP30 GITR	NP6 CP	NP14 CP	NP22 CP	NP30 CP			
g	NP7 GITR	NP15 GITR	NP23 GITR		NP7 CP	NP15 CP	NP23 CP				
h	NP8 GITR	NP16 GITR	NP24 GITR		NP8 CP	NP16 CP	NP24 CP				

Figure F.1: Figures showing the full ELISA plate layout of Round 3 GITR clones (G1-G30) against target GITR and non-target control protein (CP) on plate 1, and the round 3 NPC clones (NP1-NP30) against target GITR and non-target CP on plate 2. *The round 3 GITR polyclonal pool acted as the positive control on both plates, while the no library wells acted as the negative control.*

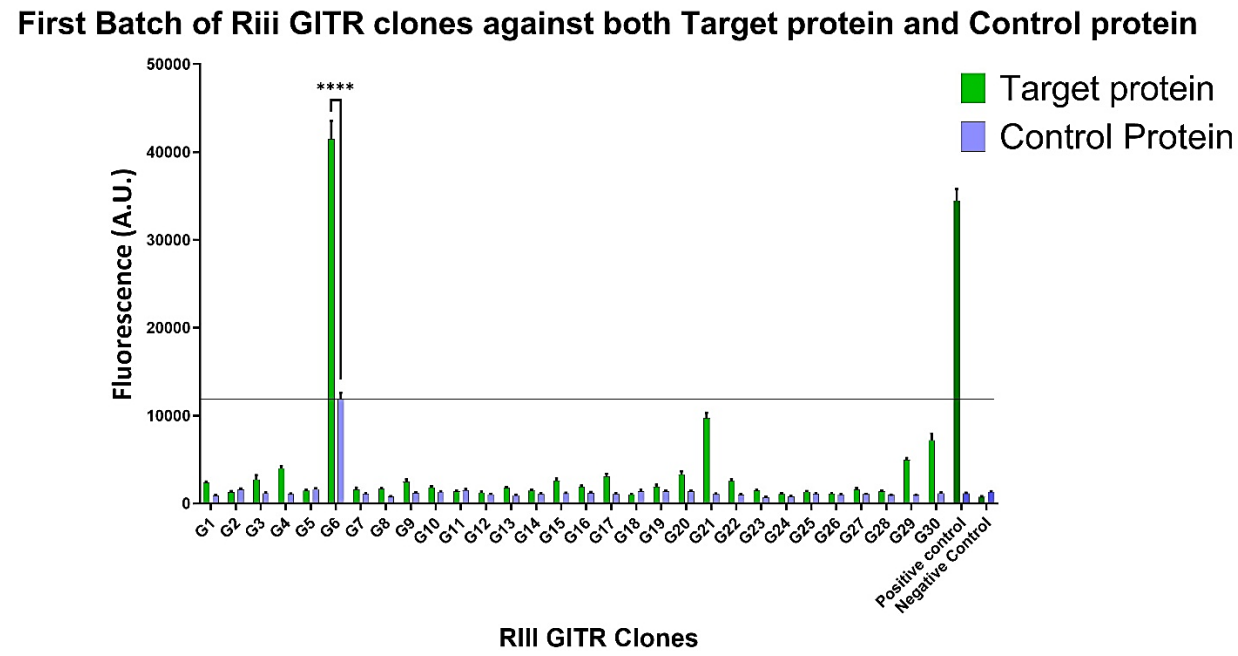

Figure F.2: A histogram showing the fluorescence readings of each GITR clone against both the target and the non-target protein. *As can be seen from the graph, only one clone out of 60 gave a level of fluorescence comparable to the positive control.*

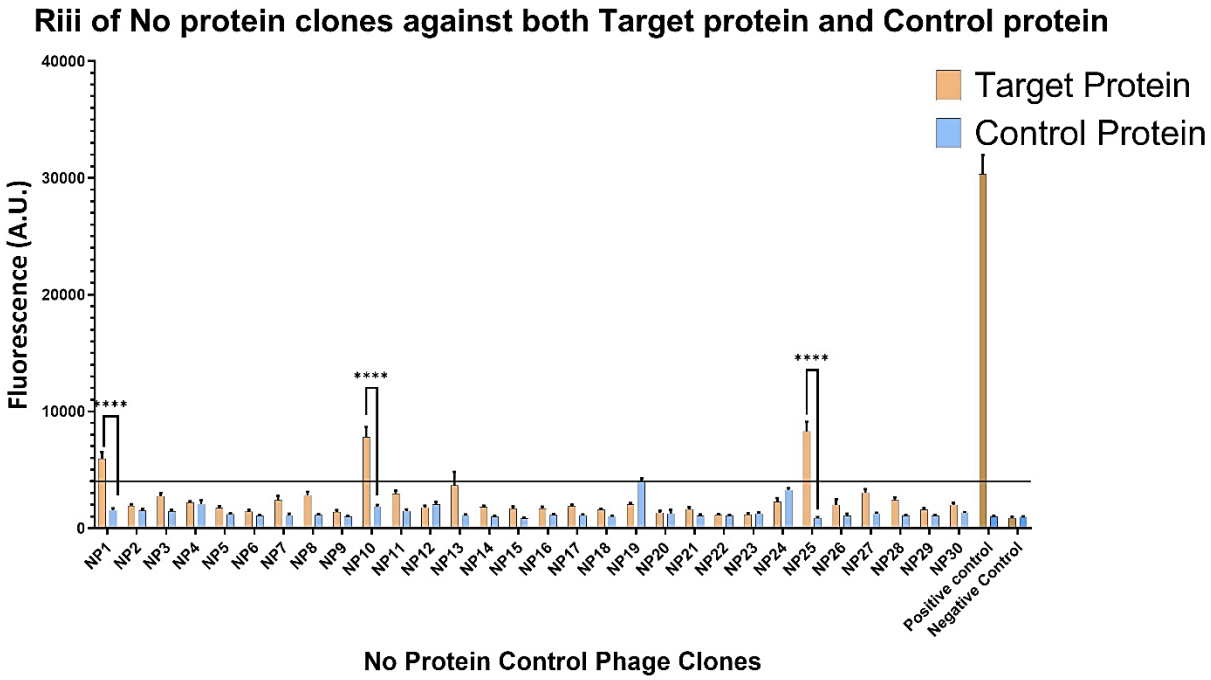

Figure F.3: A histogram showing the fluorescence readings of each NPC clone against both the GITR target and the non-target protein. *As can be seen from the graph, none of the clones reached comparable levels of fluorescence with the positive control, although there were some clones which seemingly exhibited a modicum of preferential binding to GITR over the CP.*

G. NanoDrop Readings of GITR Clones

NanoDrop readings of the extracted DNA of each clone were taken before they were sent abroad for sequencing and may be seen in **Table G.1.**

Table G.1: A table showing the NanoDrop results of all 60 final GITR clones. *The table specifies the DNA concentration, as well as the 260/280 and the 260/230 ratios indicating the purity of each sample. From these, it can be seen that most clones gave good DNA yields, and all have acceptable levels of purity.*

GITR clone	ng/µL	260/280	260/230	GITR clone	ng/µL	260/280	260/230
1	188.3	1.90	2.22	**31**	181.2	1.89	2.27
2	168.3	1.91	2.26	**32**	191.3	1.87	1.99
3	221.1	1.90	2.16	**33**	155.6	1.91	2.29
4	146.4	1.90	2.21	**34**	166.6	1.89	2.20
5	155.8	1.90	2.25	**35**	94.2	1.87	1.84
6	139.2	1.90	2.21	**36**	125.6	1.90	2.26
7	161.8	1.92	2.29	**37**	100.3	1.91	2.20
8	131.6	1.89	2.08	**38**	81.0	1.87	2.12
9	158.6	1.91	2.26	**39**	30.2	1.83	2.19
10	188.8	1.91	2.29	**40**	191.2	1.88	2.28
11	186.7	1.91	2.35	**41**	190.4	1.95	2.30
12	180.2	1.91	2.30	**42**	30.0	1.94	2.04
13	180.1	1.88	2.24	**43**	145.3	1.90	2.20
14	132.1	1.91	2.21	**44**	111.6	1.89	2.09
15	190.8	1.90	2.25	**45**	175.2	1.90	2.25
16	196.0	1.89	2.13	**46**	158.3	1.89	2.23
17	180.5	1.91	2.29	**47**	173.6	1.90	2.29
18	118.8	1.91	2.29	**48**	158.9	1.91	2.28
19	115.4	1.90	2.29	**49**	211.3	1.90	2.24
20	122.4	1.91	2.30	**50**	151.6	1.91	2.29
21	144.7	1.92	2.29	**51**	220.8	1.90	2.30
22	164.5	1.89	2.31	**52**	216.0	1.89	2.24
23	170.7	1.90	2.31	**53**	105.5	1.90	2.24
24	125.4	1.89	2.23	**54**	140.5	1.88	2.10
25	195.4	1.90	2.28	**55**	195.0	1.90	2.29
26	154.9	1.90	2.22	**56**	135.5	1.89	2.21
27	196.4	1.91	2.26	**57**	155.1	1.90	2.24
28	193.0	1.91	2.28	**58**	168.0	1.90	2.31
29	189.9	1.91	2.30	**59**	115.6	1.92	2.25
30	194.9	1.91	2.29	**60**	130.5	1.90	2.29

Some clones from the initial 30 GITR (G) and NPC (N) clones picked before the method was fully optimised were also sent abroad for sequencing. Only six of the highest affinity GITR clones, as well as six randomly selected NPC clones were chosen for DNA extraction and sequencing. The extraction method used the same Monarch DNA plasmid extraction kit and procedure as the other clones, and the NanoDrop results of these DNA extracts were also noted and may be found in **Table G.2**. It should be noted that the concentrations and the purity of the DNA measured of these initial clones were noted to be far less than the final 60 clones.

Table G.2: A table showing the NanoDrop results of the 6 GITR and 6 NP clones initially sent for sequencing. *The table specifies the DNA concentration, as well as the 260/280 and the 260/230 ratios indicating the purity of each sample. From these, it can be seen that most clones gave relatively low DNA yields, and many have lower than normally acceptable 260/230 ratio scores, showing low levels of purity of the samples.*

clone	ng/µL	260/280	260/230
G6	67.1	1.88	2.25
G21	77.3	1.86	2.34
G29	78	1.9	2.32
G30	74.4	1.81	1.71
G4	69.7	1.88	2.37
G15	89.6	1.88	2.33
N11	90.9	1.72	1.15
N25	75.8	1.86	1.83
N19	45.2	1.89	2.36
N2	58.6	1.89	1.53
N14	74	1.88	2.37
N8	68.9	1.93	2.34

H. Manual Comparisons of GITR Clones on SnapGene

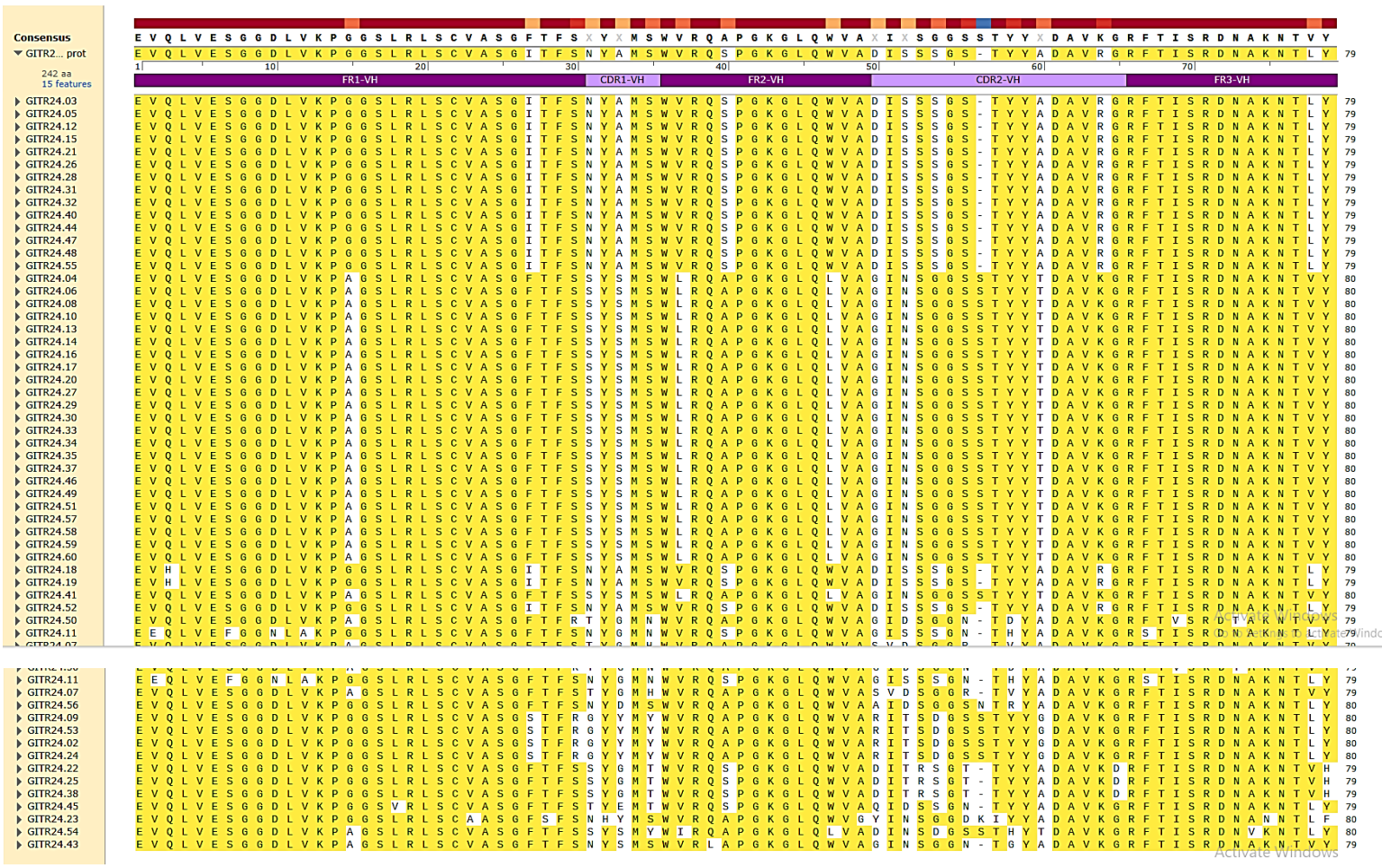

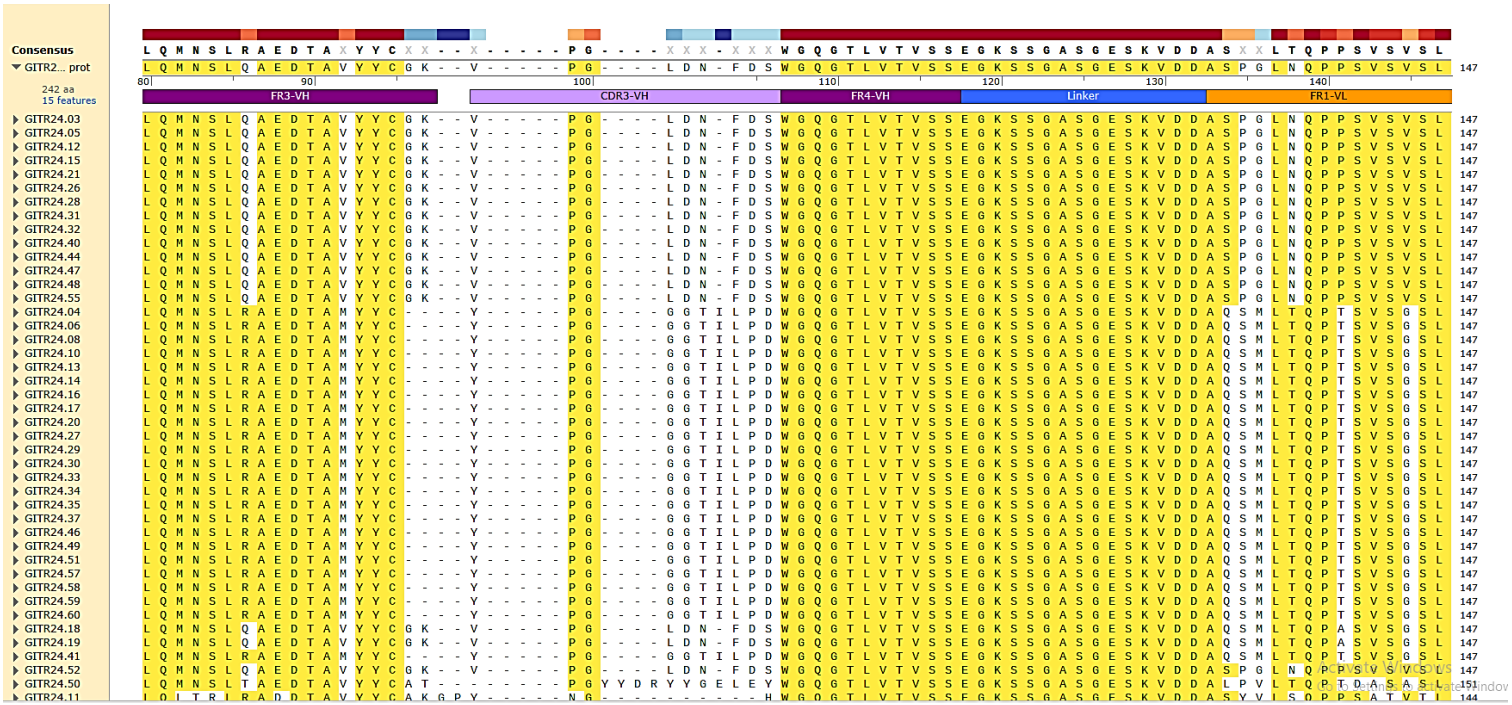

Figure H.1: Screenshots showing the full sequence and manual alignment of each of the successfully sanger sequenced GITR clones as obtained from the SnapGene software. *Clone GITR24.01 at the top shows the labelling of each framework (FR) and CDR region of the amino acid sequence and was used as a legend and guide for all other sequences.*

Also included are the full sequences and alignment of the twelve total G and N clones initially sent for sequencing. It should be noted that only 3 of the 12 total clones sent in the first batch were fully sequenced, all of which were NPC clones.

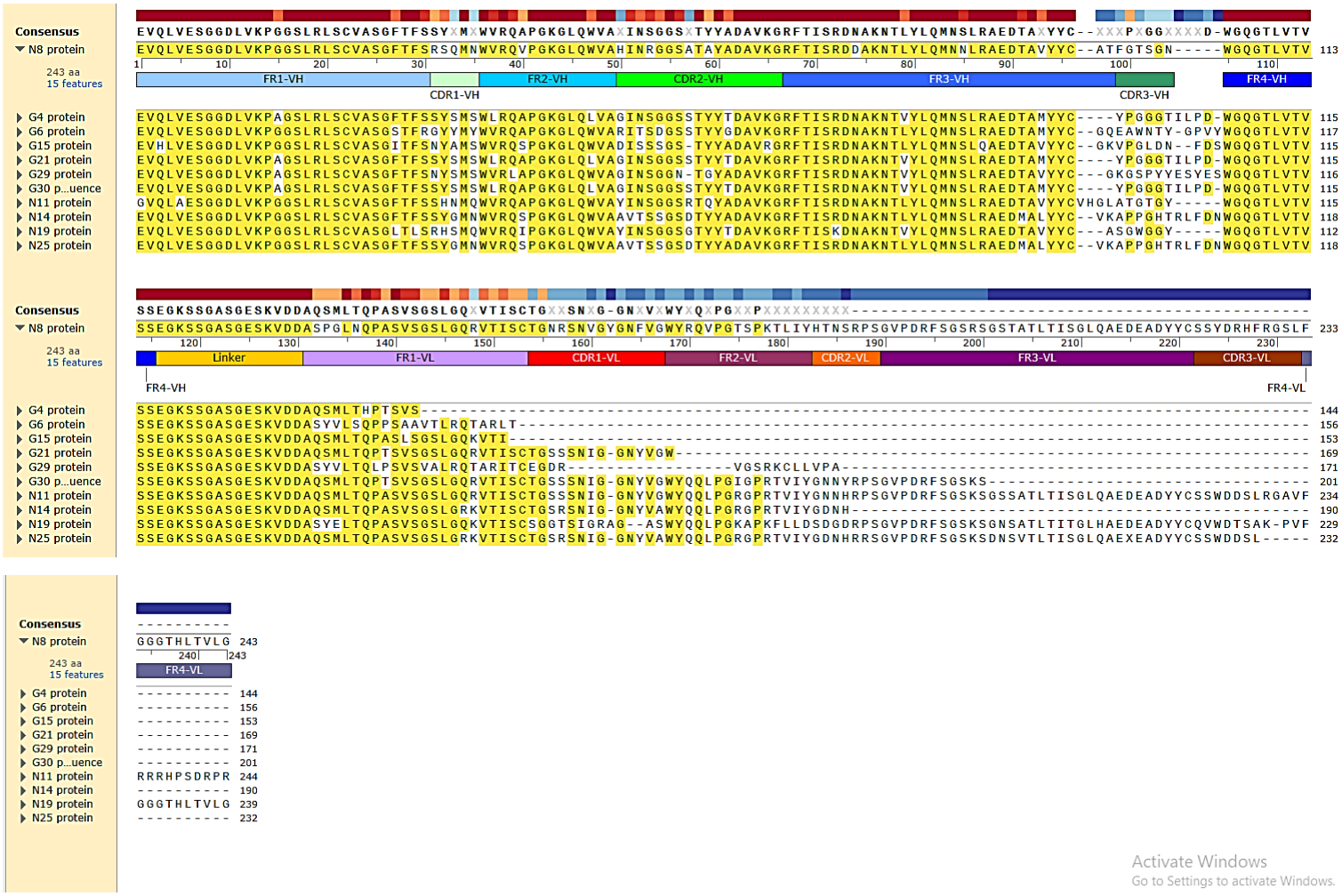

Figure H.2: Screenshots showing the full sequence and manual alignment of each of the initial GITR and NPC clones as obtained from the SnapGene software. *Clone N8 at the top shows the labelling of each framework (FR) and CDR region of the amino acid sequence and was used as a legend and guide for all other sequences. Only clone G6 showed high affinity to GITR protein.*

I. SWISS-Model Molecular Structures and Ramachandran Plots of Several GITR Clones

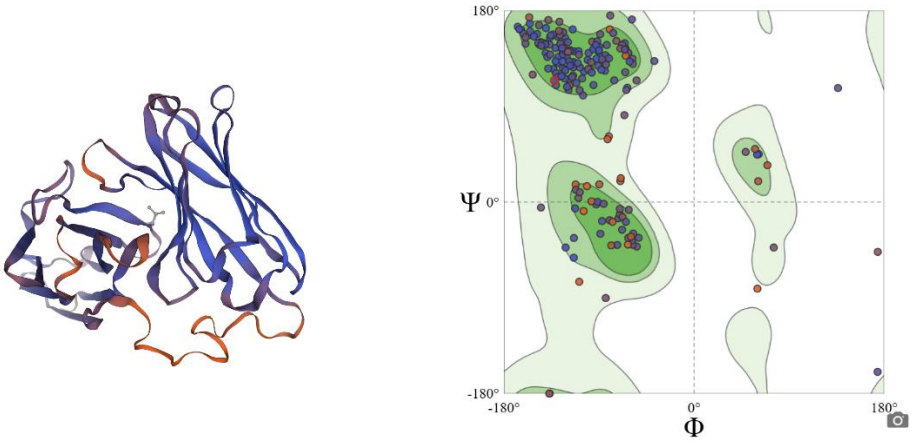

Figure I.1: The 3D structure of clone 1, composed of the VL and VH, connected by a flexible linker. *The Ramachandran plot compares the phi and psi angles of each amino acid, separated out into alpha-helical (bottom left quadrant) and beta strand (top left quadrant) conformations. The cluster in the upper right quadrant represents turns in the amino acid sequence. This was noted to be a high affinity clone of the green group. Based on the regularity of these clusters, it can be concluded the model generated for this scFv is of a good quality.*

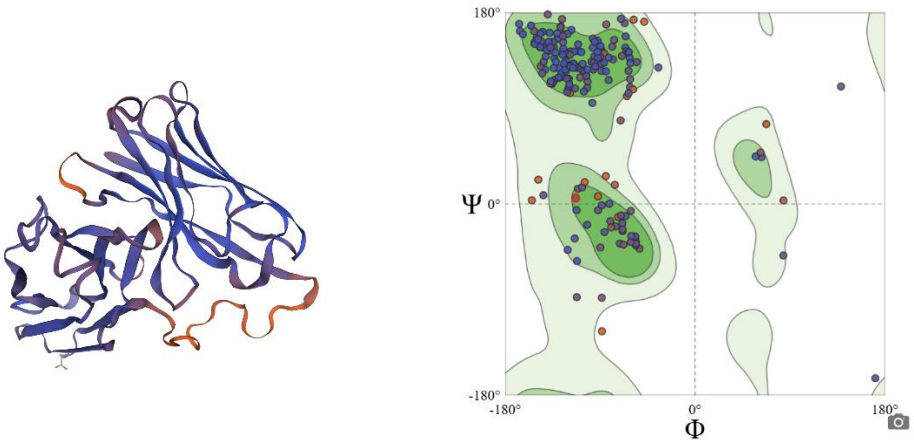

Figure I.2: The 3D structure of clone 18, composed of the VL and VH, connected by a flexible linker. *The Ramachandran plot compares the phi and psi angles of each amino acid, separated out into alpha-helical (bottom left quadrant) and beta strand (top left quadrant) conformations. The cluster in the upper right quadrant represents turns in the amino acid sequence. This was noted to be a low affinity clone of the green group. Based on the regularity of these clusters, it can be concluded the model generated for this scFv is of a good quality.*

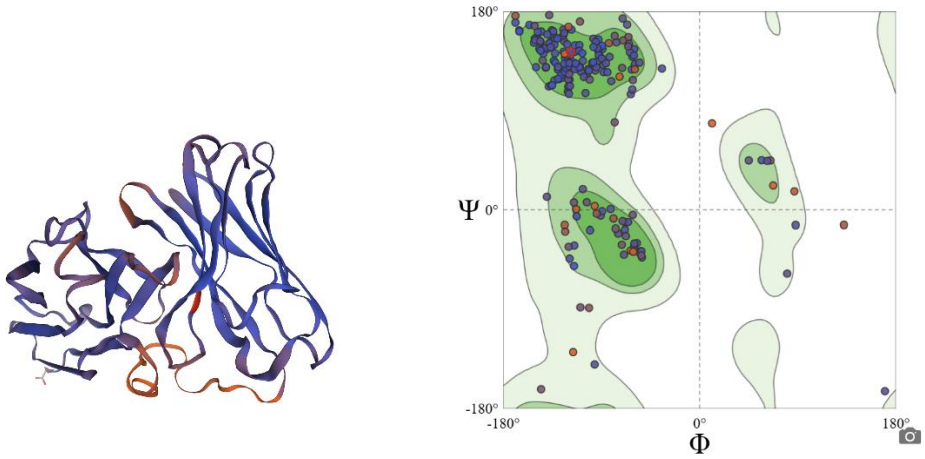

Figure I.3: The 3D structure of clone 54, composed of the VL and VH, connected by a flexible linker. *The Ramachandran plot compares the phi and psi angles of each amino acid, separated out into alpha-helical (bottom left quadrant) and beta strand (top left quadrant) conformations. The cluster in the upper right quadrant represents turns in the amino acid sequence. This was noted to be a low affinity clone of the yellow-brown group. Based on the regularity of these clusters, it can be concluded the model generated for this scFv is of a good quality.*

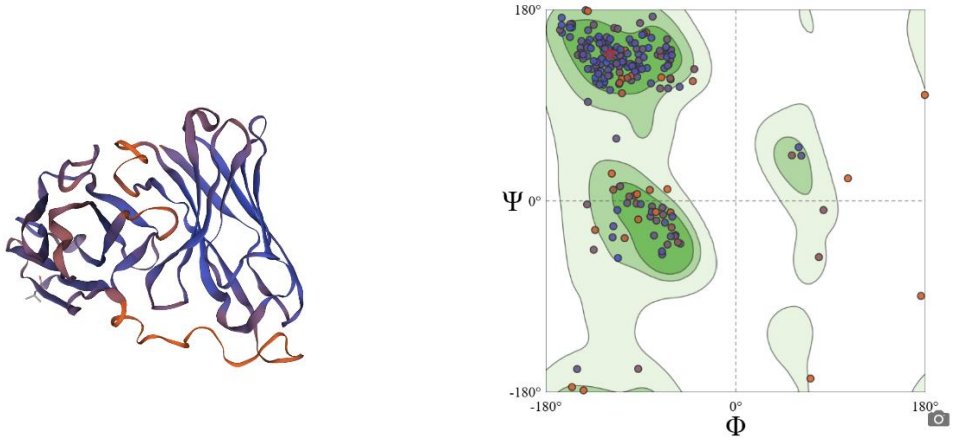

Figure I.4: The 3D structure of clone 45, composed of the VL and VH, connected by a flexible linker. *The Ramachandran plot compares the phi and psi angles of each amino acid, separated out into alpha-helical (bottom left quadrant) and beta strand (top left quadrant) conformations. The cluster in the upper right quadrant represents turns in the amino acid sequence. This was noted to be a high affinity clone of the red group with a unique CDR sequence. Based on the regularity of these clusters, it can be concluded the model generated for this scFv is of a good quality.*

J. HADDOCK Graphs and Analysis of Clone 34

The following figures showcase the steps taken and parameters used for the docking study between the scFv of clone 34 and the target protein GITR.

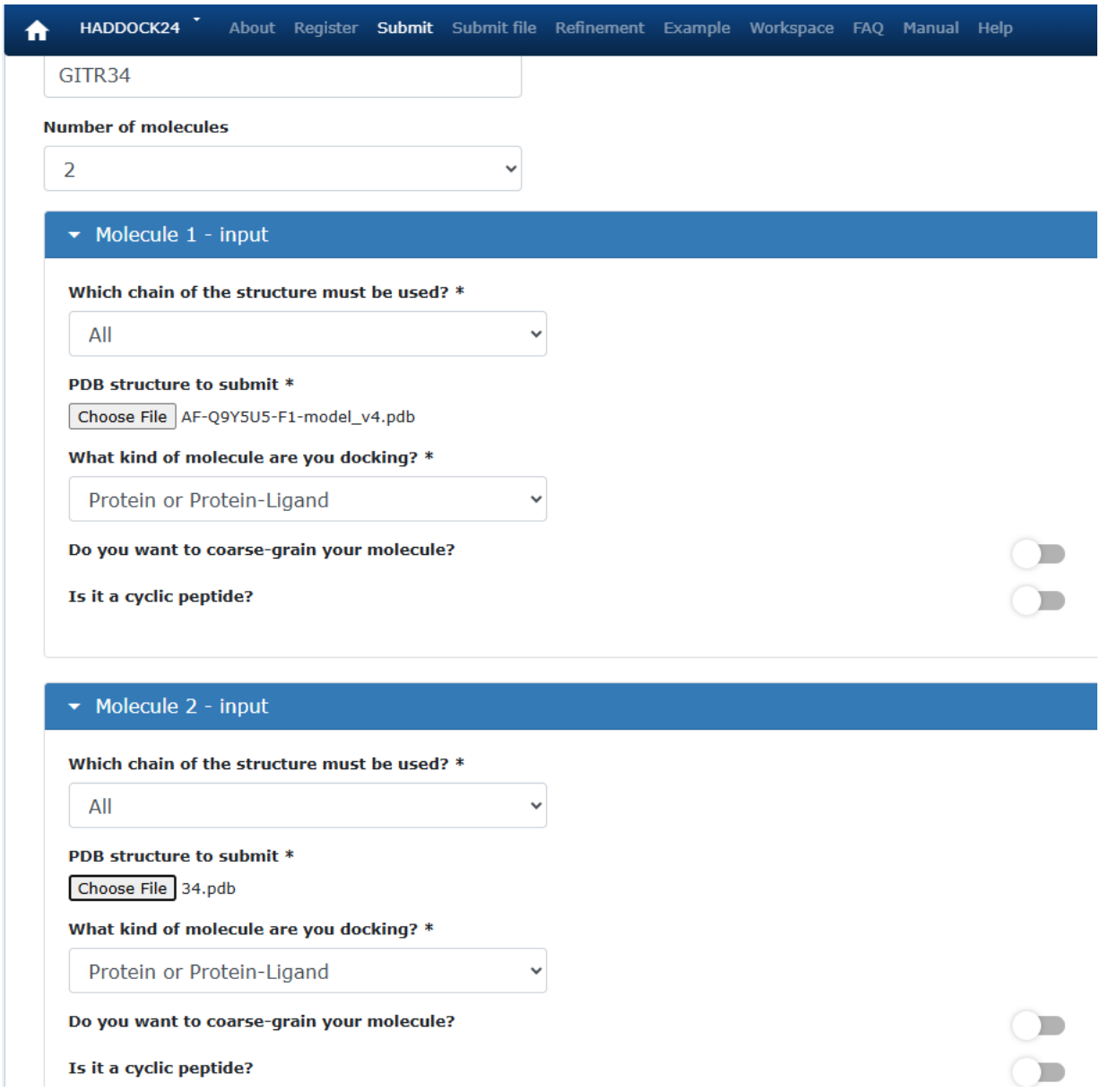

Figure J.1: A screenshot of the initial input into HADDOCK v. 2.4 protein docking software. *The number of molecules in the interaction was specified as 2, and both sequences were uploaded as pdb files. The type of molecule was also specified here, as Protein/Protein-Ligand for both GITR and the scFv of clone 34.*

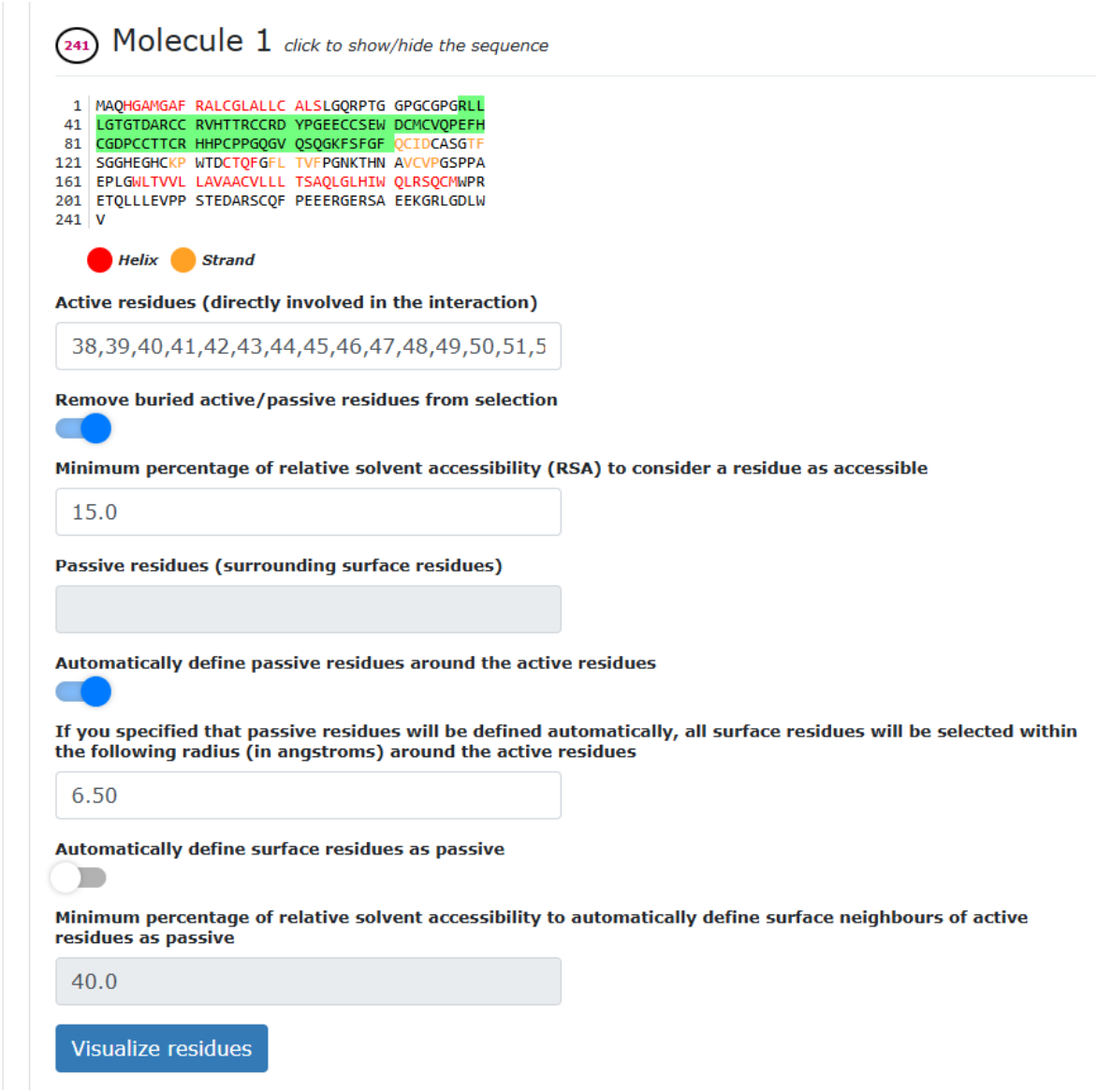

Figure J.2: A screenshot showing the selection of the active residues only for the first molecule GITR. *This selection was made after consulting available literature of the structure and functions of GITR, although the exact residues involved with binding are still under research (He, Maniyar et al. 2022).*

Figure J.3: A screenshot showing the selection of the active residues only for the second molecule, clone 34. *This involved the selection of only the CDR regions previously identified with SnapGene.*

All other parameters used were left as the default provided by the HADDOCK v. 2.4 online software.

Below are some of the graphs obtained as part of the output from HADDOCK v2.4 of the protein docking study between GITR and the scFv amino acid sequence of clone 34.

(A)

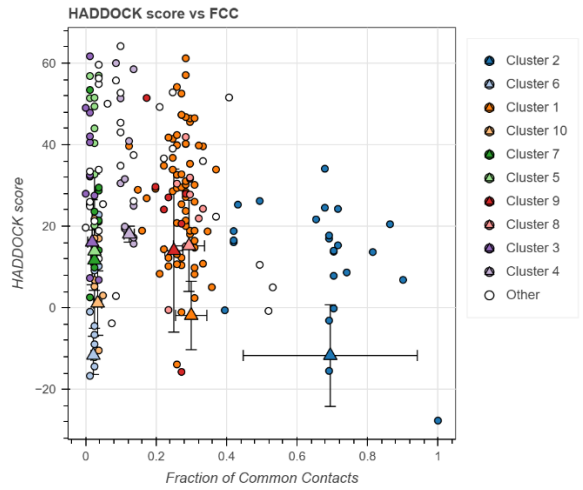
HADDOCK score vs FCC
HADDOCK score
Fraction of Common Contacts
Cluster 2
Cluster 6
Cluster 1
Cluster 10
Cluster 7
Cluster 5
Cluster 9
Cluster 8
Cluster 3
Cluster 4
Other

(B)

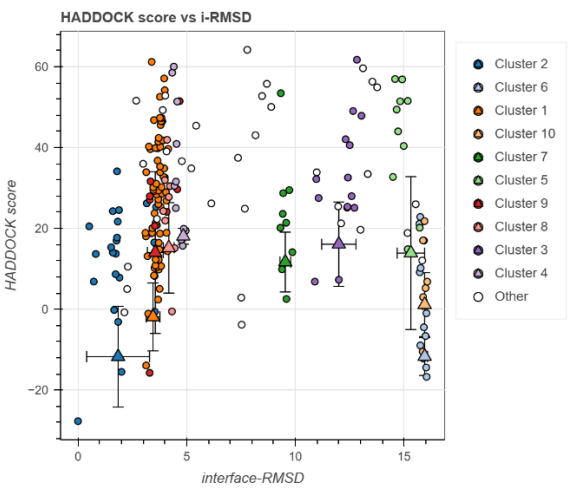
HADDOCK score vs i-RMSD
HADDOCK score
interface-RMSD
Cluster 2
Cluster 6
Cluster 1
Cluster 10
Cluster 7
Cluster 5
Cluster 9
Cluster 8
Cluster 3
Cluster 4
Other

(C)

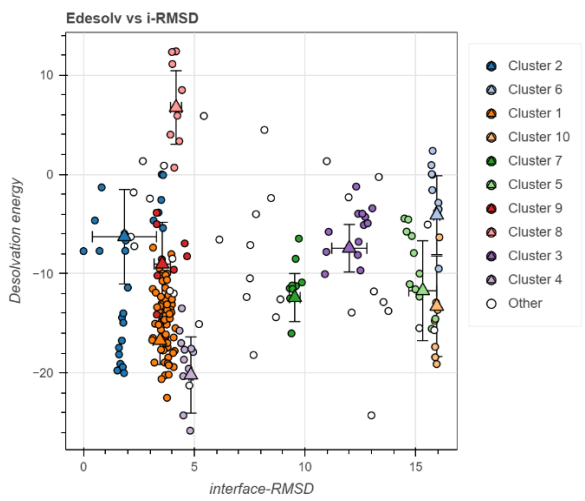
Edesolv vs i-RMSD
Desolvation energy
interface-RMSD
Cluster 2
Cluster 6
Cluster 1
Cluster 10
Cluster 7
Cluster 5
Cluster 9
Cluster 8
Cluster 3
Cluster 4
Other

(D)

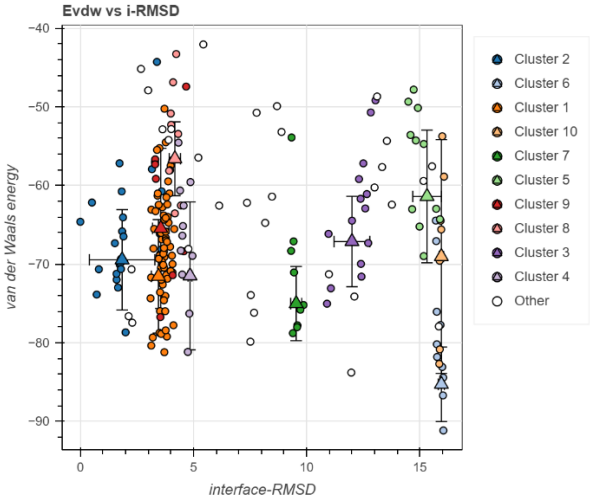
Evdw vs i-RMSD
van der Waals energy
interface-RMSD
Cluster 2
Cluster 6
Cluster 1
Cluster 10
Cluster 7
Cluster 5
Cluster 9
Cluster 8
Cluster 3
Cluster 4
Other

(E) (F)

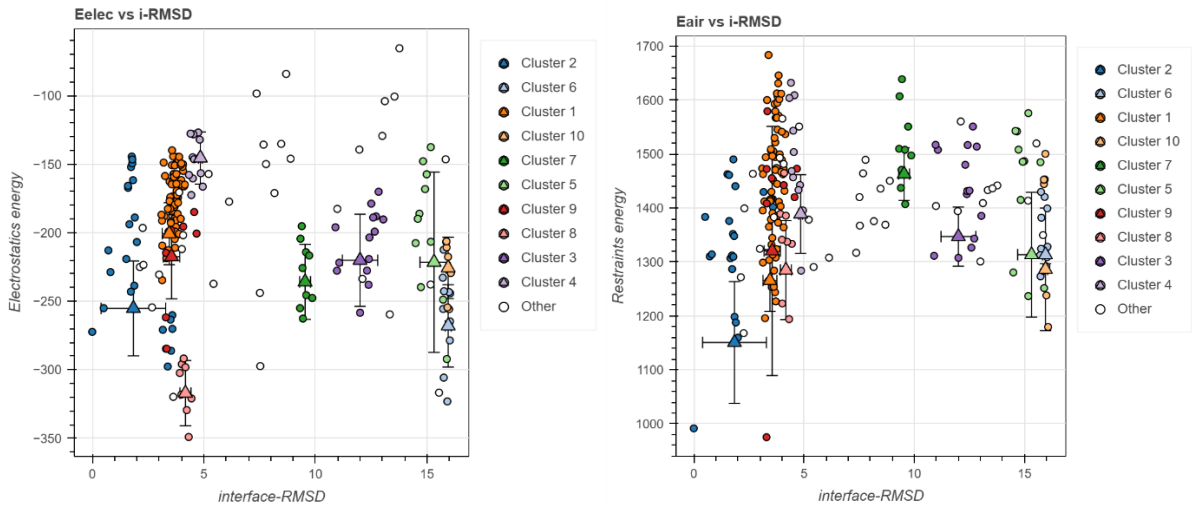

Figure J.4: HADDOCK Scatter Plots summarising the data output for all parameters tested during docking studies of clone 34 and GITR. *10 of the best clusters were selected out of the total 11 clusters identified, with each graph showing a summary of all clusters based on different calculated parameters. (A) A scatter plot showing the HADDOCK score of each cluster against the Fraction of Common Contacts (FCC) of the protein-scFv complex. (B) A scatter plot showing the HADDOCK score of each cluster against the interface Root Mean Square Deviation (i-RMSD) of the complex. (C) A scatter plot showing the Desolvation Energy (Edesolv) of each cluster against the i-RMSD. (D) A scatter plot showing the van der Waals energy (Evdw) of each cluster against the i-RSMD. (E) A scatter plot showing the Electrostatic energy (Eelec) of each cluster against the i-RSMD. (F) A scatter plot showing the Restraints energy (Eair) of each cluster against the i-RSMD.*

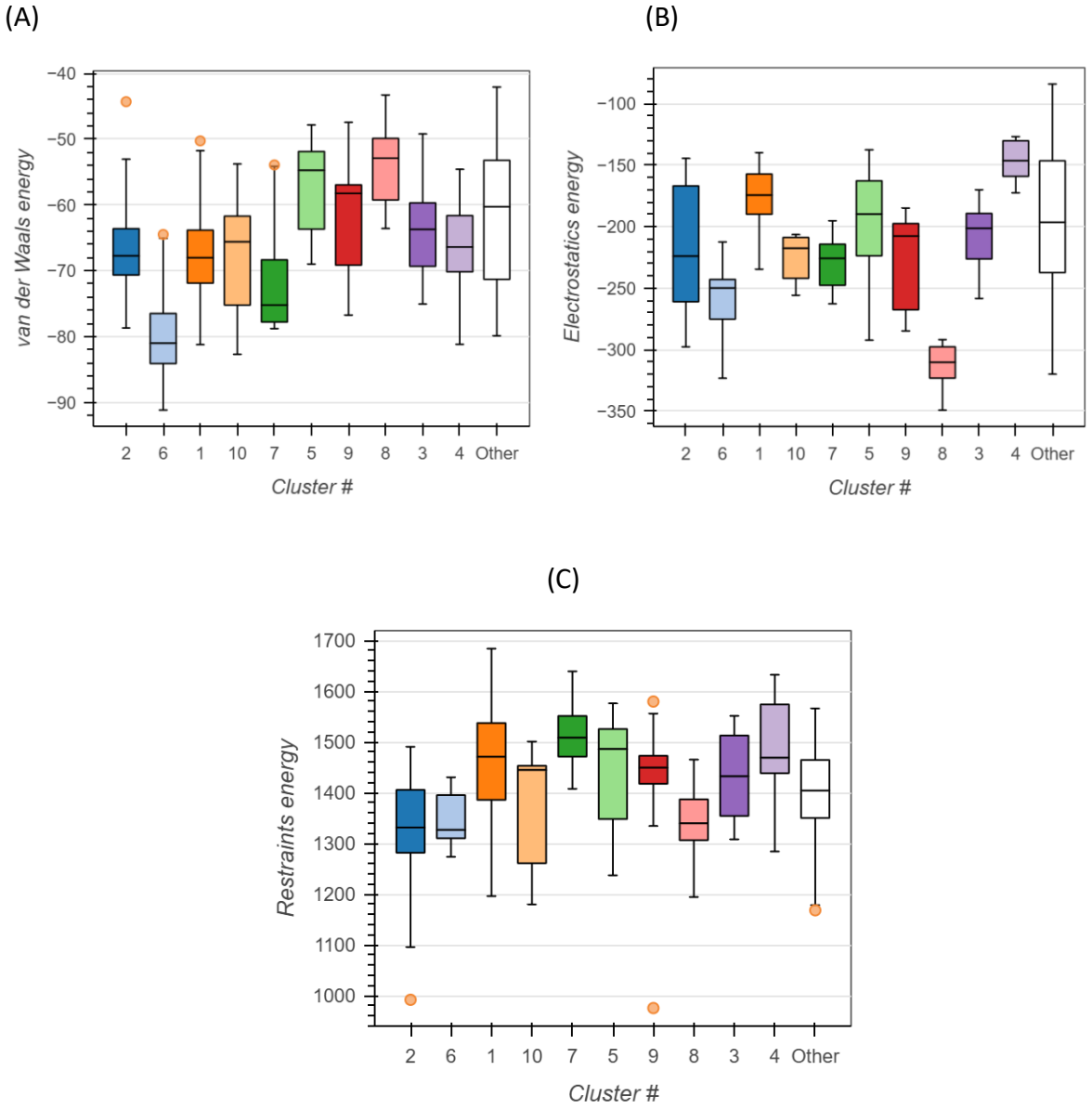

Figure J.5: HADDOCK Box Plots summarising the data output for all parameters tested during docking studies of clone 34 and GITR. *Graph (A) summarises the van der Waal energy of each cluster, starting from the most stable (2), to the least (Other). Graph (B) summarises the Electrostatic energy of each cluster, starting from the most stable (2), to the least (Other). Graph (C) summarises the Restrainst energy of each cluster, starting from the most stable (2), to the least (Other).*

Table J.1: A table summarising the main parameters used in the calculation of the HADDOCK score of the most reliable cluster (cluster 2) obtained from the docking studies of the scFv of clone 34 and GITR. *Each parameter shows a different aspect relating to protein-ligand interactions. A negative HADDOCK score typical shows a favourable interaction.*

Cluster 2	
Parameter	**Score**
HADDOCK score	-11.7 +/- 10.8
Cluster size	24
RMSD from the overall lowest-energy structure	2.4 +/- 1.8
Van der Waals energy	-69.5 +/- 5.5
Electrostatic energy	-255.2 +/- 30.0
Desolvation energy	-6.3 +/- 4.1
Restraints violation energy	1150.7+/- 97.7
Buried Surface Area	2315.2 +/- 90.1
Z-Score	-1.7